RESERVOIR-BASED DEVICES FOR THE MONITORING AND TREATMENT OF DISEASE

By Grace Young Kim

B.S., Bioengineering
University of California, Berkeley, 2001

Submitted to the Department of Materials Science and Engineering
and the
Division of Health Sciences and Technology

in Partial Fulfillment of the Requirements for the Degree of

Doctor of Philosophy in Materials Science and Medical Engineering
at the
Massachusetts Institute of Technology

June 2008

Signature of Author.....
Grace Y. Kim
May 19, 2008

Certified by.....
Michael J. Cima, Ph.D.
Sumitomo Electric Industries Professor of Engineering
Thesis Supervisor

Certified by.....
Robert S. Langer, Sc.D.
Institute Professor
HST Committee Chair

Accepted by.....
Martha L. Gray, Ph.D.
Edward Hood Taplin Professor of Medical and Electrical Engineering
Director, Harvard-MIT Division of Health Sciences and Technology

Accepted by.....
Samuel M. Allen, Ph.D.
POSCO Professor of Physical Metallurgy
Chair, DMSE Departmental Committee on Graduate Students

Dedicated to my family for their love and prayers

and

to all my teachers, in and out of the classroom

RESERVOIR-BASED DEVICES FOR MONITORING AND TREATMENT OF DISEASE

by

Grace Young Kim

Submitted to the Department of Materials Science and Engineering
and the Division of Health Sciences and Technology
on Monday, May 19, 2008
in Partial Fulfillment of the Requirements for the Degree of
Doctor of Philosophy in Materials Science and Medical Engineering

ABSTRACT

Cancer mortality still remains high despite significant investments in diagnostics, drug development, and treatment. The systemic route is convenient both for routine monitoring and for drug administration. Local cancer biomarker concentrations, however, are more indicative of the state of solid tumors and their response to therapy. Furthermore, local drug delivery can achieve efficacy where systemic treatments fail. This dissertation describes two reservoir-based devices to enable such local approaches.

We are applying superparamagnetic crosslinked iron oxide nanoparticles (CLIO) for the quantitative measurements of soluble cancer biomarkers. These nanoparticles are functionalized to react specifically in the presence of their target analyte. An implanted device with a size-exclusion membrane was used to contain the CLIO and to expose them to the cancer milieu. The system was designed to be deployed deep within the body and indirectly detect cancer cells and their activity by their secreted products, which are produced at a very high copy number by each cell. A reservoir-based polymeric device has also been applied for local chemotherapy. A biodegradable polymer microchip was designed in our group to independently deliver more than one therapeutic agent. Only *in vitro* release of active compounds had been previously demonstrated. The work in this thesis achieves local drug therapy from the polymer microchip and demonstrates efficacy against an *in vivo* tumor model of brain cancer.

The reservoir-based device approach has the potential to enable early detection of cancer recurrence, personalized drug treatments, and localized multi-drug therapy.

Thesis Committee
Professor Darrell Irvine, MIT
Professor Robert Langer, MIT (HST Chair)
Professor Michael Cima, MIT (Thesis Supervisor)

Table of Contents

Table of Figures

Table of Tables

CHAPTER 1

Introduction

1.1 Motivation

Cancer mortality still remains high despite significant investments in diagnostics, drug development and treatment. Clinical oncology relies on the systemic route for routine sampling and for administration of treatment. Not all investigations, however, can be conducted purely through measurement of serum or other easily accessible fluids such as blood, urine and tears. Furthermore, not all treatments can be administered systemically. We hypothesized that reservoir-based devices may be powerful weapons in the "War on Cancer" for both sensing and drug delivery applications.

Surveillance Bugs: The information available at a local level may provide an earlier and more accurate method of monitoring cancer and the efficacy of treatment. A tissue biopsy, cyst, or ascitic fluid gives more specialized information than systemic measurements, and biopsies are routinely performed to provide confirmation of malignancy. An estimated 1.4 million biopsies are performed annually in the United States[1]. We seek a method to leverage the large numbers of these procedures by placing a small device during biopsies to provide local measurements. Magnetic resonance imaging can be used to provide information to oncologists and patients about the molecular microenvironment around the implant

Serum human chorionic gonadotrophin (hCG), for example, is currently used to categorize patients with certain cancers[2-6], but reports indicate that local measurements may be elevated several orders of magnitude higher than systemic measurements. Animal models have shown that drug biodistribution varies widely from the systemic concentration to individual organ, but longitudinal methods of measuring local drug concentrations in humans are lacking. Drug biodistribution is of particular concern in oncology due to the abnormal vasculature of tumors[7, 8] and the increasing use of targeted drug delivery vehicles.

We are applying superparamagnetic crosslinked iron oxide nanoparticles (CLIO) for the quantitative measurements of soluble cancer biomarkers and therapeutics. These nanoparticles are functionalized to react specifically in the presence of their target analyte. Our approach uses an implanted device with a semi-permeable membrane to contain the nanoparticles and expose them to the cancer milieu. Our intent here is to design a system that can be deployed deep within the body and indirectly detect cancer cells by their secreted products, which are produced at a very high copy number by each cancer cell. Drug concentrations can be similarly measured.

Smart Bombs: Local or targeted drug delivery of cancer chemotherapeutics has the advantages of reducing total administered dose, concentrating the drug directly to needed site of action, and reducing side effects. For brain cancers, this is achieved by delivering the drug directly into the cranial cavity and bypassing the blood-brain barrier. The Gliadel® Wafer is a clinically used polymer that locally delivers carmustine, or 1,3-Bis(2-chloroethyl)-1-nitrosourea (BCNU), a common chemotherapeutic agent for the treatment of brain cancer. There is evidence that a combination of drugs may be more efficacious in cancer treatment; however, the current form of Gliadel® is not able to accommodate complex release profiles. The biodegradable polymer microchip was designed by Grayson et al.[9, 10] to independently deliver more than one therapeutic agent, but only *in vitro* release of active compounds have been demonstrated. Our work here is to deliver local drug therapy from the polymer microchip and demonstrate efficacy against an *in vivo* tumor model of brain cancer.

1.2 Thesis Objectives

The specific goals of this Ph.D. thesis are as follows:

1. To demonstrate the ability to conjugate antibodies to CLIO (Chapter 4)
2. To achieve analyte-specific aggregation of CLIO in response to two different types of cancer analyte

   a cancer biomarker, human chorionic gonadotrophin (Chapter 5)

   a cancer therapeutic, interleukin-2 (Chapter 7)
3. To characterize the T_2 change produced by a range of analyte concentrations (Chapter 5)
4. To understand the factors affecting the stability of MRSw assays (Chapter 5)
5. To increase the stability of MRSw assays (Chapter 6)

6. To demonstrate the MRSw assay within a reservoir device (Chapter 7)
7. To deliver an active chemotherapeutic drug (BCNU) with the reservoir-based microchip device (Chapter 8)
8. To demonstrate efficacy of an active chemotherapeutic drug against a cancer model *in vivo* (Chapter 8)

1.3 Organization of Thesis

Chapters 2 through 7 are devoted to the sensing application of the reservoir-based device. A review of the diagnosis and treatment of ovarian cancer, evidence supporting the need for addition methods of measuring local biomarker concentrations, and information on a specific cancer biomarker, hCG, are in Chapter 2. Chapter 3 contains background on emerging nanomaterials that are being developed for oncology applications with specific attention to one such agent, CLIO. Conjugation of CLIO is presented in Chapter 4. Characterization of CLIO as a molecular relaxation switch (MRSw) assay is presented in Chapter 5, 6, and 7. Chapter 6 focuses on a method to stabilize MRSw assay for longer applications, up to 28 days. Chapter 7 demonstrates one way that MRSw can be used in a reservoir-based device. Chapter 8 contains a short background on local drug delivery for brain cancer therapy and results on microchip-based device for local drug delivery to an animal model of brain cancer. A summary of all the thesis work is described in Chapter 9 along with recommendations for future work. Also highlighted in Chapter 9 are promising results with implanted MRSw devices, conducted in close collaboration with Karen Daniel, a fellow MIT Ph.D. candidate.

1.4 References

1. Mitka, M. (2007) New ultrasound "elasticity" technique may reduce need for breast biopsies. *Jama 297*, 455.
2. van Trommel, N. E., Massuger, L. F., Schijf, C. P., ten Kate-Booij, M. J., Sweep, F. C., and Thomas, C. M. (2006) Early identification of resistance to first-line single-agent methotrexate in patients with persistent trophoblastic disease. *J Clin Oncol 24*, 52-8.
3. Inamura, T., Nishio, S., Ikezaki, K., and Fukui, M. (1999) Human chorionic gonadotrophin in CSF, not serum, predicts outcome in germinoma. *Journal of Neurology Neurosurgery and Psychiatry 66*, 654-657.
4. Gerbes, A. L., Hoermann, R., Mann, K., and Jungst, D. (1996) Human chorionic gonadotropin-beta in the differentiation of malignancy-related and nonmalignant ascites. *Digestion 57*, 113-7.
5. Hoermann, R., Gerbes, A. L., Spoettl, G., Jungst, D., and Mann, K. (1992) Immunoreactive human chorionic gonadotropin and its free beta subunit in serum and ascites of patients with malignant tumors. *Cancer Res 52*, 1520-4.
6. Grossmann, M., Hoermann, R., Gocze, P. M., Ott, M., Berger, P., and Mann, K. (1995) Measurement of human chorionic gonadotropin-related immunoreactivity in serum, ascites and tumour cysts of patients with gynaecologic malignancies. *Eur J Clin Invest 25*, 867-73.
7. Jain, R. K. (2001) Delivery of molecular and cellular medicine. *Advanced Drug Delivery Reviews 46*.
8. Fukumura, D., and Jain, R. K. (2007) Tumor microvasculature and microenvironment: Targets for anti-angiogenesis and normalization. *Microvascular Research 74*, 72-84.
9. Grayson, A. C. R., Cima, M. J., and Langer, R. (2004) Molecular release from a polymeric microreservoir device: Influence of chemistry, polymer swelling, and loading on device performance. *Journal of Biomedical Materials Research Part A 69A*, 502-512.
10. Grayson, A. C. R., Choi, I. S., Tyler, B. M., Wang, P. P., Brem, H., Cima, M. J., and Langer, R. (2003) Multi-pulse drug delivery from a resorbable polymeric microchip device. *Nature Materials 2*, 767-772.

CHAPTER 2

Ovarian Cancer and Human Chorionic Gonadotrophin

2.1 Cancer

2.1.1 Current Diagnosis and Treatment

Ovarian cancer is the leading cause of death from gynecologic cancer in the United States. An estimated 25,000 cases are diagnosed each year, resulting in more than 16,000 deaths from ovarian cancer[1]. The needs are clear: earlier detection in potentially curable early stages, better identification of possible micro-metastatic disease during the initial diagnostic procedure, improved detection of disease remaining after treatment during follow-up procedures, and sensitive methods to monitor for reoccurrence. Research is actively in progress for sensitive and

specific serum biomarkers[2,3] and for imaging that can detect recurrent cancer[4]. Advances in chemotherapy with paclitaxel, carboplatin and surgical cytoreduction have improved remission rate and disease-free survival, but survival has only been modestly affected as treatment of drug-resistant forms of reoccurring cancer is deficient or requires improved delivery methods[5-7].

The story is similar for most forms of cancer. Current treatment methods usually involve some combination of surgery, radiation, or drug therapy. Progress is monitored by regular serum testing more for general indicators of health (such as a complete blood count) and more specific biomarkers if available. Cancer biomarkers are those that have been correlated with progression of disease, but the search for the perfect biomarker continues. One of the most well known cancer biomarker is prostate specific antigen (PSA). It is now used routinely for screening, diagnosis, and monitoring. The ideal biomarker would be elevated in a majority of malignancies, allow early detection and definitively track treatment. Realistically, a panel of biomarkers may be needed to provide the most specificity and sensitivity. Furthermore, achieving the level of individualized treatment that we seek may require more detailed information for decision making. Personalized, local information is important in cancer because each cancer is unique, with respect to genesis, location, burden, and spread. The response to therapy can be highly variable. The need for reliable methods for multiplexed sensing of tumor markers, tumor response markers or chemotherapeutic agents exists despite many recent advances.

2.1.2 Measuring Soluble Biomarkers in vivo

A wide variety of methods are employed for preclinical and clinical diagnostics. Experimental methods can be used in preclinical studies in animal models. The distribution and concentrations of administered compounds, such as chemotherapeutic drugs or microparticles,

can be traced using radioactive or fluorescent markers, imaging, or explanted tissue. Tumor activity can be similarly measured by administering an agent that is targeted to the tumor, imaging, or sacrificing the animal at regular intervals. These methods provide more detailed information but are unsuitable for routine or repeated use in humans due to safety, toxicity, tissue damage, financial, and time considerations.

Clinical oncology relies on routine sampling of easily accessible fluids such as blood, urine and tears. The samples are then analyzed by methods such as a dipstick, light scattering analysis, agglutination assay, ELISA, and Western blot. The information from easily accessible fluids tends to provide a systemic measurement, reflecting concentrations from the whole body. A tissue biopsy, cyst, or ascitic fluid gives more specialized information but is more difficult to obtain. A surgical procedure is required which can be minimally invasive, performed through a large bore needle, or require an open incision. A tissue biopsy, for example, can be used to

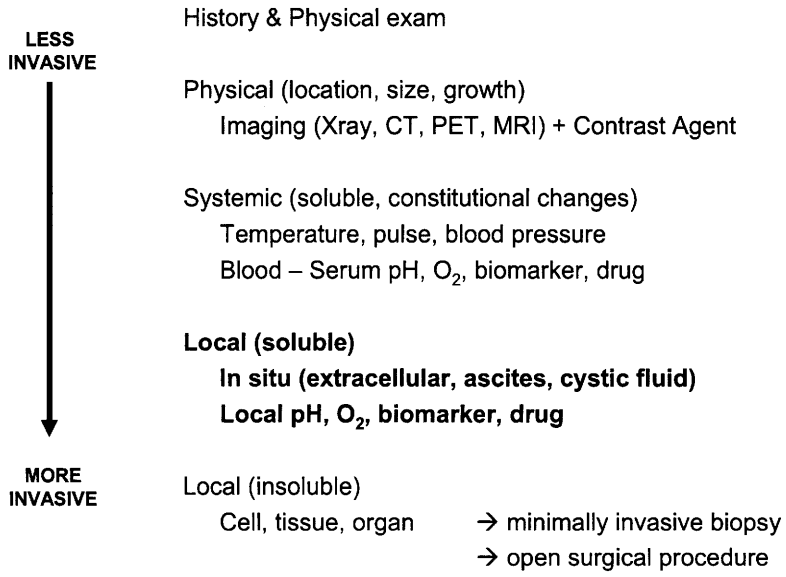

Figure 2–1. Soluble molecules *in vivo* are measured by a range of methods with different degrees of invasiveness. Molecules of interest for oncology applications include drugs, cancer biomarkers, and measures of tumor activity such as O_2, pH, apoptosis markers.

measure intratumoral or interstitial concentrations of drugs and endogenous materials. The information obtained in this manner is more specific to the site.

The utility of local biomarker concentrations was demonstrated by Sedlaczek et al.[8] in a comparative analysis of 67 patients with various ovarian cancers. The concentrations of CA125, tissue polypeptide specific antigen (TPS), and soluble interleukin-2 receptor alpha (sIL-2Rα) were compared in sera, cystic fluid, and ascitic fluid of these patients. The data were classified into, malignant with FIGO Scoring I/II, or malignant with FIGO Scoring III/IV categories (Table 2–1, Table 2–2, Table 2–3). A range of concentrations were measured from these patients, but trends do emerge (Figure 2-2). CA125 and TPS are generally elevated in cystic and ascites fluid compared to serum.

Table 2–1. CA125 Levels in Serum, Cyst Fluid, and Ascites from Patients with Ovarian Neoplasms. Reproduced from [8]. Copyright 2002 Cancer.

	CA125 (U/mL)								
	Serum			Cyst fluid			Ascites		
Histologic type	Positive/ total[a]	Median	Range	Positive/ total[a]	Median	Range	Positive/ total[a]	Median	Range
Serous carcinoma	32/33	696.0	34.1–12,408.7	10/10	44,850.0	1390.0–171,300.0	22/22	18,563.0	2610.0–74,477.0
Endometrioid carcinoma	14/16	661.0	22.5–3256.5	10/10	32,150.0	1156.0–120,410.0	10/10	14,415.5	930.0–50,900.0
Mucinous adenocarcinoma	4/7	67.0	5.2–195.0	6/6	3930.5	389.3–125,574.0	4/4	3521.5	570.0–5503.0
Undifferentiated carcinoma	11/11	860.7	327.0–5774.7	—	—	—	8/8	3909.5	710.0–17,020.0
Serous cystadenoma	1/6	7.1	3.4–71.1	6/6	42150.0	1450.0–86,940.0	—	—	—
Serous cyst	1/20	4.8	1.8–59.3	20/20	6851.5	150.0–82,210.0	—	—	—
Mucinous adenoma	0/6	10.8	5.1–18.3	6/6	5691.5	370.0–47,490.0	—	—	—

[a] Cut-off used level for CA125 was 35 U/mL.

Table 2–2. Tissue Polypeptide Specific Antigen Levels in Serum, Cyst Fluid, and Ascites from Patients with Ovarian Neoplasms
Reproduced from [8]. Copyright 2002 Cancer.

	TPS (U/L)								
	Serum			Cyst fluid			Ascites		
Histologic type	Positive/ total[a]	Median	Range	Positive/ total[a]	Median	Range	Positive/ total[a]	Median	Range
Serous carcinoma	25/33	188.2	35.7–947.7	10/10	113,140.0	11,570.0–229,300.0	23/23	25,610.0	1468.0–82,600.0
Endometrioid carcinoma	13/16	233.4	31.5–831.7	10/10	218,200.0	34,850.0–276,100.0	10/10	34,650.0	1100.0–216,700.0
Mucinous adenocarcinoma	6/7	158.4	22.7–2205.0	6/6	144,320.0	2020.0–268,600.0	4/4	206,210.0	30,460.0–352,100.0
Undifferentiated carcinoma	9/11	431.0	44.3–2224.0	—	—	—	8/8	24,035.0	3540.0–242,600.0
Serous cystadenoma	1/6	53.5	13.8–137.3	6/6	7845.0	750.0–15,190.0	—	—	—
Serous cyst	3/20	37.3	13.2–356.2	20/20	1768.5	185.0–39,540.0	—	—	—
Mucinous adenoma	2/6	26.9	14.1–157.7	6/6	4015.0	950.0–114,000.0	—	—	—

TPS: tissue polypeptide specific antigen.
[a] The cut-off level used for TPS was 80 U/L.

Table 2–3. Soluble Interleukin 2 Receptor α Levels in Serum, Cyst Fluid, and Ascites from Patients with Ovarian Neoplasms
Reproduced from [8]. Copyright 2002 Cancer.

	sIL-2Rα (pg/mL)								
	Serum			Cyst fluid			Ascites		
Histologic type	Positive/ total[a]	Median	Range	Positive/ total[a]	Median	Range	Positive/ total[a]	Median	Range
Serous carcinoma	28/33	5172.0	359.6–15,292.0	10/10	7230.0	2418.4–15,672.0	23/23	15,120.0	3645.6–42,724.8
Endometrioid carcinoma	12/16	4326.0	1049.6–16,216.0	7/10	9300.5	843.2–17,280.0	10/10	17,280.0	4960.0–49,712.4
Mucinous adenocarcinoma	6/7	4860.0	1495.2–9212.0	4/6	6990.5	1197.4–17,652.0	4/4	36,648.0	6042.6–46,731.6
Undifferentiated carcinoma	8/11	5428.0	1407.6–26,816.0	—	—	—	7/8	13,098.0	0.0–28,798.2
Serous cystadenoma	0/6	1064.6	772.0–1272.2	1/6	610.2	30.4–2765.6	—	—	—
Serous cyst	1/20	655.6	300.0–5227.7	2/20	352.4	0.0–6372.0	—	—	—
Mucinous adenoma	0/6	961.8	335.2–2138.9	1/6	914.0	18.4–6863.4	—	—	—

sIL-2Rα: soluable interleukin 2 receptor α.
[a] The cut-off level used for sIL-2Rα was 2140 pg/mL.

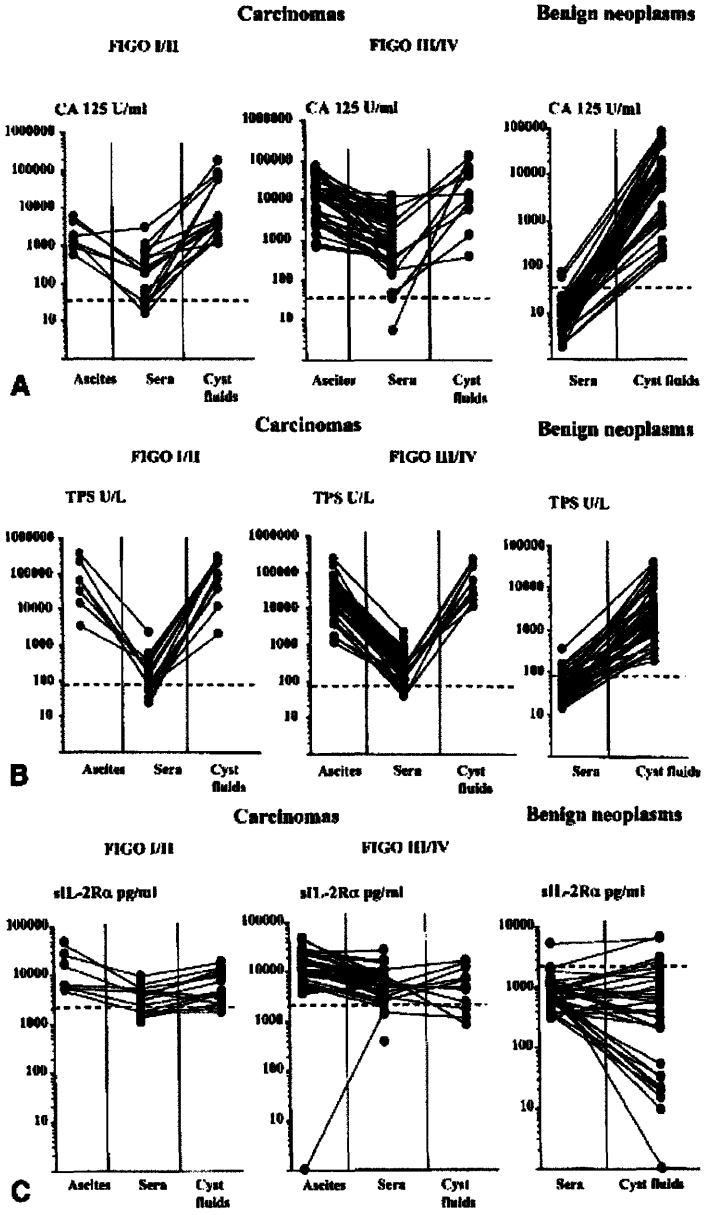

Figure 2–2. Levels of CA125 (A), tissue polypeptide specific antigen (TPS) (B), and soluble interleukin-2 receptor α (sIL-2Rα) in sera, cyst, and ascitic fluids from individual patients with ovarian carcinoma according to International Federation of Gynecology and Obstetrics (FIGO) disease stage and in serum and cyst fluid from patients with benign ovarian neoplasms. The upper reference limits for CA125 (35 U/mL), TPS (80 U/L), and sIL-2R α (2140 pg/mL) are indicated by dashed lines. Reproduced from [8]. Copyright 2002 Cancer.

This type of differential study of biomarkers is important and more is needed. Not all studies, however, can be conducted purely through serum measurements. There is still a need for additional noninvasive or minimally invasive methods in oncology research and clinical practice.

One need involves a type of cancer therapy that uses oncolytic viruses to kill tumor cells[9]. Peng et al. generated a viral tracking method to meet this need as current methods are inadequate to characterize the efficiency and timing of viral therapy. Peng states that PET imaging, in particular, lacks the sensitivity and resolution for this application. An oncolytic measles virus was engineering to secrete their own soluble marker peptide[10]. This method allows independent monitoring of the therapeutic vehicle and its efficacy. They chose marker peptides that are also cancer biomarkers themselves, human carcinoembryonic antigen (hCEA) and the beta-subunit of human chorionic gonadotrophin (hCG-β). They chose these markers for tracking the kinetic profile of gene expression because they are non-immunogenic, have no interfering biological function, and have a long circulation half-life (2-5 hrs, and 11 hours, respectively, in mouse serum). The rationale behind tracking cancer killing efficacy with an agent that itself secretes a cancer biomarker is not clear as it limits the use of the virus to application in which hCEA and hCG-β are not secreted by the cancer. Nevertheless, this approach using traceable oncolytic viruses may improve preclinical development and provide clinical data regarding efficacy, clearance, dose response, and variability between patients. This approach works because Peng is delivering a live cancer treatment. Most other therapies, however, do not have the capacity both to secrete an indicator of activity and as well as to perform their cancer killing action. Another problem with this approach and others employing a systemically delivered agent is that it is highly dependent on the ability of the agent to access the investigation site. It is difficult to distinguish if a lower signal is due to inactivation of the agent (inadequate viral replication, dissociation of radiolabel, photobleaching of dye) or inefficiency of delivery to the investigation site. This is of particular concern in oncology due to the abnormal vasculature of tumors[11, 12]

2.2 Human Chorionic Gonadotrophin

HCG is a placenta-derived glycoprotein hormone composed of an α and β subunit[13]. The hCG-α (14.5 kDa) is similar in structure to many other hormones, whereas hCG-β (28 kDa) has a more specific function. HCG-β has a serum half-life of 30 hours in humans[14] and 11 hours in mice[15]. The biological function is minimal without the α subunit[14]. It is well-characterized as it is a convenient marker in serum or urine for pregnancy[16] and a variety of malignancies in human and rodent models[14, 15].

Serum concentration is typically very low in healthy men and women but can vary widely with disease (Table 2–4). Serum concentrations of hCG-β are specifically elevated in testicular and ovarian cancer[17-21]. Serum concentrations of up to 16 μg/ml hCG were reported in persistent trophoblastic disease were reported, whereas they are usually less than 0.005 μg/ml in normal men and women[17].

Table 2–1. Range of hCG and hCG-β Concentrations.

Sample, population	[hCG] μg/ml
Serum, in men*:	< 0.003
Serum, in women during normal menstrual cycle*:	< 0.005
Urine, pregnancy early test concentration*:	0.015-0.025
Urine, pregnancy peak concentration (week 9-11)*:	180 – 300[22]
Serum, cancer patients	0.006 - 16**,[17]

*converted using 10 IU per μg hCG; 10 mIU/mL = 10 ng/ml
** Pre-chemotherapy, persistent trophoblastic disease

It is hypothesized that local biomarker concentration may provide a more accurate method of categorizing patients for staging and treatment. Serum HCG is currently used to categorize patients in certain gynecologic disorders. Van Trommel reported in 2006 a

retrospective study in which he compared data from patients with persistent trophoblastic disease (PTD)[17]. Patients were divided into two populations, those who responded to treatment with a single agent such as methotrexate, or those who required alternate or multi-drug treatment. Multi-drug treatment is avoided when possible due to harmful side effects, including an increased risk of secondary malignancies[23] and earlier menopause[24, 25]. Serum hCG, within the first few courses of methotrexate treatment, was different in patients for whom the single agent would be sufficient compared to patients who would eventually require more aggressive therapy. Early categorization into low and high risk status may allow the appropriate treatment to be given sooner rather than waiting for failure with the single agent and then giving the more hazardous multi-drug treatment later.

A study by Inamura et al.[18] found that hCG elevations in cerebrospinal fluid (CSF) may be a better indication of disease severity than by hCG in serum alone. Intracranial germinomas containing syncytiotrophoblastic giant cells (STGC) are currently treated more aggressively if serum hCG is elevated. The normal ranges for hCG in CSF are unknown, probably because invasiveness of the procedure, considerations of neurological damage, or risk of infection limits its determination compared to serum. A sense of the range of values is still possible (Table 2–5). CSF values tend to be more elevated than serum measurements. The CSF is contained in a relatively confined, isolated compartment surrounding the brain and spinal cord, and is closely in contact with the germinomas and STGC cells. HCG concentrations in CSF may not be the definitive answer for identifying and categorizing patients with malignancy, it remains a good model biomarker. These examples do highlight the need for more information about cancer biomarkers and that local concentrations are different from systemic concentrations. Scientists continue to look for biomarkers with strong correlations with the disease state.

Table 2–2. HCG Serum positive group in germinoma patients. Reproduced with permission[18]. Copyright 1999 BMJ Publishing Group Ltd.

Case	Age/ sex	Site	HCG serum/ CSF (mIU/ml)	HCG-β serum/ CSF (ng/ml)	Initial treatment	Recurrence	Treatment at recurrence	Latest follow up
1	13/M	P	40/88	0.41/1.5	R	—	—	12 y/ alive
2	12/M	BG	130/90	3.5/6.3	R	—	—	15 y/ alive
3	9/M	S	78/96	0.57/1.34	Chem	—	—	7 y/ alive
4	13/M	P	-/-	0.3/2.3	Chem	6 months; local	Cranial irradiation	2 y/ alive
5	16/M	P	56/70	0.54/0.78	R	14 months; spinal	Spinal irradiation	4 y/ died of tumour
6	22/M	P	6.9/22	0.47/1.1	Chem	5 y; Local CSF HCG-β (+), normal serum HCG- β	Cranial irradiation	7 y/ alive
7	16/M	BG	6.4/8.0	0.4/0.9	Chem	3 y; local	Cranial irradiation	7 y/ alive

BG=basal ganglia; P=pineal; S=suprasellar; R=radiotherapy (whole brain, 30 Gy; local 20 Gy); Chem=chemotherapy; HCG=human chorionic gonadotrophin;
HCG- β =human chorionic gonadotrophin β -subunit; -/- =not tested.

2.3 References

1. Jemal, A., Clegg, L. X., Ward, E., Ries, L. A. G., Wu, X. C., Jamison, P. M., Wingo, P. A., Howe, H. L., Anderson, R. N., and Edwards, B. K. (2004) Annual report to the nation on the status of cancer, 1975-2001, with a special feature regarding survival. *Cancer 101*, 3-27.
2. Zhang, Z., Bast, R. C., Yu, Y. H., Li, J. N., Sokoll, L. J., Rai, A. J., Rosenzweig, J. M., Cameron, B., Wang, Y. Y., Meng, X. Y., Berchuck, A., van Haaften-Day, C., Hacker, N. F., de Bruijn, H. W. A., van der Zee, A. G. J., Jacobs, I. J., Fung, E. T., and Chan, D. W. (2004) Three biomarkers identified from serum proteomic analysis for the detection of early stage ovarian cancer. *Cancer Research 64*, 5882-5890.
3. McIntosh, M. W., Drescher, C., Karlan, B., Scholler, N., Urban, N., Hellstrom, K. E., and Hellstrom, I. (2004) Combining CA 125 and SMR serum markers for diagnosis and early detection of ovarian carcinoma. *Gynecologic Oncology 95*, 9-15.
4. Tammela, J., and Lele, S. (2004) New modalities in detection of recurrent ovarian cancer. *Current Opinion in Obstetrics & Gynecology 16*, 5-9.
5. Agarwal, R., and Kaye, S. B. (2003) Ovarian cancer: strategies for overcoming resistance to chemotherapy. *Nat Rev Cancer 3*, 502-16.
6. Sood, A. K., and Buller, R. E. (1998) Drug resistance in ovarian cancer: from the laboratory to the clinic. *Obstet Gynecol 92*, 312-9.
7. Kamat, A. A., Kim, T. J., Landen, C. N., Jr., Lu, C., Han, L. Y., Lin, Y. G., Merritt, W. M., Thaker, P. H., Gershenson, D. M., Bischoff, F. Z., Heymach, J. V., Jaffe, R. B., Coleman, R. L., and Sood, A. K. (2007) Metronomic chemotherapy enhances the efficacy of antivascular therapy in ovarian cancer. *Cancer Res 67*, 281-8.
8. Sedlaczek, P., Frydecka, I., Gabrys, M., van Dalen, A., Einarsson, R., and Harlozinska, A. (2002) Comparative analysis of CA125, tissue polypeptide specific antigen, and soluble interleukin-2 receptor alpha levels in sera, cyst, and ascitic fluids from patients with ovarian carcinoma. *Cancer 95*, 1886-1893.
9. Russell, S. J., and Peng, K. W. (2007) Viruses as anticancer drugs. *Trends in Pharmacological Sciences 28*, 326-333.
10. Peng, K. W., Facteau, S., Wegman, T., O'Kane, D., and Russell, S. J. (2002) Non-invasive in vivo monitoring of trackable viruses expressing soluble marker peptides. *Nature Medicine 8*, 527-531.
11. Jain, R. K. (2001) Delivery of molecular and cellular medicine. *Advanced Drug Delivery Reviews 46*.
12. Fukumura, D., and Jain, R. K. (2007) Tumor microvasculature and microenvironment: Targets for anti-angiogenesis and normalization. *Microvascular Research 74*, 72-84.
13. Gam, L. H., and Latiff, A. (2005) SDS-PAGE electrophoretic property of human chorionic gonadotropin (hCG) and its beta-subunit. *Int J Biol Sci 1*, 103-9.
14. Bidart, J. M., Thuillier, F., Augereau, C., Chalas, J., Daver, A., Jacob, N., Labrousse, F., and Voitot, H. (1999) Kinetics of serum tumor marker concentrations and usefulness in clinical monitoring. *Clinical Chemistry 45*, 1695-1707.
15. Shih, I. M., Torrance, C., Sokoll, L. J., Chan, D. W., Kinzler, K. W., and Vogelstein, B. (2000) Assessing tumors in living animals through measurement of urinary beta-human chorionic gonadotropin. *Nat Med 6*, 711-4.

16. Cole, L. A., Seifer, D. B., Kardana, A., and Braunstein, G. D. (1993) Selecting human chorionic gonadotropin immunoassays: consideration of cross-reacting molecules in first-trimester pregnancy serum and urine. *Am J Obstet Gynecol 168*, 1580-6.
17. van Trommel, N. E., Massuger, L. F., Schijf, C. P., ten Kate-Booij, M. J., Sweep, F. C., and Thomas, C. M. (2006) Early identification of resistance to first-line single-agent methotrexate in patients with persistent trophoblastic disease. *J Clin Oncol 24*, 52-8.
18. Inamura, T., Nishio, S., Ikezaki, K., and Fukui, M. (1999) Human chorionic gonadotrophin in CSF, not serum, predicts outcome in germinoma. *Journal of Neurology Neurosurgery and Psychiatry 66*, 654-657.
19. Gerbes, A. L., Hoermann, R., Mann, K., and Jungst, D. (1996) Human chorionic gonadotropin-beta in the differentiation of malignancy-related and nonmalignant ascites. *Digestion 57*, 113-7.
20. Hoermann, R., Gerbes, A. L., Spoettl, G., Jungst, D., and Mann, K. (1992) Immunoreactive human chorionic gonadotropin and its free beta subunit in serum and ascites of patients with malignant tumors. *Cancer Res 52*, 1520-4.
21. Grossmann, M., Hoermann, R., Gocze, P. M., Ott, M., Berger, P., and Mann, K. (1995) Measurement of human chorionic gonadotropin-related immunoreactivity in serum, ascites and tumour cysts of patients with gynaecologic malignancies. *Eur J Clin Invest 25*, 867-73.
22. Braunstein, G. D., Karow, W. G., Gentry, W. C., Rasor, J., and Wade, M. E. (1978) First-trimester chorionic gonadotropin measurements as an aid in the diagnosis of early pregnancy disorders. *Am J Obstet Gynecol 131*, 25-32.
23. Secki, M. J., and Rustin, G. J. (1997) Late toxicity after therapy of gestational trophoblastic tumors, in *Gestational trophoblastic disease* (Hancock, B. W., Newlands, E. S., and Berkowitz, R. S., Eds.) pp viii, 266 p., Chapman & Hall Medical, London ; New York.
24. Rustin, G. J. S., Newlands, E. S., Lutz, J. M., Holden, L., Bagshawe, K. D., Hiscox, J. G., Foskett, M., Fuller, S., and Short, D. (1996) Combination but not single-agent methotrexate chemotherapy for gestational trophoblastic tumors increases the incidence of second tumors. *Journal of Clinical Oncology 14*, 2769-2773.
25. Bower, M., Rustin, G. J. S., Newlands, E. S., Holden, L., Short, D., Foskett, M., and Bagshawe, K. D. (1998) Chemotherapy for gestational trophoblastic tumours hastens menopause by 3 years. *European Journal of Cancer 34*, 1204-1207.

CHAPTER 3

Nanomedicine

and Superparamagnetic Nanoparticles

3.1 Nanomedicine

Nanomedicine has emerged as a promising weapon in the war against cancer. Nanomedicine refers to the use of nano-scale components in medical applications. It was identified as a key area of research by the National Cancer Institute (NCI) and resulted in the launch of the Alliance for Nanotechnology in Cancer in September 2004. A grant component of that program, Center of Cancer Nanotechnology Excellence, was awarded to Harvard-MIT in October 2005 and has produced collaborative research projects for improved cancer diagnosis and treatment[1]. Nanomedicine involves a broad array of technologies, but most can be grouped

into six main areas: nanoshells, carbon nanotubes, dendrimers, quantum dots, liposomes, and superparamagnetic nanoparticles[3]. These agents have lengths from 1 to 100 nm in two or three dimensions[4]. Their size imbues them with special properties. Quantum dots, for example, can be tuned to have specific wavelengths of emission. The size of superparamagnetic nanoparticles imparts its magnetic properties as they are small enough to encompass only a single magnetic domain. These agents can be combined with detection moieties (antibodies, aptamers), therapeutics agents (chemotherapeutics, siRNA), or imaging agents (fluorophors, radiolabels) or serve as an imaging agent themselves and have been applied for diagnostic, therapeutic, or imaging purposes.

The utility of these agents increases with combination approaches that feature multi-platform tracking or that merge therapeutics and monitoring functionality into a "theranostic." Nanomedicine platforms are being designed to "home in" to a disease area, highlight the target cells, and release their drug payload directly where it is needed[5, 6]. This multifunctional and responsive nature is why these platforms have often been termed "smart" or "intelligent." This intelligence has special promise in oncology applications to due to the potential of these agents to reduce chemotherapeutic side effects that, in traditional therapeutic methods, cause extreme complications or termination of therapy. These agents are diverse in shape and feature exotic materials, though biocompatibility is usually conferred by coating with a more familiar polymeric shell, typically of dextran or PEG. This coating has the added advantage of reducing immunogenicity and clearance while increasing circulation time. This is important because nanomedicine platforms rely heavily on the enhanced permeability and retention (EPR) effect for cancer targeting[7]. Concerns with these agents include lack of data regarding the effect of repeat administration and long-term safety. The Nanotechnology Characterization Laboratory,

established by NCI in collaboration with the National Institute of Standards and Technology and the United States Food and Drug Administration, aims to spearhead the testing and approving of nanomaterials for cancer, but clinical acceptance may still be very difficult in the case of some agents, such as cadmium-based quantum dots. Other nanoscale agents, however, are already making an impact clinically. Liposomes are the oldest and most successful nanomedicine agent. Formally described by Alec D. Bangham in a seminal paper in 1965[8], it is the first nanomaterial introduced into the clinical market. Doxil® is a pegylated liposome that carries doxorubicin and was FDA approved in November 1995[9, 10]. Nanomedicine continues to expand with many nanoparticle-based therapeutics now clinically approved or under clinical trials[11, 12].

3.2 Superparamagnetic Iron Oxide Nanoparticles

3.2.1 Magnetic Nanoparticles

Iron oxides are categorized into three general groups based on their magnetization curves at about 300 Kelvin: ferromagnetic, paramagnetic and superparamagnetic (Figure 3–1). Superparmagnetic iron oxides nanoparticles (SPION) attain superparamagnetic behavior when the material is in a particle form containing single domains of about 10-20 nm in diameter. They can be maghemite, δ-Fe_2O_3, or magnetite, Fe_3O_4 [13]. The individual nanoparticles are magnetic, but a solution of nanoparticles shows no net magnetization in the absence of an external field as the particles are randomly oriented. It has been suggested that this lack of magnetic remanence is of benefit in biological applications though the true effects of remanent magnetic materials *in vivo* is unknown[14].

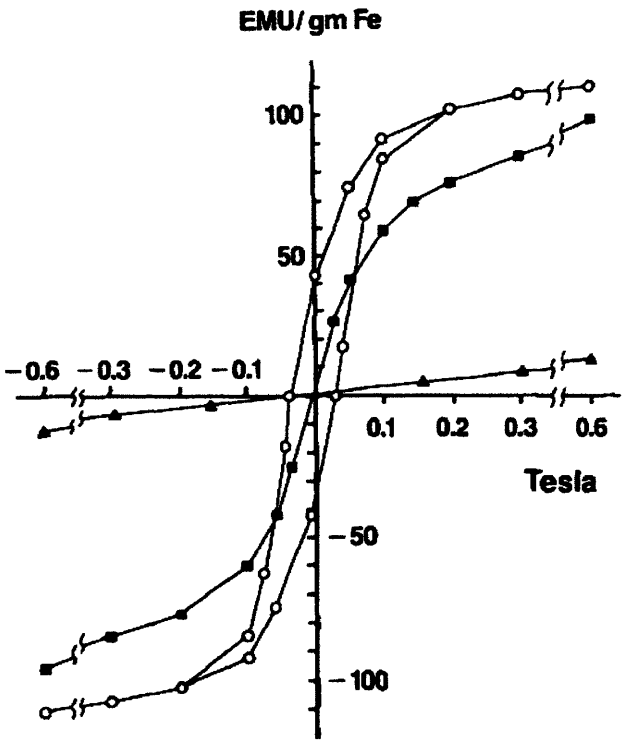

Figure 3–1. Superparamagnetic iron oxides (AMI-25, square) show high magnetization and saturation in high magnetic field but when have no magnetic remanence when the field is removed (0 T). This is in contrast with paramagnetic iron oxides (triangle) which shows low magnetization and ferromagnetic iron oxide which does have a magnetic remanence (open circle). Reproduced by permission from [15]. Copyright 1999 Magnetic Resonance Imaging.

The synthetic method and the coating are important as they determine the properties of SPION, and are highly specialized for each application. SPION are synthesized by multiple methods including co-precipitation, thermal decomposition and/or reduction, micelle synthesis, hydrothermal synthesis, and biosynthesis [14, 16-18]. These methods succeed to different degrees in controlling the size and polydispersity, and thus the critical characteristics that not only determines if it is a true nanoparticle but also influences its superparamagnetic behavior. The coating of SPION is especially important as bare metallic nanoparticles can be highly reactive, hydrophobic, and toxic. They are susceptible to oxidization, degradation, or non-specific agglomeration due to magnetic dipole-dipole attractions [19]. Coating is accomplished with surfactants, polymers, inorganic materials, or organic means. They confer biocompatibility,

reduced cytotoxicity, improve stability, enhance biodistribution, and provide a surface for easy chemical modification and functionalization [16, 20]. SPION are rapidly cleared through extravasation, the reticulo-endothelial system, and renal excretion. Crosslinked iron oxide (CLIO) is one particular type of SPION. It has a non-biodegradable dextran coating and, as such, it is primarily used as an experimental material, but in certain applications and given the rapid clearance of some nanomaterials, biodegradation may not always be necessary. The CLIO coating also contains abundant free amines, which are convenient for functionalization as Sun et al. demonstrated (Figure 3–2) [21].

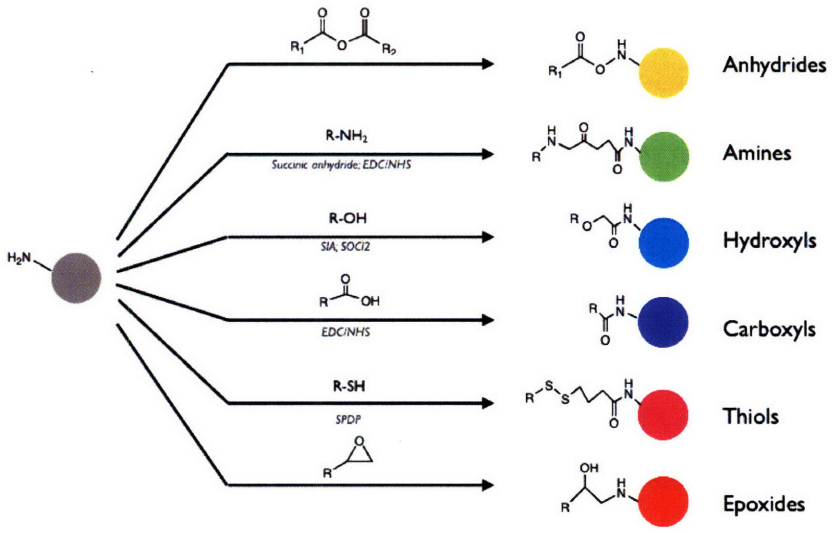

Figure 3–2. Conjugation strategies to magnetofluroescent nanoparticles. Aminated magnetofluorescent nanoparticles were reacted with small molecules with different reactivities. Reproduced from [21]. Copyright 2006 American Chemical Society.

3.2.2 Biomedical Applications of SPION

Magnetic nanoparticles are used for a variety of applications: hyperthermia, drug delivery, magnetic resonance imaging contrast enhancement, tissue repair, immunoassay[18], detoxification of biological fluids, and bioseparation[13, 16, 22]. One of the earliest biomedical

applications of small iron oxide particles was traced to 40 years ago by Gilchrist[23] for hyperthermia research and thermal ablation of lymph nodes. Ohgushi demonstrated its T_2 shortening ability in 1978[24] and since then, its use in *in vitro* diagnostic assays and *in vivo* imaging has proliferated. SPION are efficient at dephasing the spins of protons in neighboring water molecules. Solutions containing SPION, thus, have a change in the transverse relaxation time T_2 from the solvent alone. T_2 varies not only with the concentration of SPION but also with the configuration of SPION, whether it is dispersed or clustered. Clustered SPION are more efficient at decreasing T_2 than dispersed SPION (Figure 3–1)[15]. Differential contrast with clustering has been exploited and specifically controlled through the use of the surface functional groups[25-27].

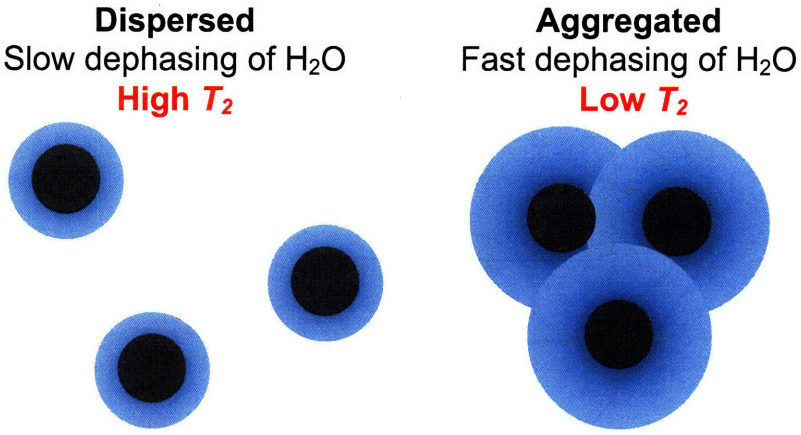

Figure 3–1. Clustered superparamagnetic iron oxide nanoparticles are more efficient at dephasing the neighboring protons, resulting in a decreasing T_2 compared with superparamagnetic iron oxide nanoparticles.

Since Gilchrist and Ohgushi, applications of SPION to magnetic resonance imaging (MRI) and, specifically, oncology have been changing cancer treatment[2, 3, 28]. One of the most well-known applications has used CLIO for detection of lymph node metastases that are missed by currently available means (Figure 3–4)[2, 29]. Furthermore, "smart" MRI contrast agents are

now being designed to produce specific contrast in response to cells, biomolecules or small drug molecules. This responsiveness is achieved in some MRI contrast agents by functionalization with receptors, proteins, or other ligands[30]. Others are being specifically engineered to have

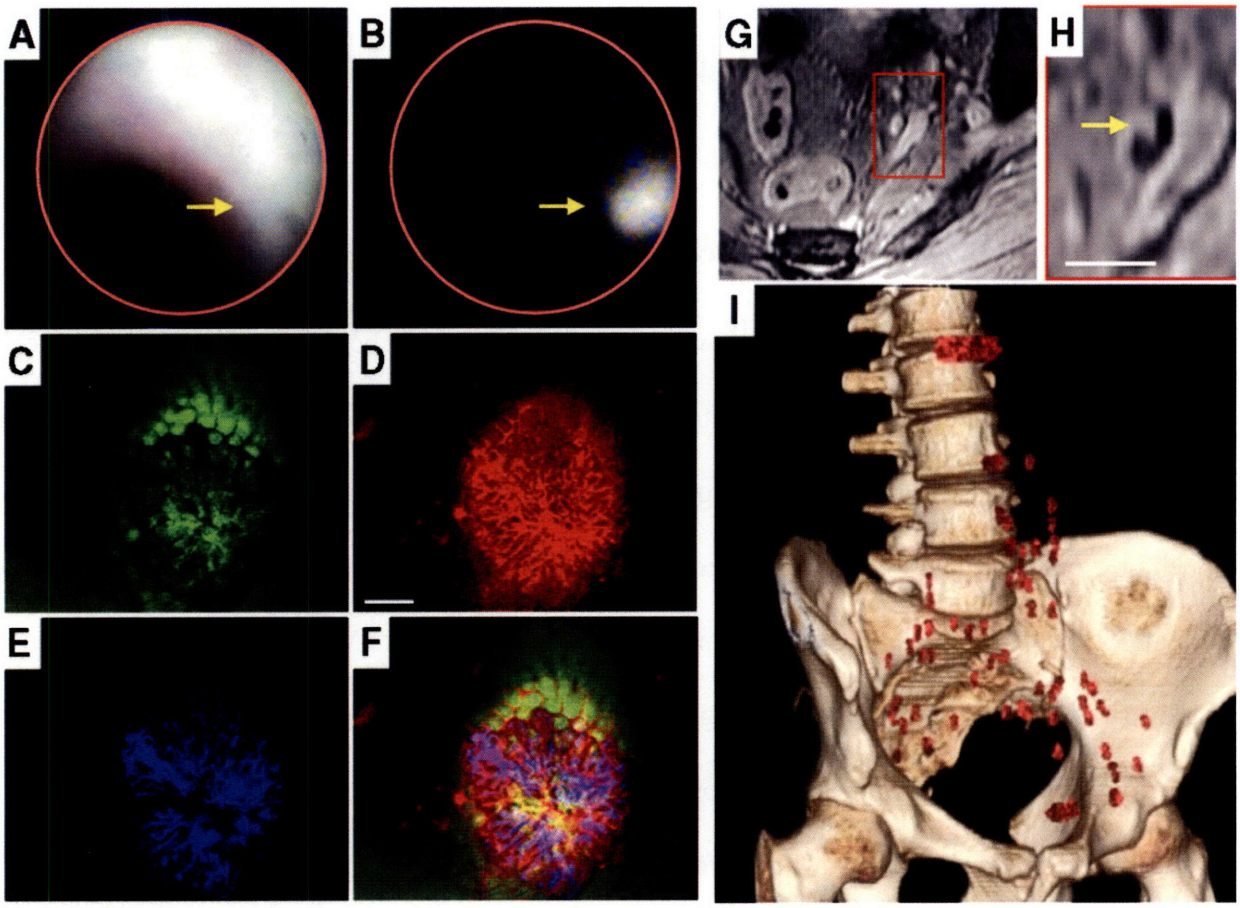

Figure 3–1 Molecular imaging used for early detection of cancer in mice and humans. Dysplastic colonic adenoma in *Apc*$^{Min/-}$ mice imaged by fiberoptic endoscopy (A and B) and endomicroscopy (C to F). The 2-mm lesion is not detectable by regular colonoscopy (A) but becomes readily apparent by imaging cathepsin protease activity in the near infrared channel (B). Arrows indicate location of adenoma. [(C) to (F)] show that endomicroscopy of an adenomatous lesion in a living mouse provides cellular resolution of this early lesion (C), cathepsin expression (D) (scale bar, 1 mm), and microvascularity (E). (F) is a merged image. (G and H) MRI of a human male pelvis showing prostate cancer metastasis. (G) shows an axial MRI of the pelvis. The square highlights a region of nonenlarged lymph nodes and vessels. Magnetic nanoparticles with affinity for lymph node macrophages were administered systemically to detect intranodal metastases. (H) is a magnified region after nanoparticle administration, which shows 1.3-mm micrometastases in a 4 x 7 mm lymph node. Scale bar, 10 mm. Arrow points to micrometastases within dark lymph node. (I) Reconstruction of lymph node metastases detected in 34 patients by the above technique. The extensive, unpredictable spread of prostate cancer to these nodes (red) is one of the reasons that imaging in individual patients is so important. Reproduced with permission from [2]. Copyright 2006 Science.

variable contrast with binding of a molecule of interest[31]. These "smart" agents may reveal information about the mechanisms of cancer origin and metastasis and their response to therapy[2]. Their role in clinical oncology is of particular interest because they may extend current imaging techniques of determining cancer borders to include visualizing the local molecular activity of the cancer, they may inform early detection of disease, they may allow personalized medicine, and they may aid in the development and study of new cancer drugs[2].

3.2.3 SPION in Diagnostic and Molecular Relaxation Switch Assays

The same SPION used for *in vivo* applications can also be used for *in vitro* diagnostic measurements of specific targets, including nucleotides[32], viruses[33], cells[34], and ions[31]. The sensitivity of detection has been demonstrated from 10^{-21} M for DNA to 10^{-6} M for Ca^{2+} depending on a variety of factors, including binding affinity, particle concentration, and sensor format. These particles are called magnetic relaxation switches (MRSw) because they can be made to "switch" from dispersed to aggregated in the presence of a target molecule or analyte (Figure 3–1a). The aggregation is accomplished by the presence of functional groups on the particle surface that have an affinity for the analyte. The change of state from dispersed to aggregated affects the T_2 of the aqueous medium that surrounds the particles (Figure 3–1). Thus, aggregation can be detected by magnetic means, enabling measurements in turbid and opaque solutions as well as real-time measurements in patients. Magnetic detection, therefore, has a distinct advantage over optical or electrochemical assays [35, 36].

Aggregation of multivalent systems is actively being studied[37-39]. Functional group balance has been found to be important in the formation of aggregates [38]. An optimum ratio of particle to analyte exists where the analytes form interparticle bridges or crosslinks between two

nanoparticles ((Figure 3–1c). A network or branched aggregate can be created if the nanoparticle has more than one receptor or if the analyte is multivalent. The low analyte regime has insufficient analyte to cause aggregation and very few bridges are created (Figure 3–1b). High concentrations of analyte will, however, saturate the receptors and prevent crosslinking of nanoparticles (Figure 3–1d). This phenomenon is known as the prozone effect or high-dose hook effect and is a limitation of all agglutination assays. Colloidal stability is also a concern for the MRSw-based assay[14].

The main advantages of MRSw assays are that they have a simple and fast operating principle, requiring putting the functionalized SPION in contact with the solution containing the analyte. MRSw assays can provide qualitative measurements with minimal hardware and time. Quantitative MRSw-based measurements may be advantageous in certain applications compared with more labor intensive methods such as ELISA or HPLC. Research on these MRSw assays is actively ongoing, and further development is needed for accurate, sensitive, and robust measurements for *in vitro* and *in vivo* oncology applications.

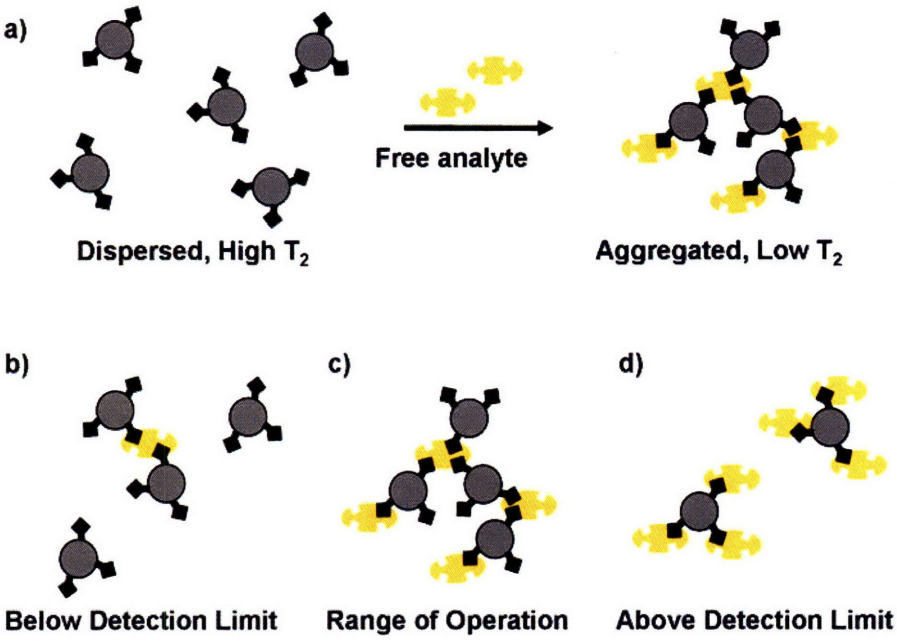

Figure 3–1. a) Schematic of analyte-induced aggregation. b-d) Schematic of the effect of increasing analyte to particle ratio. Adapted from Costanzo[38]. b) Low analyte to particle ratio causes insufficient aggregation for detection. c) The range of aggregate formation relies on a stoichiometric balance of analyte to particle. d) The prozone effect is seen at high analyte to particle ratio, where analytes have saturated the particles such that crosslinking of particles is impaired. Reproduced in part with permission from [40]. Copyright 2007 American Chemical Society.

3.3 References

1. http://nano.cancer.gov/alliance_awards/fact/centers.asp. (Accessed on April 17, 2008.).
2. Weissleder, R. (2006) Molecular imaging in cancer. *Science 312*, 1168-71.
3. Kim, K. Y. (2007) Nanotechnology platforms and physiological challenges for cancer therapeutics. *Nanomedicine-Nanotechnology Biology and Medicine 3*, 103-110.
4. ASTM-E-2456-06. (2006) Terminology for Nanotechnology. *ASTM International.*
5. Nasongkla, N., Bey, E., Ren, J., Ai, H., Khemtong, C., Guthi, J. S., Chin, S. F., Sherry, A. D., Boothman, D. A., and Gao, J. (2006) Multifunctional polymeric micelles as cancer-targeted, MRI-ultrasensitive drug delivery systems. *Nano Lett 6*, 2427-30.
6. Hong, G., Yuan, R., Liang, B., Shen, J., Yang, X., and Shuai, X. (2008) Folate-functionalized polymeric micelle as hepatic carcinoma-targeted, MRI-ultrasensitive delivery system of antitumor drugs. *Biomed Microdevices.*
7. Maeda, H. (2001) The enhanced permeability and retention (EPR) effect in tumor vasculature: The key role of tumor-selective macromolecular drug targeting. *Advances in Enzyme Regulation, Vol 41 41*, 189-207.
8. Bangham, A. D., Standish, M. M., and Watkins, J. C. (1965) Diffusion of univalent ions across the lamellae of swollen phospholipids. *J Mol Biol 13*, 238-52.
9. Northfelt, D. W., Dezube, B. J., Thommes, J. A., Miller, B. J., Fischl, M. A., Friedman-Kien, A., Kaplan, L. D., Du Mond, C., Mamelok, R. D., and Henry, D. H. (1998) Pegylated-liposomal doxorubicin versus doxorubicin, bleomycin, and vincristine in the treatment of AIDS-related Kaposi's sarcoma: Results of a randomized phase III clinical trial. *Journal of Clinical Oncology 16*, 2445-2451.
10. Northfelt, D. W., Dezube, B., Miller, B., Mamelok, R. D., DuMond, C. E., and Henry, D. (1995) Randomized comparative trial of DOXIL(R) vs adriamycin, bleomycin, and vincristine (ABV) in the treatment of severe AIDS-related Kaposi's sarcoma (AIDS-KS). *Blood 86*, 1515-1515.
11. Farokhzad, O. C., and Langer, R. (2006) Nanomedicine: Developing smarter therapeutic and diagnostic modalities. *Advanced Drug Delivery Reviews 58*, 1456-1459.
12. Zhang, L., Gu, F. X., Chan, J. M., Wang, A. Z., Langer, R. S., and Farokhzad, O. C. (2007) Nanoparticles in Medicine: Therapeutic Applications and Developments. *Clin Pharmacol Ther.*
13. Gupta, A. K., and Gupta, M. (2005) Synthesis and surface engineering of iron oxide nanoparticles for biomedical applications. *Biomaterials 26*, 3995-4021.
14. Tartaj, P., Morales, M. D., Veintemillas-Verdaguer, S., Gonzalez-Carreno, T., and Serna, C. J. (2003) The preparation of magnetic nanoparticles for applications in biomedicine. *Journal of Physics D-Applied Physics 36*, R182-R197.
15. Josephson, L., Lewis, J., Jacobs, P., Hahn, P. F., and Stark, D. D. (1988) The Effects of Iron-Oxides on Proton Relaxivity. *Magnetic Resonance Imaging 6*, 647-653.
16. Lu, A. H., Salabas, E. L., and Schuth, F. (2007) Magnetic nanoparticles: synthesis, protection, functionalization, and application. *Angew Chem Int Ed Engl 46*, 1222-44.
17. Babes, L., Denizot, B., Tanguy, G., Le Jeune, J. J., and Jallet, P. (1999) Synthesis of iron oxide nanoparticles used as MRI contrast agents: A parametric study. *Journal of Colloid and Interface Science 212*, 474-482.

18. Osaka, T., Matsunaga, T., Nakanishi, T., Arakaki, A., Niwa, D., and Iida, H. (2006) Synthesis of magnetic nanoparticles and their application to bioassays. *Anal Bioanal Chem 384*, 593-600.
19. Hamley, I. W. (2003) Nanotechnology with soft materials. *Angewandte Chemie-International Edition 42*, 1692-1712.
20. Lewinski, N., Colvin, V., and Drezek, R. (2008) Cytotoxicity of nanoparticles. *Small 4*, 26-49.
21. Sun, E. Y., Josephson, L., Kelly, K. A., and Weissleder, R. (2006) Development of nanoparticle libraries for biosensing. *Bioconjugate Chemistry 17*, 109-113.
22. Liang, Y. Y., Zhang, L. M., Jiang, W., and Li, W. (2007) Embedding magnetic nanoparticles into polysaccharide-based hydrogels for magnetically assisted bioseparation. *Chemphyschem 8*, 2367-72.
23. Gilchrist, R. K., Medal, R., Shorey, W. D., Hanselman, R. C., Parrott, J. C., and Taylor, C. B. (1957) Selective inductive heating of lymph nodes. *Ann Surg 146*, 596-606.
24. Ohgushi, M., Nagayama, K., and Wada, A. (1978) Dextran-Magnetite - New Relaxation Reagent and Its Application to T_2 Measurements in Gel Systems. *Journal of Magnetic Resonance 29*, 599-601.
25. Bogdanov, A., Jr., Matuszewski, L., Bremer, C., Petrovsky, A., and Weissleder, R. (2002) Oligomerization of paramagnetic substrates result in signal amplification and can be used for MR imaging of molecular targets. *Mol Imaging 1*, 16-23.
26. Perez, J. M., Josephson, L., O'Loughlin, T., Hogemann, D., and Weissleder, R. (2002) Magnetic relaxation switches capable of sensing molecular interactions. *Nat Biotechnol 20*, 816-20.
27. Yigit, M. V., Mazumdar, D., Kim, H. K., Lee, J. H., Dintsov, B., and Lu, Y. (2007) Smart "Turn-on" magnetic resonance contrast agents based on aptamer-functionalized superparamagnetic iron oxide nanoparticles. *ChemBioChem 8*, 1675-1678.
28. Weissleder, R., and Mahmood, U. (2001) Molecular imaging. *Radiology 219*, 316-33.
29. Weissleder, R., Elizondo, G., Josephson, L., Compton, C. C., Fretz, C. J., Stark, D. D., and Ferrucci, J. T. (1989) Experimental lymph node metastases: enhanced detection with MR lymphography. *Radiology 171*, 835-9.
30. Weissleder, R., Kelly, K., Sun, E. Y., Shtatland, T., and Josephson, L. (2005) Cell-specific targeting of nanoparticles by multivalent attachment of small molecules. *Nat Biotechnol 23*, 1418-23.
31. Atanasijevic, T., Shusteff, M., Fam, P., and Jasanoff, A. (2006) Calcium-sensitive MRI contrast agents based on superparamagnetic iron oxide nanoparticles and calmodulin. *Proc Natl Acad Sci U S A 103*, 14707-12.
32. Josephson, L., Perez, J. M., and Weissleder, R. (2001) Magnetic nanosensors for the detection of oligonucleotide sequences. *Angew. Chem. Int. Ed. 40*, 3204-3206.
33. Perez, J. M., Simeone, F. J., Saeki, Y., Josephson, L., and Weissleder, R. (2003) Viral-induced self-assembly of magnetic nanoparticles allows the detection of viral particles in biological media. *J Am Chem Soc 125*, 10192-3.
34. Schellenberger, E. A., Reynolds, F., Weissleder, R., and Josephson, L. (2004) Surface-functionalized nanoparticle library yields probes for apoptotic cells. *ChemBioChem 5*, 275-9.

35. von Lode, P., Rainaho, J., and Pettersson, K. (2004) Quantitative, wide-range, 5-minute point-of-care immunoassay for total human chorionic gonadotropin in whole blood. *Clin Chem 50*, 1026-35.
36. Chen, J., Tang, J., Yan, F., and Ju, H. (2006) A gold nanoparticles/sol-gel composite architecture for encapsulation of immunoconjugate for reagentless electrochemical immunoassay. *Biomaterials 27*, 2313-21.
37. Shapiro, M. G., Atanasijevic, T., Faas, H., Westmeyer, G. G., and Jasanoff, A. (2006) Dynamic imaging with MRI contrast agents: quantitative considerations. *Magn Reson Imaging 24*, 449-62.
38. Costanzo, P. J., Patten, T. E., and Seery, T. A. (2004) Protein-Ligand Mediated Aggregation of Nanoparticles: A study of synthesis and assembly mechanism. *Chem Mater 16*, 1775-1785.
39. Costanzo, P. J., Patten, T. E., and Seery, T. A. (2006) Nanoparticle agglutination: acceleration of aggregation rates and broadening of the analyte concentration range using mixtures of various-sized nanoparticles. *Langmuir 22*, 2788-94.
40. Kim, G. Y., Josephson, L., Langer, R., and Cima, M. J. (2007) Magnetic relaxation switch detection of human chorionic gonadotrophin. *Bioconjug Chem 18*, 2024-8.

CHAPTER 4

Conjugation of Crosslinked Iron Oxide Nanoparticles

4.1 Introduction & Motivation

Crosslinked iron oxide nanoparticles (CLIO) have been conjugated by many methods. We demonstrate conjugation of CLIO and IgG antibodies following previously established protocols. It was important to validate our ability to conjugate CLIO before proceeding with additional characterization of the magnetic relation switches and assay development.

CLIO have an iron oxide core 5-10 nm diameter, containing approximately 8000 Fe atoms[1, 2]. The core is surrounded by a dextran coating which has been crosslinked with

epichlorohydrin and aminated by reacting with ammonia. The resulting particle is 40-80 nm, water soluble, biocompatible, and stable[3]. The coating also provides approximately 40-60 free surface amines and a convenient route for conjugation[4]. Conjugation of CLIO to antibodies, proteins, virus, nucleic acids, and others have been previously reported[5-9]. Regulatory approval and the cost associated with production of a biological agent for clinical use has motivated the investigation of additional conjugates. CLIO were conjugated via the surface amines with different small molecules and reactive handles as demonstrated by Sun et al. in 2006[10, 11]. The amine can be used to form other amines, anhydrides, hydroxyls, carboxyls, thiols and epoxides (Figure 4–1). Analytical methods employed with CLIO must take into consideration the strong absorption due to the iron oxide themselves from 250 and 450 nm, the superparamagnetic property, and the presence of oxidizing ferrous ions and reducing ferric ions[10]. A successful conjugates should preserve the activity of the original species and avoid surface denaturation.

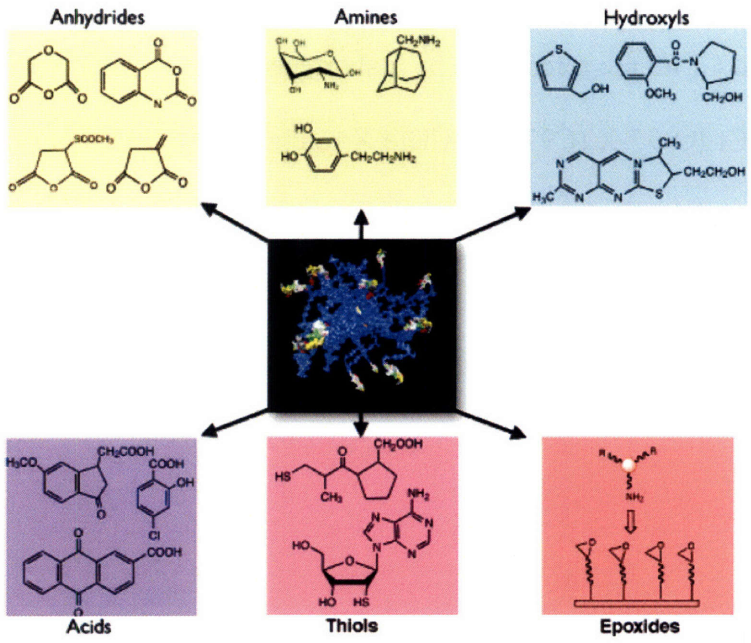

Figure 4–1. Nanoparticle library. Examples of small molecules attached to amino-CLIO to create a 96-member library (to fill one microtiter plate) that was subsequently used. Reproduced from [10]. Copyright 2006 American Chemical Society.

4.2 Materials and Methods

4.2.1 Nanoparticle Conjugation

Magnetic iron oxide nanoparticles with amine-terminated dextran shell (CLIO-NH_2) were produced as described previously[12]. CLIO-NH_2 was treated with sulfo-succinimidyl-4-(N-maleimidomethyl)cyclohexane-1-carboxylate (Sulfo-SMCC, Pierce, Rockford, IL) to create a maleimide functional group. Antibodies were activated with N-succinimidyl-S-acetylthioacetate (SATA, Pierce) to generate a blocked sulfanyl group which was deprotected with hydroxylamine. The CLIO-SMCC was incubated with the prepared antibody solutions for 4 to 8 h at 4°C. The reaction was quenched with 2-sulfanylethanol and purified with a Sephacryl 300 column (Sigma). Antibodies conjugated were mouse IgG (Sigma), anti-hCG-β (Scripps Laboratories, San Diego, CA), and anti-IL-2 (R & D Systems). Anti-hCG-β monoclonal antibody-conjugated CLIO are referred to by a shortened form of their product numbers, CLIO-95-X (C95-X) and CLIO-97-X (C97-X), where X refers to the batch number. The antibodies for C95 and C97 are a matched pair to separate, nonoverlapping epitopes on hCG-β, with K_d values of 10^{-10} M and 5×10^{-9} M, respectively. The second batch of each conjugate, C95-2 and C97-2, was produced by starting with a 3-fold volumetric scaleup of reactants. All other batches were not scaled up.

4.2.2 Relaxation Rate

Relaxivities (r_2 and r_1) were determined as the slope of a plot of $1/T_2$ or $1/T_1$ (s^{-1}) as a function of the CLIO iron concentration (mM).

4.2.3 Nanoparticle Valency Estimation

Iron concentrations were determined by absorbance at 410 nm after aliquots were incubated for 1 h in 6 N HCl and H_2O_2 to dissolve CLIO. Samples were compared to an iron standard curve. Protein concentrations were determined by bicinchoninic acid assay (Pierce). The protein concentration was divided by the iron concentration to estimate the number of antibody conjugated to each nanoparticle, assuming 8000 iron molecules per CLIO[1].

4.2.4 Dynamic Light Scattering and Zeta Potential Measurements

Particle sizes and zeto potential were determined using a 90 Plus Particle Size Analyzer (Brookhaven Instrument Corporation, Holtsville, NY). Samples were measured at 237°C in PBS, $\lambda = 658$ nm, 90° fixed angle. The log-normal intensity-weighted effective diameter was reported. Zeta potential solutions were prepared in PBS at 8 μg/ml Fe. Measurements were obtained after at least 40 cycles.

4.3 Results

CLIO-NH_2 starting material was generously provided by the Center for Molecular Imaging Research (CMIR, CLIO-NH_2 Batch #9) with the parameters in Table 4–1. It was estimated to have 41 free amines per nanoparticle. Several batches of CLIO-NH_2 were conjugated with antibodies according to the protocol described (Figure 4–1). SATA is a non-site-specific coupling agent and has the potential to interfere with some antibody functionality. Higher antibody functionality, if necessary, may be achieved with site-specific coupling such as mercaptoethylamine, which directs modification away from the antibody binding region.

The relaxivity and valency of the unconjugated CLIO-NH_2 and conjugated CLIO are also reported in Table 1. The relaxivities of conjugated CLIO are similar to those of unconjugated CLIO-NH_2. The same initial concentration of antibody was used in all conjugations. No specific attempt was made to increase the degree of conjugation; however, C95-2 and C97-2 resulted in higher valencies than C95 and C97, yielding approximately 1 to 2 more antibodies per nanoparticle. Effective diameters were found to increase after conjugation. The variability in the valencies obtained suggest that additional parameter exist that should be more closely controlled. The variability, however, provides an opportunity to examine the role of antibody valency in the function of molecular relaxation switch assays (Chapter 5).

Zeta potential measurements of select CLIO conjugates including some matched pairs reveal that the CLIO conjugates are relatively neutral in PBS. This may be important in understanding its solution stability, especially as aggregates are deliberately formed. Efforts to specifically control the zeta potential may aid it its colloidal stability.

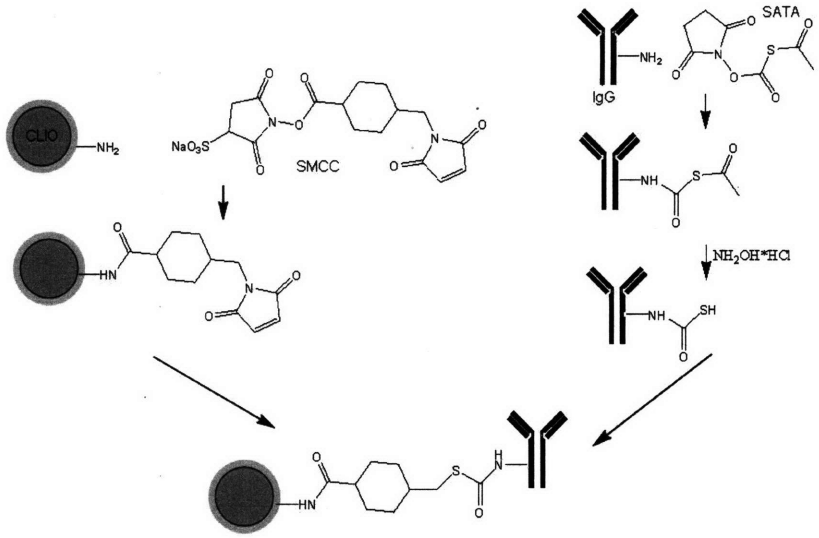

Figure 4–1. Conjugation of CLIO and antibody

Table 4–1. Characterization of CLIO conjugates. Reproduced in part with permission from [13]. Copyright 2007 American Chemical Society.

Sample	Analyte	r_2 Relaxivity $(mM \bullet sec)^{-1}$	r_1 Relaxivity $(mM \bullet sec)^{-1}$	r_2/r_1	Valency (# Ab per CLIO)	Effective diameter (nm)	Zeta potential ± std. error (mV)
PBS	--	--	--	--	--	13.3	0.43 ± 0.51
CLIO-NH_2*	--	54.2	21.5	2.52	--	58	
CLIO-NH_2	--	54.3	23.7	2.29	--	58	
CLIO-IgG	protein A	47.0	n/m	n/a	--	117	
CLIO-95 (C95)	hCG-β, hCG	44.1	n/m	n/a	2.2	66	2.33 ± 0.59
CLIO-97 (C97)	hCG-β, hCG	44.9	n/m	n/a	3.1	66	
CLIO-95-2 (C95-2)	hCG-β, hCG	67.9	17.8	3.81	4.1	128**	1.36 ± 0.29
CLIO-97-2 (C97-2)	hCG-β, hCG	76.4	20	3.82	4.5	128**	
CLIO-95-3 (C95-3)	hCG-β, hCG	83.7	23.5	3.56	4.0	125	
CLIO-97-3 (C97-3)	hCG-β, hCG	79.9	22.9	3.49	1.9	126	
CLIO-95-4 (C95-4)	hCG-β, hCG	tbd	tbd	tbd	2.0	97	1.14 ± 1.77
CLIO-97-4 (C97-4)	hCG-β, hCG	tbd	tbd	tbd	2.3	100	
CLIO-3000	hCG-β, hCG					70.2	0.62 ± 0.72
CLIO-anti-IL-2	IL-2	tbd	tbd	tbd	tbd	308	-1.28 ± 0.53

* as reported by CMIR

-- not applicable

n/m not measured

4.4 References

1. Reynolds, F., O'Loughlin, T., Weissleder, R., and Josephson, L. (2005) Method of determining nanoparticle core weight. *Anal Chem 77*, 814-7.
2. Shen, T. T., Bogdanov, A., Bogdanova, A., Poss, K., Brady, T. J., and Weissleder, R. (1996) Magnetically labeled secretin retains receptor affinity to pancreas acinar cells. *7*, 311-316.
3. Lewin, M., Carlesso, N., Tung, C. H., Tang, X. W., Cory, D., Scadden, D. T., and Weissleder, R. (2000) Tat peptide-derivatized magnetic nanoparticles allow in vivo tracking and recovery of progenitor cells. *Nat Biotechnol 18*, 410-4.
4. Zhao, M., Kircher, M. F., Josephson, L., and Weissleder, R. (2002) Differential conjugation of tat peptide to superparamagnetic nanoparticles and its effect on cellular uptake. *Bioconjug Chem 13*, 840-4.
5. Josephson, L., Perez, J. M., and Weissleder, R. (2001) Magnetic nanosensors for the detection of oligonucleotide sequences. *Angewandte Chemie-International Edition 40*, 3204-3206.
6. Perez, J. M., O'Loughin, T., Simeone, F. J., Weissleder, R., and Josephson, L. (2002) DNA-based magnetic nanoparticle assembly acts as a magnetic relaxation nanoswitch allowing screening of DNA-cleaving agents. *J Am Chem Soc 124*, 2856-7.
7. Perez, J. M., Simeone, F. J., Saeki, Y., Josephson, L., and Weissleder, R. (2003) Viral-induced self-assembly of magnetic nanoparticles allows the detection of viral particles in biological media. *J Am Chem Soc 125*, 10192-3.
8. Grimm, J., Perez, J. M., Josephson, L., and Weissleder, R. (2004) Novel nanosensors for rapid analysis of telomerase activity. *Cancer Res 64*, 639-43.
9. Perez, J. M., Simeone, F. J., Tsourkas, A., Josephson, L., and Weissleder, R. (2004) Peroxidase substrate nanosensors for MR imaging. *4*, 119-122.
10. Sun, E. Y., Josephson, L., Kelly, K. A., and Weissleder, R. (2006) Development of nanoparticle libraries for biosensing. *Bioconjugate Chemistry 17*, 109-113.
11. Sun, E. Y., Josephson, L., Kelly, K. A., and Weissleder, R. (2006) Development of nanoparticle libraries for biosensing. *Bioconjug Chem 17*, 109-13.
12. Josephson, L., Tung, C. H., Moore, A., and Weissleder, R. (1999) High-efficiency intracellular magnetic labeling with novel superparamagnetic-Tat peptide conjugates. *Bioconjug Chem 10*, 186-91.
13. Kim, G. Y., Josephson, L., Langer, R., and Cima, M. J. (2007) Magnetic relaxation switch detection of human chorionic gonadotrophin. *Bioconjug Chem 18*, 2024-8.

CHAPTER 5

Characterization of MRSw-based Assays

5.1 Summary

Magnetic relaxation switches (MRSw) were prepared to detect protein A and the hCG-β subunit of human chorionic gonadotrophin (hCG-β). Crosslinked iron oxide nanoparticles (CLIO) are a T_2 MRI contrast agent. Antibodies were attached to CLIO using standard peptide chemistry. Protein A was used as a simple model analyte, as it is naturally multivalent and can bind multiple CLIO-IgG simultaneously. The addition of PA to CLIO-IgG resulted in transverse relaxation time (T_2) decreases compared to a blank control as seen by homogenous field magnetic relaxometry (HFMR). A two-particle system was designed to measure hCG-β, as it is

not multivalent and requires conjugation of a matched pair of monoclonal antibodies to CLIO (referred to as C95 and C97). Measurement of hCG-β is of interest as elevated serum levels are associated with malignancies including testicular and ovarian cancers[1]. The addition of hCG-β to C95 and C97 resulted in T_2 decreases with a linear dynamic concentration range of 0.1 to 1 molecules of analyte per nanoparticle. Similar data were obtained for the hCG dimer. Other parameters important in this assay, such as the stoichiometry of analyte to nanoparticle and MRSw valency, were also investigated. The MRSw assay was found to be compatible with a variety of buffers and selective in the presence of other proteins. Analyte-induced aggregation was confirmed by light scattering particle size analysis. T_2 kinetic and particle size kinetic measurements were also made and suggest that control of aggregate size is an important component of stable MRSw measurements.

5.2 Introduction & Motivation

Functionalized nanoparticle MRI contrast agents are being are being used for many applications[2, 3]. T_2 measurements are radiofrequency-based and can be made in opaque solutions and within deep tissues. It is, thus, ideal for *in vitro* diagnostic as well as *in vivo* applications. CLIO and their conjugates have been studied by Weissleder et al. for use as a responsive T_2 modifying agent (Section 3). One area of study is the ideal functional group valency for a particular application. The role of valency on the efficacy of cell targeting was reported by Weissleder and his colleagues. CLIO were targeted via cyclic-RGD sequences (cRGD) to $\alpha_v\beta_3$ integrins that are overexpressed on the surface of angiogenic endothelial cells and tumor cells[4]. CLIO-cRGD was found to bind highly to BT-20 human breast cancer cells and resulted in

tumoral accumulation of CLIO-cRGD. The effect of multivalency was studied by conjugating variable numbers of cRGD to CLIO (low, medium and high valency conjugates had 4, 20, and 52 cRGD per CLIO, respectively)[5]. Multivalency was seen to have effect with as few as four peptides, and when the peptide density on the particle was higher than the density of integrin binding sites, the higher valency did not confer additional benefits.

In vitro diagnostic applications of CLIO may have an entirely different optimum valency that needs to be tailored for each assay type. MRSw assays have simple mix-and-read methodology[6-9]; however, validation of our ability to conjugate antibodies to CLIO and achieve analyte-specific aggregation needs to be established before work can commence on a more detailed characterization of the aggregation reaction. Furthermore, colleagues of Weissleder had suggested that solution stability of MRSw could be problematic under certain conditions. We set out to better understand the parameter space of stable MRSw operation.

The aggregation reaction between the MRSw and the analyte relies on the specificity of antibody recognition to yield a simple mix-and-read system in which the superparamagnetic nanoparticles amplify antibody:analyte binding events for enhanced sensitivity[10, 11]. Characterization of the aggregation reaction was achieved mainly through two methods. The primary observable was the analyte concentration range that induces MRSw switching. The accuracy and speed of MRSw switching are obvious corollary investigations. The antibodies used for conjugation have been protein A or affinity purified, but the specificity of the antibodies after conjugation to CLIO should be confirmed by testing MRSw switching in various buffers. The kinetics of the switching reaction is important for determining the incubation time and the ideal window for T_2 measurements. ELISA assays, for example, often require incubation steps of 15 minutes to 1 hour for analytes and antibodies to interact. They also employ a "stop solution"

to achieve an endpoint read or at least slow the continued development of colored products before saturation. MRSw reaction kinetics can be monitored by serial relaxation time measurements and by particle size, which can also provide an estimate of the evolving cluster size.

The MRSw-based assay was studied initially with two analytes: protein A (PA) and human chorionic gonadotrophin (hCG). PA is a stable cell surface receptor that is naturally multivalent and serves as a simple model system for aggregation. One PA molecule can bind to the Fc portion of least two molecules of IgG at the same time, and thus forms a simple aggregating system (Figure 5–1a). Other proteins, however, may not naturally be multivalent and require a matched pair of antibodies to form a "sandwich" with the analyte in the middle, similar to an ELISA. Detection of hCG requires such a strategy to form networked aggregates, since hCG is not multivalent (Figure 5–1a). hCG is a heterodimer, consisting of an α and β subunit. Many other hormones share a similar structure to hCG-α, whereas the hCG-β serum level is elevated in testicular and ovarian cancers and locally elevated in cystic fluid and ascites often to concentrations greater than in serum[12, 13]. It is one of the more well-characterized soluble cancer biomarkers, as it is also a pregnancy marker.

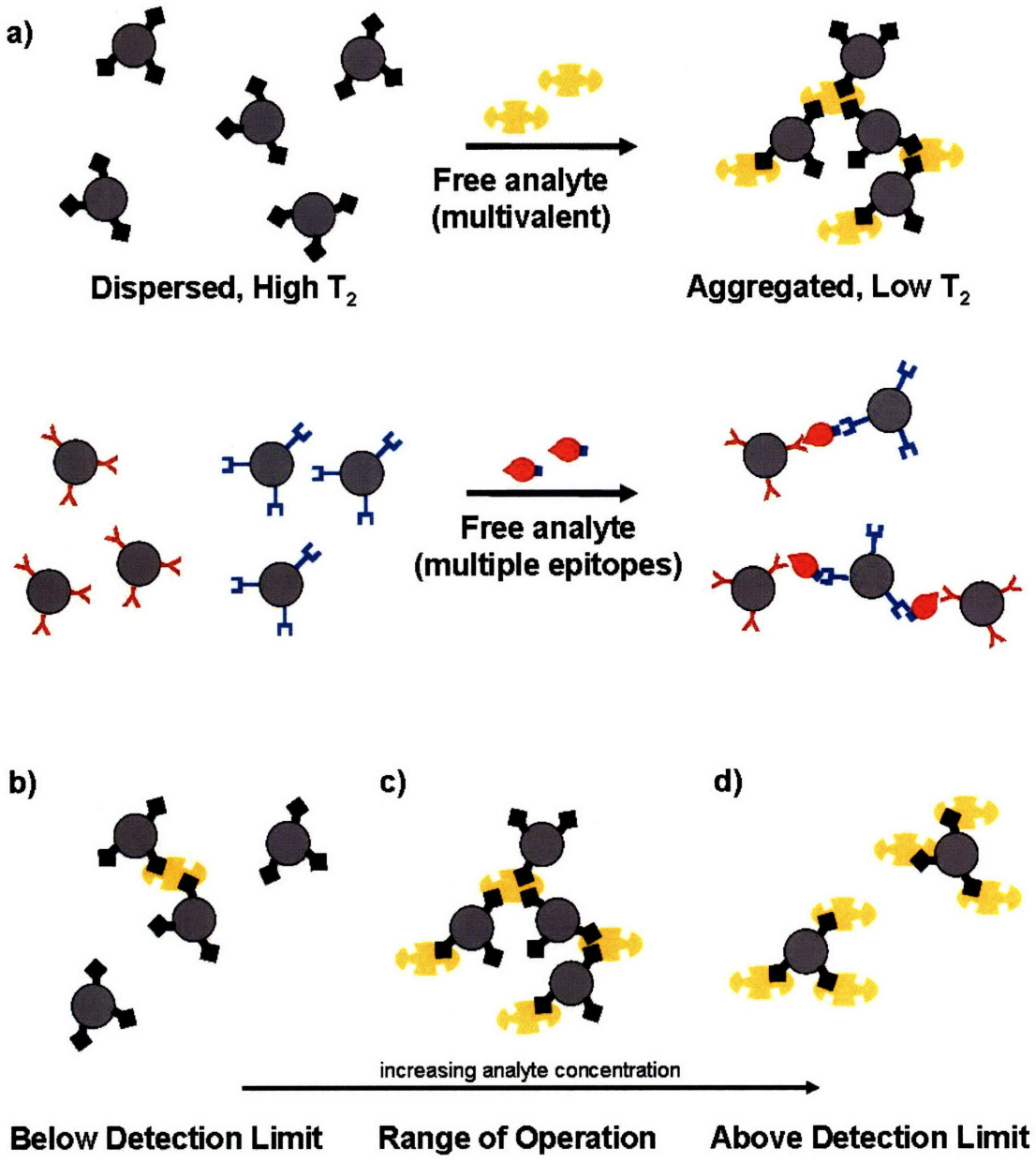

Figure 5–1. a) Schematic of MRSw aggregation wit ha multivalent analyte and a non-multivalent analyte. Protein A is a multivalent analyte and requires only one CLIO conjugate. HCG is not multivalent, and thus, two different CLIO conjugates (both C95 and C97) directed against a separate epitope on hCG are needed. b-d) Schematic of the effect of increasing analyte to particle ratio. Adapted from Costanzo[14]. b) Low analyte to particle ratio causes insufficient aggregation for detection. c) The range of aggregate formation relies on a stoichiometric balance of analyte to particle. d) The prozone effect is seen at high analyte to particle ratio, where analytes have saturated the particles such that crosslinking of particles is impaired.

5.3 Materials and Methods

5.3.1 Aggregation Experiments

Aggregation experiments were performed by mixing equal volumes of CLIO reagent and analyte solutions. CLIO-IgG was conjugated to assay for PA (Section 4). CLIO-IgG was prepared in PBS to have a final concentration of 10 μg/ml Fe after analyte addition. CLIO-95-X and CLIO-97-X (C95-X, C97-X for short, where X indicates a generic batch number) was conjugated to assay for hCG and hCG-β (Section 4). An equal blend of C95 and C97 (C95/C97) or C95-2 and C97-2 (C95-2/C97-2) solutions were prepared in PBS to have final concentrations of 8 μg/ml Fe C95-X and 8 μg/ml Fe C97-X after analyte addition except for the experiment in which the ratio of C95 to C97 was specifically varied. The sandwich-behavior of the assay was tested using controls of C95-X or C97-X alone. Analyte dilutions of PA (Sigma, 45 kDa), hCG-β (Scripps Laboratories, 28 kDa), hCG (Sigma, 37.9 kDa), TH, LH, or FSH (Sigma) were prepared in phosphate buffered saline pH 7.4 with 1% penicillin-streptomycin and 0.1% bovine serum albumin (PBS) to reduce nonspecific adsorptive loss of analyte. Aggregation experiments with various buffers used PBS, artificial urine solution (Surine®, Dynatek Industries, Lenexa, KS), DMEM cell culture media (Invitrogen), cell culture media + 10% fetal bovine serum (10% FBS, Invitrogen), and fetal bovine serum (100% FBS). Aspirated conditioned media from cell culture studies were mixed with equal volumes of C95/C97 reagent. Reported concentrations are the final analyte concentrations obtained after mixing. The limit of detection (LOD) is defined by the concentration where the standard deviation does not overlap with the standard deviation of the PBS control

5.3.2 Cell Culture

CRL-8400, JAR, and JEG-3 cell lines (ATCC) were cultured according to the manufacturer's instructions. Cells were harvested and plated at 10^5 cells/ml in a 6-well plate. Conditioned cell culture media was aspirated from wells on subsequent days. The media was tested in aggregation experiments as is and hCG-β concentration was independently measured by ELISA (United Biotech Inc). Cells were also counted using a hemocytometer to track cell growth rates.

5.3.3 ^1H Relaxation Time Measurements

Proton relaxation time measurements were performed on two different instruments: a homogeneous field magnetic relaxometer (HFMR; 0.47 T and 40°C; Bruker the Minispec, Bruker Optics, Billerica, MA) or a single-sided MR (0.43 T and 25°C; Profile NMR MOUSE, ACT Center for Technology, Aachen, Germany). Samples for the HFMR were mixed in a microcentrifuge tube to ensure adequate mixing before being transferred to a 7" long, 5 mm diameter NMR tube and thermally equilibrated at 40°C for 1 h before measurements were taken. The transverse relaxation time (T_2) was measured using a Carr Purcell Meiboom Gill (CPMG) pulse sequence with the following parameters: TE = 0.5 ms, 900 echoes, 8 scans, and TR = 1.5 s. The single-sided MR sensor was retrofitted with a programmable motion stage and 96-well plate holder. Single-sided MR samples were directly pipetted and mixed in the wells of a 96-well plate at room temperature and were read automatically in sequence. Measurements were obtained within one minute after mixing or at the specified times for T_2 kinetic experiments. Transverse relaxation times for the single-sided MR ($T_{2,eff}$) were measured using a CPMG sequence with the following parameters: TE = 0.035 ms, 2143 echoes, 20 scans, and TR = 1.25 s. The echo peak

intensities were fit to the equation $I = I_0 e^{-t/T_2}$ using a custom script running on MATLAB (The Mathworks, Natick, MA). T_2 or $T_{2,eff}$ were plotted as measured and are within 0.1 ms and 0.5 ms respectively for most the reported values with 95% confidence.

5.3.4 Dynamic Light Scattering

Particle sizes were determined using a 90 Plus Particle Size Analyzer (Brookhaven Instrument Corporation, Holtsville, NY). Samples were measured at 37°C in PBS, λ = 658 nm, 90° fixed angle. CLIO and analyte solutions were separately equilibrated to 37°C before being mixed in the instrument chamber for particle size kinetic experiments. The log-normal intensity-weighted effective diameter was reported. Population distribution was determined by peak integration of the volume-weighted scattering intensity.

5.4 Results

5.4.1 CLIO-IgG + Protein A Aggregation, T_2 and Particle Size Kinetics

CLIO-IgG was used as a simple model system to assess the conjugation scheme and aggregate formation without the need for a matched pair of antibodies to two nonoverlapping epitopes on the analyte. CLIO-IgG were mixed with increasing concentration of PA from 0.1 to 8 μg/mL. The T_2 relaxation time of a CLIO-IgG + PBS control was 93.4 ms. The T_2 of CLIO-IgG with PA solutions all exhibited lower values compared with the control. Concentrations between 0.1 and 2 μg/mL correlate with the dynamic concentration range of CLIO-IgG for the given CLIO concentration (Figure 5–1c). The largest T_2 change was seen at 2 μg/mL PA (20%).

Concentrations higher than 2 μg/mL PA did not show further T_2 decreases. The flattened response at the higher concentrations tested may be due to saturation of the CLIO-IgG. CLIO-IgG of a higher nanoparticle concentration resulted in the same trend with T_2 decreases up to 40% (data not shown).

A single PA concentration was selected for additional investigation by dynamic light scattering. The formation of aggregates was confirmed by measurements of the particle size (Table 5-1). The mean particle size of CLIO-IgG alone was 117 nm. PA solution alone showed no detectable particles by light scattering. Mixing CLIO-IgG and PA to a final PA concentration of 2 μg/mL produced two peaks. The major particle population with a size of 76.1 nm comprised 90% of the volume-weighted scattering efficiency, and the remainder of the population was 620 nm in size. Dynamic light scattering measurements support that the change in T_2 upon addition of PA solution was attributable to PA-induced aggregation of CLIO-IgG. The bimodal distribution formed at 2 minutes indicates that some particles reacted extensively to create large aggregates while the smaller 76.1 nm population may comprise single CLIO-IgG nanoparticles

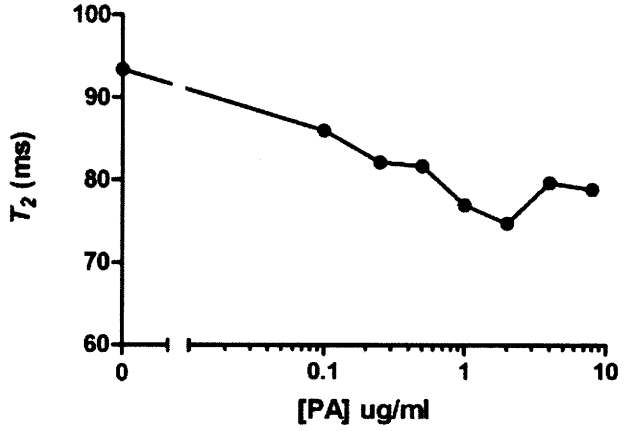

Figure 5–1. a) CLIO-IgG were incubated with increasing concentrations of protein A. Aggregation of CLIO-IgG is indicated by the decrease in T_2. The data are plotted as average ± standard deviation (n=4). All concentrations refer to final concentrations after incubation.

or CLIO-IgG:PA complexes. The time for temperature equilibration on the HFMR precludes rapid T_2 measurements; however, unequilibrated measurements of room-temperature samples suggest that T_2 is sensitive to the formation of small populations of aggregates as quickly as it can be measured. This further implies that the small aggregates formed in the initial minutes contribute to the majority of the T_2 changes.

The smaller clusters formed at 2 minutes combined into larger aggregates such that nearly half of the particles were in an aggregate at 24 h (Table 5-1). These aggregates were stable for up to 5 days at room temperature as confirmed by particle size measurements and HFMR. T_2 values varied from the initial T_2 drop by 6% for the 2 μg/mL PA concentration over this 5 day period. A variation in T_2 of 6-12% was observed for all other PA samples. This drift in T_2 over time was further examined with the C95-X/C97-X system (Section 5.4.7) using the single-sided MR that does not require temperature equilibration. Additional aggregate growth kinetics was also further investigated with the C95-X/C97-X system (Section 5.4.9).

The conjugation was performed with N-succinimidyl-S-acetylthioacetate (SATA) reagent (Section 4.3.1). SATA is not a site-specific coupling agent and has the potential to interfere with some antibody functionality, but the formation of PA-induced aggregates confirms that sufficient antibody functionality is retained with this conjugation reaction. Higher antibody functionality may be achieved with site-specific coupling such as mercaptoethylamine, which directs modification away from the antibody binding region. PA-induced aggregation of CLIO-IgG indicates that the conjugation scheme can produce a single component CLIO reagent which is suitable in an MRSw assay with a multivalent analyte.

Table 5-1. Particle Size Measurements of CLIO-IgG + Protein A[a]. Reproduced with permission from [15]. Copyright 2007 American Chemical Society.

	Population 1		Population 2	
Time	Size (nm)	percent of sample	size (nm)	percent of sample
No analyte	52.3	100	--	--
2 min	76.1	89.7	619.8	10.3
1 day	97.9	58.7	375.5	41.3
5 days	63.4	55.1	551.9	44.9

[a] Particle size analysis of CLIO-IgG upon addition of protein A (final concentration 2 μg/ml).

Population distribution was determined by peak integration of the volume-weighted scattering intensity. No particles were detected in PA solution alone.

5.4.2 CLIO-95/CLIO-97 Aggregation requires both CLIO-95 and CLIO-97

A matched pair of monoclonal antibodies was conjugated to CLIO to create an ELISA-like sandwich assay in solution form. CLIO-95/CLIO-97 (C95/C97) blends were mixed with PBS or hCG (Figure 5–1). T_2 dropped in the solution containing hCG as compared to PBS. Furthermore, hCG added to C95 alone or C97 alone did not cause a change in T_2 from the respective PBS control (Figure 5–1), supporting the hypothesis that both antibody-conjugated nanoparticles are required to form a "sandwich," which created aggregates upon additional binding (Figure 5–1a). Control solutions (C95 or C97 alone) contained dispersed nanoparticles as confirmed by dynamic light scattering (DLS). The addition of analyte to C95 or C97 can produce analyte:antibody-CLIO complexes, but this is not sufficient to induce a measurable T_2 change. MRS assays require agglomeration of at least two CLIO for "switching" of this sensor. The T_2 and particle size changes indicate that the conjugation scheme can produce a sandwich-type two component CLIO reagent. Similar results were observed with hCG-β (data not shown).

The monoclonal antibodies used here form a sandwich with hCG or hCG-β and subsequently form CLIO aggregates.

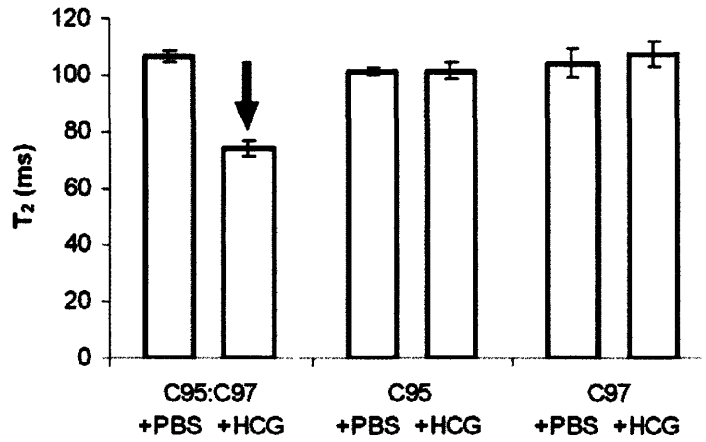

Figure 5–1. C95:C97 solutions were incubated with PBS or hCG. A T_2 decrease is observed with the addition of hCG to C95:C97. Both C95 and C97 are required for hCG induced T_2 changes. Similar results are observed with hCG-β. Data are plotted as the average +/- standard deviation of three determinations. Reproduced in part with permission from [15]. Copyright 2007 American Chemical Society.

5.4.3 Dissociation of CLIO-95/CLIO-97 in large hCG excess

The reversibility of C95/C97 aggregation was studied. MRSw aggregation was hypothesized to be reversible as governed by dissociation constant of the antibody (K_d). An excess of hCG at concentrations far above the K_d, which was 0.5 and 1.0 nM for these antibodies, would cause the aggregates to dissociate as all the antibodies become saturated with hCG and very few hCG form crosslinks (Figure 5–1d). Relaxation time is sensitive to both the state of aggregation and the iron concentration of the CLIO nanoparticles. Measurements must be compared to a control value of the same iron concentration in order to attribute T_2 changes to the aggregation state. The addition of hCG to C95/C97 resulted in aggregation induced T_2 reductions compared to the addition of PBS (Figure 5–1). The T_2 relaxation time of an equal

blend of C95 and C97 was 110.1 ms in the absence of hCG and dropped to 79.8 ms when hCG was added (8 μg/ml Fe, 13.5 nM hCG, final concentration).

PBS or a concentrated hCG solution was added to the aggregated solution (Figure 5–1). The addition of PBS to the aggregated solution did not cause dissociation, but the T_2 increases due to dilution of the nanoparticles. The addition of concentrated hCG solution (4 μg/ml Fe, 919 nM, final concentration) resulted in a higher T_2 than when PBS is added to the aggregated solution. The difference in T_2 can be attributed to dissociation of some aggregates. The reversibility of this sensor may be further explored using a semi-permeable membrane system, such as a dialysis cassette, if proper reference values are available. As volumetric fluctuations are often observed in dialysis, T_2 changes due to iron concentration would need to be carefully isolated from that induced by aggregation. Presumably, this system is reversible as governed by antibody-antigen binding kinetics, and in a fixed volume device, the T_2 would reflect the dynamically aggregating and dissociating CLIO in response to the hCG concentration in the local environment. MRSw with low avidity (both low valency and, more importantly, antibodies with favorable K_d) may be investigated for reversible MRSw sensing.

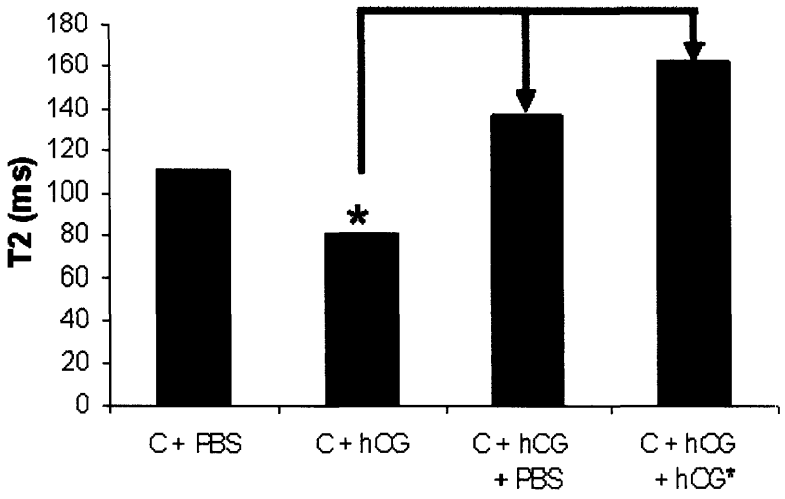

Figure 5–1. Large excess of hCG induces dissociation and concomitant T_2 change. PBS or a concentrated hCG solution was added to the aggregated solution (*). Addition of PBS caused a rise in T_2 due to dilution of the CLIO. The addition of a concentrated hCG solution resulted in a larger rise in T_2. The difference is attributed to dissociation of the aggregates (*).

5.4.4 Ratio of CLIO-95:CLIO-97

The stoichiometric relationship among the two populations of functionalized CLIO (C95, C97) and the hCG crosslinker was explored by varying the relative ratios of antibodies. The total number of antibodies in a CLIO solution is described by the following:

$$n_{TOT} = n_{95} + n_{97} = V_{C95} * C_{C95} = V_{C97} * C_{C97}$$

where n is the number of antibodies, V is the valency or number of antibodies per particle, and C is the concentration of particles. It was hypothesized that a scarcity of one of the matched pairs of antibody hinders aggregation formation when the total amount of CLIO was fixed. An extreme example of this would be the case where the CLIO are all C95 or C97 as demonstrated in Section 5.4.2. The valencies of C95 and C97 are not matched (Table 4-1), and it was hypothesized that the largest change in T_2 would occur when an equal number of 95 and 97 antibodies were present, i.e., $n_{95} = n_{97}$.

This condition was calculated to be true when the CLIO blend contains 0.7 C97 per C95 nanoparticle. The relative concentration of C97 to C95 was varied while keeping the total iron concentration fixed at 8 μg/ml. Final analyte concentrations were 5 μg/ml for both hCG and hCG-β. The percent T_2 change was found to vary with relative ratios of antibody with the most pronounced change in T_2 found when there was less C97 compared to C95 (Figure 5–1). This is in agreement with our calculation as C97 has a greater valency than C95.

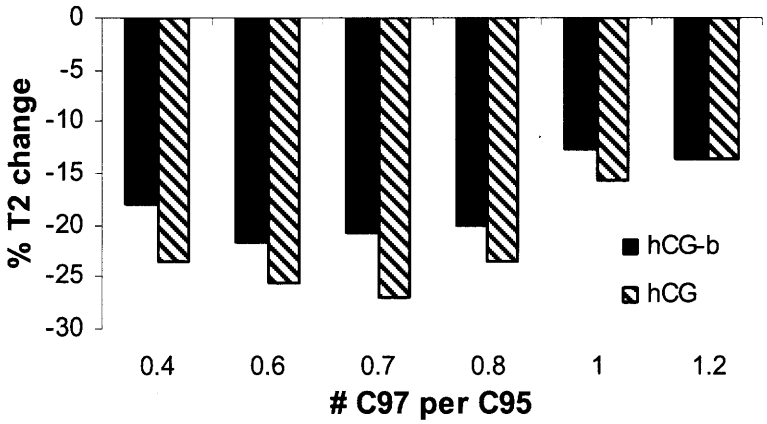

Figure 5–1. Stoichiometric dependence of aggregation. An optimum T_2 change is exhibited with the ratio of C95 to C97 is adjusted to match the total number of antibodies of each conjugate.

5.4.5 Comparison of Low and High Valency CLIO; hCG-β and hCG Analytes

A larger concentration range was studied to estimate the dynamic range of this MRSw assay. Responses to both the hCG-β subunit and hCG dimer were evaluated with a 50/50 C95/C97 blend (Figure 5–1a,b). Concentrations are reported in the unit of equivalents (or molecules of analyte per CLIO) using the theoretical molecular weight and the CLIO concentration to facilitate a stoichiometric comparison between hCG-β and hCG. This conversion facilitates the comparison between hCG and hCG-β and interpretation of the stoichiometric nature of this sensor. The T_2 of the C95/C97 + PBS control was 92.7 ms (Figure 5–1a). The T_2 varied inversely with the amount of hCG-β, with the largest decrease observed at 2.5 equivalents per CLIO (T_2 = 74.9 ms, 19% decrease). These aggregates were stable over 6 days at room temperature as measured by HFRM (data not shown). A change in T_2 was found with the addition of either hCG-β subunit or hCG heterodimer. The sensitivity was higher with the heterodimer, but both analytes showed a flattened response at analyte concentrations higher than 1 equivalent (Figure 5–1a,b). The more significant response to equivalent numbers of hCG molecules as compared with hCG-β may be due to stronger avidity and cooperative binding of the antibodies to the hCG molecule over hCG-β alone.

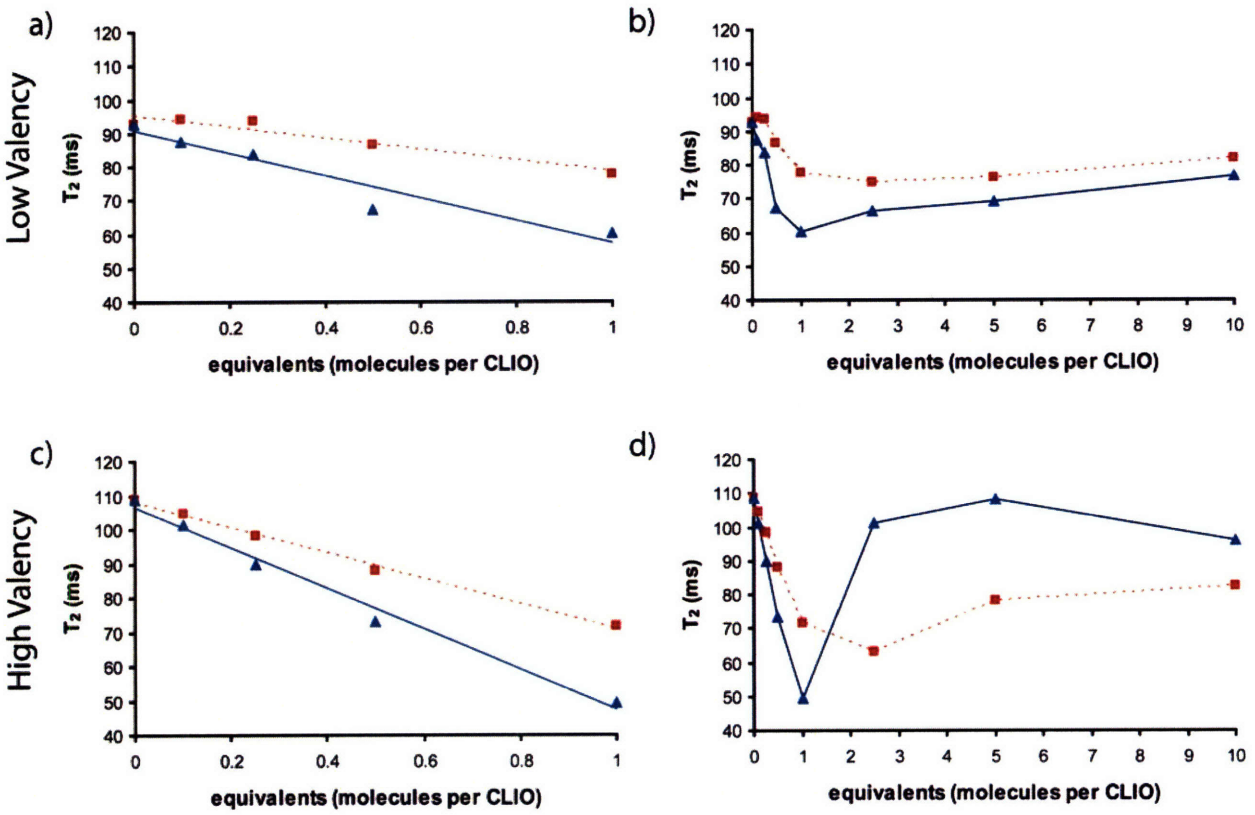

Figure 5–1. Comparison of Low and High Valency CLIO reagent. a) Low valency C95/C97 CLIO reagent and b) high valency C95-2/C97-2 CLIO reagent were incubated with hCG-β (■) and hCG dimer (▲). T_2 varies linearly with analyte concentration between 0.1 and 1 molecules of analyte per CLIO nanoparticle; inset shows the wider concentration range for a) lower valency C95:C97 blend and b) higher valency C95-2:C97-2. Both show enhanced T_2 decreases with hCG compared to hCG-β. The higher valency C95-2:C97-2 particles are more sensitive to analyte; however, instabilities at the higher analyte regime becomes more pronounced with additional incubation time. Reproduced in part with permission from [15]. Copyright 2007 American Chemical Society.

The limit of detection (LOD) was 0.5 equivalents hCG-β and 0.1 equivalents of hCG for C95/C97 as defined by the concentration where the standard deviation does not overlap with the standard deviation of the PBS control. The limit of detection is an order of magnitude greater than the K_d of the antibody (0.1 nM). Thus, the sensitivity of this stoichiometric sensor at the given CLIO concentrations is not limited by the dissociation constant of the antibody. Sensitivity can be enhanced by using a lower CLIO concentration, as fewer total analyte molecules are needed to induce a T_2 change.

Aggregation behavior with the second, higher-valency CLIO blend (C95-2/C97-2) was compared to the initial lot of lower valency C95/C97 (Figure 5–1c,d). Similar trends were observed in both lots. The linear dynamic concentration range was the same, with the largest T_2 changes for both of the C95-2/C97-2 and C95/ C97 lots observed at 2.5 molecules of hCG-β per CLIO and 1 molecule of hCG per CLIO. The magnitude of changes in T_2 was larger with hCG over that observed for hCG-β. The response was steeper for the higher valency blend and may lead to higher sensitivity at the lower concentrations. The LOD is 0.1 equivalents or better, since 0.1 equivalents is the lowest concentration tested in this experiment. A decrease in T_2 was, however, not observed at the higher hCG analyte concentrations (2.5, 5, and 10 analyte molecules per CLIO) with C95-2/C97-2. Repeated measurements of these samples yielded a T_2 that was rapidly changing, and in certain cases, a precipitate could be seen to settle overnight. These were studied in detail elsewhere (Section 5.4.10). These data are in agreement with a recent study that found the largest stable T_2 change at approximately 1.2 equiv of avidin per biotin-functionalized nanoparticle.[6] Unstable measurements with coefficients of variation above 2% were seen when larger equivalents of avidin were added.

It has been predicted that increasing number of functional groups would decrease the time constant for aggregation.[16] This effect was not observed in the employed incubation time, and higher valency, in fact, may be a disadvantage, especially in the higher analyte regime, wherein a greater degree of aggregation may occur. These larger valency particles may form much larger networks, which are prone to insolubility and precipitation. The addition of approximately one antibody more per CLIO has a dramatic effect on aggregation kinetics at these experimental conditions. Thus, a high T_2 may occur when CLIO precipitate in the presence of high analyte concentrations or also when antigen excess results in the formation of

antigen:antibody-CLIO complexes without crosslinking (Figure 5–1d). Thus, it seems that solution stable CLIO agglutination is subject to an upper limit of approximately 1 equiv of analyte per nanoparticle and that higher valency may have higher sensitivity, but lower valency particles are preferred for stability.

5.4.6 Single-sided MR as a Suitable Alternative to Homogenous Field Relaxometer

The homogeneous field magnetic relaxometer (HFMR) is a standard instrument for determining relaxation time. The HFMR is amenable to low sample numbers due to the single serial sample port and the need for thermal equilibration of samples, but a large standard plate assay with calibration standards and multiple unknown samples would benefit from automated sample handling, ideally, in a industry-standard format such as a 96-well or 384-well microplate. Custom instruments, such as one featuring a microfabricated coil[17], a portable sensor[18], or a single-sided magnetic relaxometer (MR), allow these dilute nanoparticle solutions to be measured with more compact instrumentation in small volumes for higher throughput screening and research purposes than is possible with conventional methods. The large number of samples motivated the use of a custom-built high-throughput single-sided magnetic relaxometer (single-sided MR) fitted with a programmable sample stage. Thus, measurements from the homogeneous field relaxometer were compared to those from the single-sided MR to validate the single-sided MR as a suitable alternative.

The addition of hCG to the C95-2/C97-2 CLIO reagent resulted in an aggregation-induced decrease in T_2 compared to a blank PBS control as reported previously [15] (Figure 5–1). It should be noted that the concentrations hereon will be reported in μg/ml, a more commonly reported format since the stoichiometric relationship of MRSw aggregation has already been

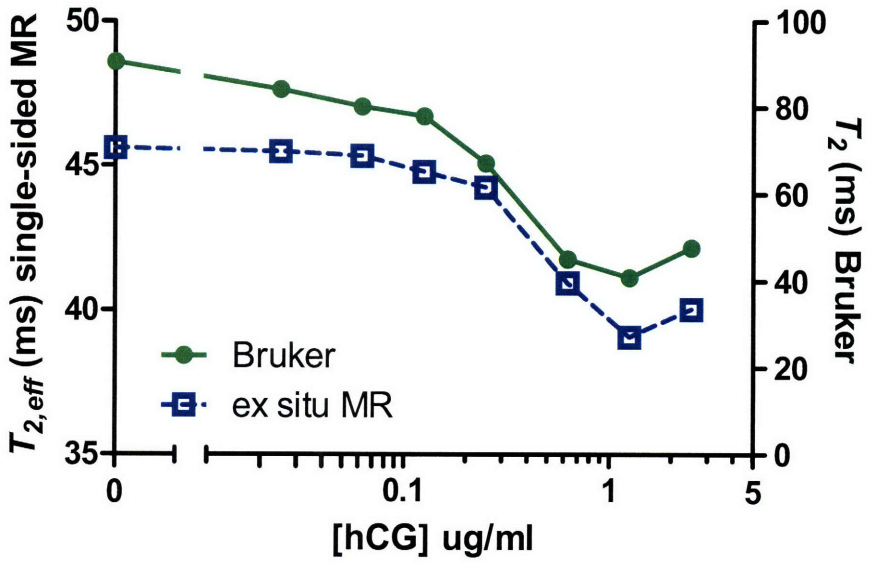

Figure 5–1. T_2 response from HFRM are compared to $T_{2,eff}$ from single-sided MR. T_2 and $T_{2,eff}$ exhibit similar trends with different magnitudes due to the drastically different magnetic field homogeneities.

established. The measurements on both instruments follow the same trend and thus the single-sided MR can be used to rapidly measure MRSw samples in a plate format.

Transverse relaxation times measured on the single-sided MR are lower in general than T_2 measured on the HFMR. The amount by which the value is reduced is dependent upon the field gradient, the pulse sequence parameters, the T_1 , and the T_2 of the sample[19]. The measured time constant is thus reported as an effective T_2 ($T_{2,eff}$). Samples for the HFMR are prepared in a microcentrifuge tube to ensure adequate mixing before being transferred to a NMR tube for measurement. Samples are then manually introduced into the single measurement port and measured serially. Samples for the single-sided MR, in contrast, are prepared directly in the wells of a 96-well plate and sample handling is automated thereafter. The single-sided MR, thus, is a more convenient alternative to the HFMR.

5.4.7 *Buffer Compatibility and Specificity of CLIO95-2/CLIO97-2*

The compatibility of the MRSw-based assay with colored, turbid, or protein-rich samples was tested using the single-sided MR. The buffers investigated were PBS, artificial urine solution (Surine®), cell culture media, cell culture media + 10% fetal bovine serum (10% FBS), and fetal bovine serum (100% FBS). The buffers were prepared with increasing concentrations of hCG, mixed with C95-2/C97-2 by pipetting in the well, and read on the single-sided MR (Figure 5–1a). No significant functional differences were observed among the various buffers. The versatility of MRSw-based assay was further tested using cell culture supernatants. Cell culture supernatants were tested as is without centrifugation, washes, or other processing to remove phenol red or other interferences. Conditioned media from different cell lines secreting hCG were assayed using the CLIO reagent. The media was aspirated from the cell culture plate and directly mixed with the CLIO reagent. The T_2 response was found to correlate with duration of conditioning. Conditioned media contains many secreted cell products and cell debris, but these were found not to interfere significantly with the MRSw.

MRSw specificity was tested using homologous proteins. HCG shares similar structure with follicle-stimulating hormone (FSH), luteinizing hormone (LH) and thyroid hormone (TH). The monoclonal antibody used was reported by the manufacturer to have no cross-reactivity with these hormones. The CLIO reagent was tested to see if specificity was preserved after conjugation to CLIO. Solutions of FSH, LH, and TH were mixed with C95-2/C97-2 (Figure 5–2). No T_2 changes were seen with these analytes. Only hCG containing solutions showed a T_2 change. This MRSw-based assay was thus shown to be compatible with these biological solutions without interference from colored solutions or other proteins.

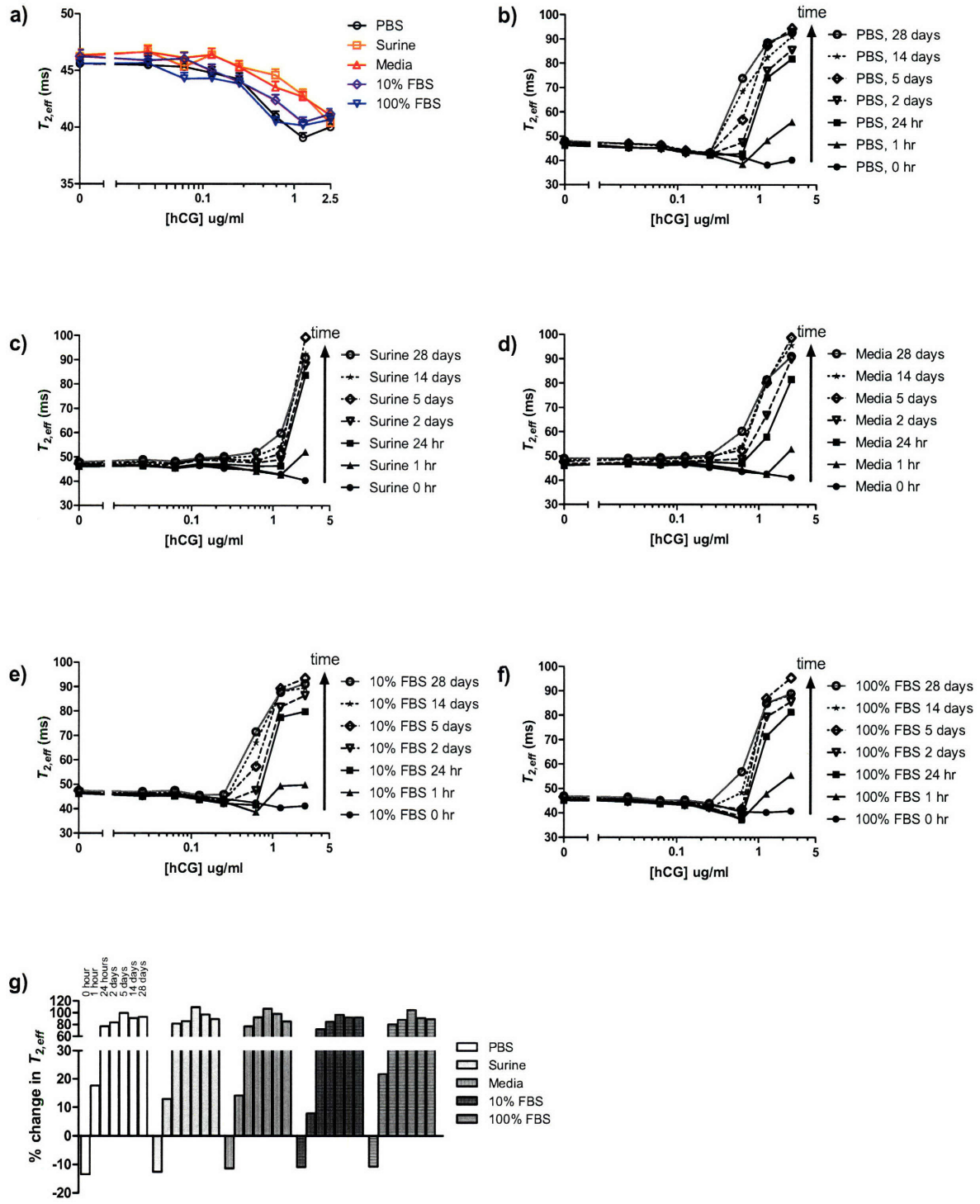

Figure 5–1. $T_{2,\text{eff}}$ of hCG using fluid C95-2/C97-2 CLIO reagent in various physiologic buffers. a) Immediately after mixing (0 hr), C95-2/C97-2 CLIO reagent performs comparably in all buffers tested (○ PBS, □ Surine, △ Media, ◇ 10% FBS, ▽100% FBS). b-f) Repeat measurements of CLIO reagent at the indicated timepoints up to 28 days later show that the $T_{2,\text{eff}}$ drifts up over time, especially in the higher hCG concentrations in b)

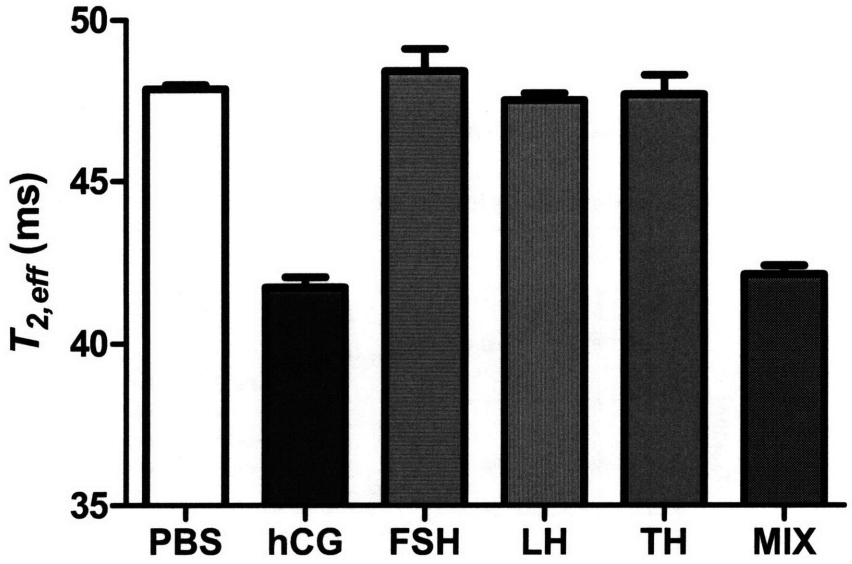

Figure 5–2. The specificity of the CLIO reagent. $T_{2,eff}$ changes with hCG but not FSH, LH, or TH (all 1 μg/ml final concentration), showing that there no cross-reactivity with these analytes. Furthermore, the $T_{2,eff}$ of CLIO reagent is comparable when hCG is prepared in PBS or in a mixture of FSH, LH, and TH (MIX).

PBS, c) Surine, d) Media, e) 10% FBS, and f) 100% FBS. g) The highest concentration tested, 2.5 μg/ml, shows the most drift in $T_{2,eff}$ in all the buffers tested.

5.4.8 Effect of CLIO Concentration on Sensitivity and Dynamic Range

The effect of CLIO concentration on MRSw sensitivity and dynamic range were investigated. It was hypothesized that since the MRSw relies on stoichiometric reaction between the analyte and the CLIO, a lower CLIO concentration may yield a more sensitive assay. Four concentrations of CLIO were investigated (2, 4, 8, and 16 μg/ml Fe) with increasing concentrations of hCG (Figure 5–1). The concentration profiles show markedly different $T_{2,eff}$ as $T_{2,eff}$ has a strong dependence on the CLIO concentration (Figure 5–1a). The higher CLIO concentrations show a lower $T_{2,eff}$ overall as there are more nanoparticles to dephase the protons in solution. The data were also plotted as $\Delta T_{2,eff}$, the difference from the control sample (Figure 5–1b). Higher CLIO concentrations require more HCG to cause aggregation and a $T_{2,eff}$ change

in the ensemble. Lower CLIO concentrations may be used if more sensitivity is required to lower analyte concentrations. Nontrivial gains can be made the LOD by adjusting the CLIO concentration. Measurement parameters (Section 5.3.3) may be adjusted accordingly to accurately obtain high $T_{2,eff}$ and may result in longer acquisition times.

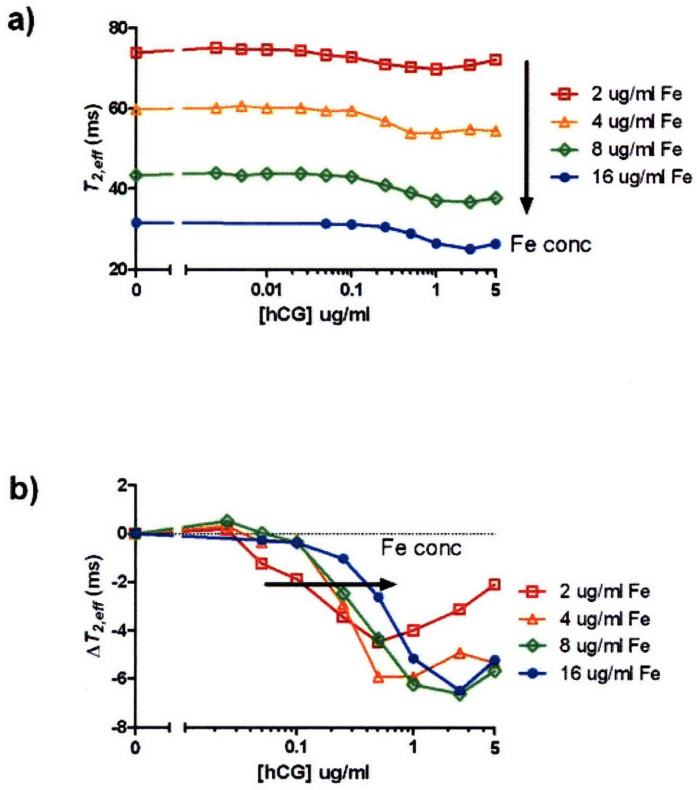

Figure 5–1. CLIO concentration affects the sensitivity and dynamic range. a) $T_{2,eff}$ has a strong dependence on the CLIO concentration. b) The effect of CLIO C95-2/C97-2 concentration on the concentrations profiles is clearer when plotted as $\Delta T_{2,eff}$. Lower CLIO concentrations show increased sensitivity. Higher CLIO concentrations require more HCG to cause a $T_{2,eff}$ change in the solution.

5.4.9 T_2 Kinetics of High Valency CLIO-95-2/CLIO-97-2

T_2 measurements of C95-2/C97-2 were followed over time in the various biological buffers (Figure 5–1b-f). The samples showed a concentration dependent response only with immediate measurement. Measurement after longer times did not show concentration dependence. Some samples showing an initial $T_{2,eff}$ decrease with respect to controls, for

example, were found to have an elevated $T_{2,eff}$ from the initial value 1 hour after mixing. This drift was particularly dramatic at the higher concentrations of hCG. The highest concentration tested, 2.5 μg/ml hCG, showed the largest elevations in $T_{2,eff}$ (Figure 5–1), but the drift behavior was also observed at 1.25 μg/ml and 0.5 μg/ml hCG. This observation was consistent in all the buffers (Figure 5–1b-f). These extremely high $T_{2,eff}$ reflect that few nanoparticles remain in solution. The nanoparticle aggregates grow to become insoluble and precipitate (Section 5.4.10); thus, they no longer contribute to the magnetic susceptibility of the solution and the $T_{2,eff}$ rises.[15] This instability can lead to erroneous measurements or false negatives if the samples are not read immediately. Thus, the reliability of this assay has been compromised by the uncontrolled aggregation. Some solutions reported to be stable in Kim et al.[15] when replicated on the single-sided MR were found to have drifting $T_{2,eff}$. The magnetic field gradient on the single-sided MR applies a downward force on the particles, and this force is believed to accelerate or accentuate any precipitation and results in increased measurement instability on the single-sided MR compared to the HFMR.

5.4.10 Particle Size Kinetics

The kinetics of aggregation were examined by particle size analysis to track the progress of the aggregation reaction (Figure 5–1). A secondary goal was to investigation a possible mechanism for unstable T_2 measurements (Section 5.4.9). It has been suggested that the aggregates are of a fractal nature[16], whereas dynamic light scattering assumes a hard-sphere hydrodynamic model. Nevertheless, the effective diameter produces a convenient, single value which represents relative changes in the entire particle population. The effective diameter for the low valency C95/C97 and the high valency C95-2/C97-2 CLIO are initially between 100-140 nm

and are stable (Figure 5–1a,b). The addition of hCG (final concentration, 1 μg/ml) causes the effective diameter in the low valency CLIO to rise modestly and plateaus below 200 nm in size for all hCG concentrations tested. The same analyte concentration, however, causes the effective diameter of the high valency CLIO to increase dramatically. The effective diameter was approximately 140 nm for the unaggregated C95-2/C97-2 particles and increased with the addition of hCG to form micron-sized aggregates (Figure 5–1b). The rate of effective diameter increase is related to the analyte concentration (Figure 5–1c). The initial rates of increase were 17 ± 1 nm/hr and 21 ± 1 nm/hr for 0.5 and 2.5 μg/ml hCG, respectively. The effective diameter of the aggregates reached 1 μm in 2 hours for 0.5 μg/ml sample. That size was reached even sooner for 2.5 μg/ml sample. Particle size measurements by dynamic light scattering at that size are imprecise due to the heterogeneous population of aggregates formed and the settling of precipitates. Nevertheless, they do indicate that particles are aggregating, forming very large aggregates in cases. Indeed, precipitates can be observed by eye at the bottom of high CLIO concentration samples. Measurements of these settled solutions show that the autocorrelation function has difficulty establishing a baseline and no particles are detected. Micrometer-sized particles are again reported upon resuspension of the particles by mixing. Particle size analysis supports the stable T_2 measurements that were made with CLIO-IgG and C95/C97 days later and the rapidly changing measurements made with the higher valency C95-2/C97-2.

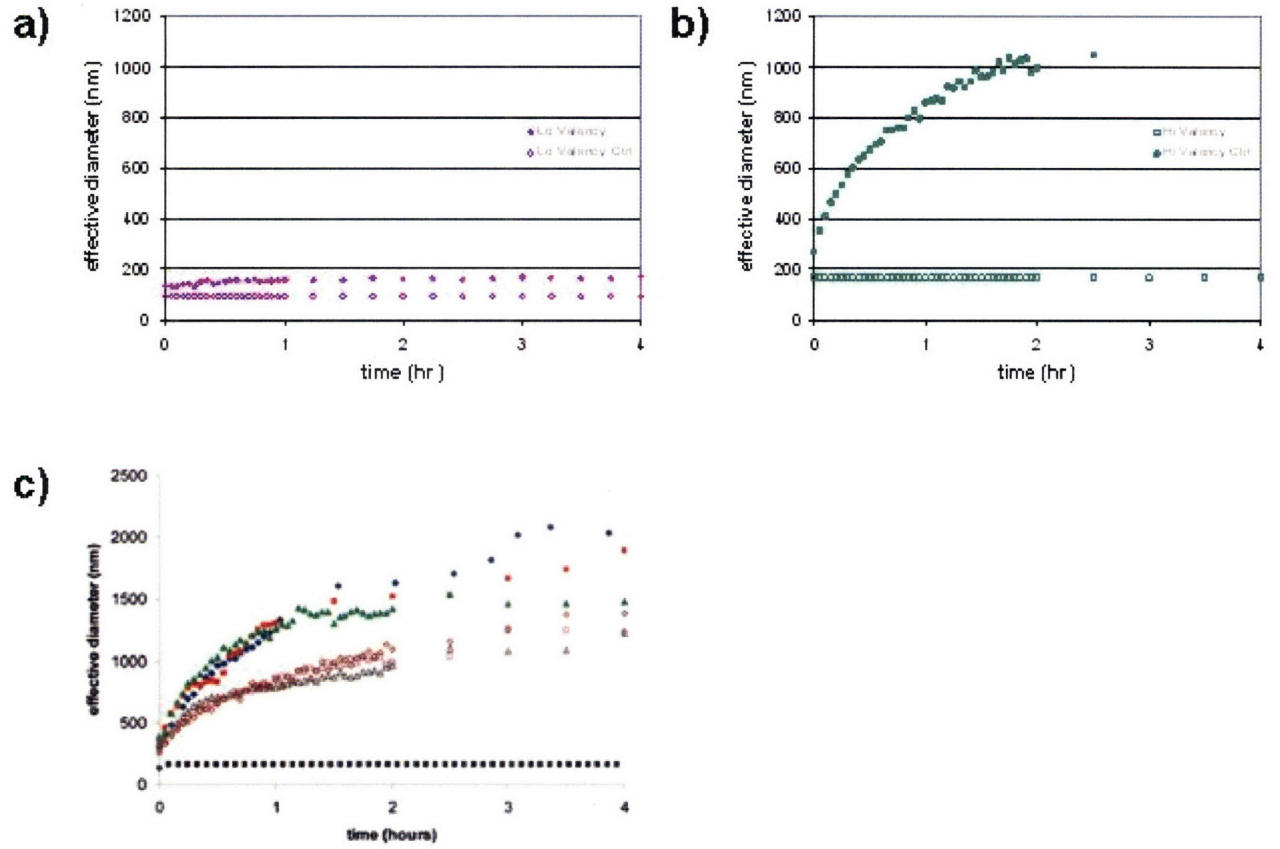

Figure 5–1. Particle size increases during aggregation. Particle size data for a) low C95/C97 and b) high C95-2/C97-2 valency CLIO. Both control samples (open symbols, no hCG) are stable in size. The addition of hCG (1 µg/ml) to the low valency particles forms modest clusters under 200 nm in size whereas the high valency particles results in the formation of micron-sized aggregates in hours. c) The size of the aggregates formed varies with analyte concentration. Effective diameter of the C95-2:C97-2 aggregates formed in 0.5 µg/ml hCG (open symbols, ◊ □ Δ) and 2.5 µg/ml hCG (solid symbols, ♦ ■ ▲). Triplicate data are shown. Unaggregated particles show no change in size (dotted line). Particle aggregation kinetics as measured by dynamic light scattering. Reproduced in part from [15]. Copyright 2007 American Chemical Society.

5.5 Conclusion

Antibodies were conjugated to CLIO using standard peptide chemistry. The MRSw assay was then tested by measuring T_2 change by magnetic relaxometry and aggregate formation by dynamic light scattering. The conjugation scheme was found to successfully generate a one and two component CLIO reagent. A stoichiometric dependence of analyte-induced T_2 changes was observed. The presence of hCG caused the CLIO to aggregate as measured by a decrease in T_2

compared to a blank control. The aggregates were made to dissociate by introducing a large excess of analyte. The most pronounced change in T_2 was observed when the number of 95 and 97 antibodies was equalized. The size of the particles increased with the addition of analyte, independently confirming that aggregation was occurring.

Higher valency CLIO showed better sensitivity but at the expense of stability. Particle size measurements also suggest that control of aggregate size will be important in enhancing the dynamic range and stability of this type of assay. CLIO solutions showed a concentration dependent response only with immediate measurement. Analytical methods require stable samples for the duration of the measurement. Current operating parameters on the single-sided MR require a 30 minute acquisition time for an entire 96-well plate. This acquisition time may be reduced with instrument optimizations or relaxing accuracy requirements; however, the CLIO assay remains sensitive to incubation time (time between mixing reagents and reading) due to the fast reaction time and uncontrolled growth of aggregates.

Problems at high analyte concentrations are not unique to MRSw-based assays. Other agglutination-based assays are subject to the prozone effect when analyte excess results in the formation of analyte:antibody-particle complexes without crosslinking (Figure 5–1d). The prozone effect or high-dose hook effect is also seen in other agglutination-based assays[20, 21]. It is of particular concern for false-negative assay results in personal and public health concerns such as syphilis and HIV/AIDS testing[22, 23]. Measurements are typically repeated with a one-tenth dilution when a false negative is suspected to obtain concentrations within the dynamic range of the assay[24]. This technique, however, is not feasible for all applications.

Solution-based magnetic aggregation measurements have an additional limitation due to precipitation. Higher-valency particles produced more pronounced changes in T_2 and have been

predicted to aggregate faster[16]. Higher valency may also be a disadvantage, especially in the higher analyte regime, wherein a greater degree of aggregation may form much larger networks that are prone to insolubility and precipitation. It is interesting that the addition of approximately one antibody more per CLIO has a dramatic effect on aggregation kinetics under these experimental conditions. Thus, both the prozone and insolubility effects may be occurring above the one analyte per nanoparticle ratio to various extents depending on the nanoparticle (size, density, and valency), extent of analyte excess, K_d, and kinetics of aggregate growth. Stabilization of nanoparticle aggregates and control of aggregate growth in favor of nucleation of smaller aggregates will be important to the further development of these types of assays.

This one-pot sensor system has the advantages of being able to work with an opaque sample with a single mixing step at the expense of the sensitivity that can be obtained by ELISA. This may be useful in instances where fast or sequential measurements are required. Additional applications may exploit the reversible nature of antibody/analyte binding by removal of analyte, such as through a dialysis membrane[7]. Thus, the same nanoparticle solution can be used for continuous measurements if a fixed volume container is used to achieve a constant nanoparticle concentration. The stability of the MRSw, however, is a key area that needs to be addressed.

5.6 References

1. Daniel, K. D., Kim, G. Y., Vassiliou, C. C., Galindo, M., Guimaraes, A., Weissleder, R., Charest, A., Langer, R., and Cima, M. J. Implantable Diagnostic Device for Cancer Monitoring. (Submitted).
2. Hooker, J. M., Datta, A., Botta, M., Raymond, K. N., and Francis, M. B. Magnetic resonance contrast agents from viral capsid shells: a comparison of exterior and interior cargo strategies. *Nano Lett, 7:* 2207-2210, 2007.
3. Weissleder, R. Molecular imaging in cancer. *Science, 312:* 1168-1171, 2006.
4. Montet, X., Montet-Abou, K., Reynolds, F., Weissleder, R., and Josephson, L. Nanoparticle imaging of integrins on tumor cells. *Neoplasia, 8:* 214-222, 2006.
5. Montet, X., Funovics, M., Montet-Abou, K., Weissleder, R., and Josephson, L. Multivalent effects of RGD peptides obtained by nanoparticle display. *Journal of Medicinal Chemistry, 49:* 6087-6093, 2006.
6. Taktak, S., Sosnovik, D., Cima, M. J., Weissleder, R., and Josephson, L. Multiparameter magnetic relaxation switch assays. *Anal Chem, 79:* 8863-8869, 2007.
7. Sun, E. Y., Weissleder, R., and Josephson, L. Continuous analyte sensing with magnetic nanoswitches. *Small, 2:* 1144-1147, 2006.
8. Yigit, M. V., Mazumdar, D., Kim, H. K., Lee, J. H., Dintsov, B., and Lu, Y. Smart "Turn-on" magnetic resonance contrast agents based on aptamer-functionalized superparamagnetic iron oxide nanoparticles. *ChemBioChem, 8:* 1675-1678, 2007.
9. Lowery, T. J., Palazzolo, R., Wong, S. M., Prado, P. J., and Taktak, S. Single-coil, multisample, proton relaxation method for magnetic relaxation switch assays. *Anal Chem, 80:* 1118-1123, 2008.
10. Osaka, T., Matsunaga, T., Nakanishi, T., Arakaki, A., Niwa, D., and Iida, H. Synthesis of magnetic nanoparticles and their application to bioassays. *Anal Bioanal Chem, 384:* 593-600, 2006.
11. Josephson, L., Lewis, J., Jacobs, P., Hahn, P. F., and Stark, D. D. The Effects of Iron-Oxides on Proton Relaxivity. *Magnetic Resonance Imaging, 6:* 647-653, 1988.
12. Hoermann, R., Gerbes, A. L., Spoettl, G., Jungst, D., and Mann, K. Immunoreactive human chorionic gonadotropin and its free beta subunit in serum and ascites of patients with malignant tumors. *Cancer Res, 52:* 1520-1524, 1992.
13. Grossmann, M., Hoermann, R., Gocze, P. M., Ott, M., Berger, P., and Mann, K. Measurement of human chorionic gonadotropin-related immunoreactivity in serum, ascites and tumour cysts of patients with gynaecologic malignancies. *Eur J Clin Invest, 25:* 867-873, 1995.
14. Costanzo, P. J., Patten, T. E., and Seery, T. A. Protein-Ligand Mediated Aggregation of Nanoparticles: A study of synthesis and assembly mechanism. *Chem Mater, 16:* 1775-1785, 2004.
15. Kim, G. Y., Josephson, L., Langer, R., and Cima, M. J. Magnetic relaxation switch detection of human chorionic gonadotrophin. *Bioconjug Chem, 18:* 2024-2028, 2007.
16. Shapiro, M. G., Atanasijevic, T., Faas, H., Westmeyer, G. G., and Jasanoff, A. Dynamic imaging with MRI contrast agents: quantitative considerations. *Magn Reson Imaging, 24:* 449-462, 2006.

17. Sillerud, L. O., McDowell, A. F., Adolphi, N. L., Serda, R. E., Adams, D. P., Vasile, M. J., and Alam, T. M. 1H NMR Detection of superparamagnetic nanoparticles at 1T using a microcoil and novel tuning circuit. *J Magn Reson, 181:* 181-190, 2006.
18. Perlo, J., Demas, V., Casanova, F., Meriles, C. A., Reimer, J., Pines, A., and Blumich, B. High-resolution NMR spectroscopy with a portable single-sided sensor. *Science, 308:* 1279, 2005.
19. Hurlimann, M. D. and Griffin, D. D. Spin dynamics of Carr-Purcell-Meiboom-Gill-like sequences in grossly inhomogeneous B-0 and B-1 fields and application to NMR well logging. *Journal of Magnetic Resonance, 143:* 120-135, 2000.
20. Bermes, E. W., Jr. and Isaacs, J. H. Evaluation of a direct agglutination latex particle test for human chorionic gonadotropin. *Am J Obstet Gynecol, 104:* 865-870, 1969.
21. Taborda, C. P., Rivera, J., Zaragoza, O., and Casadevall, A. More is not necessarily better: prozone-like effects in passive immunization with IgG. *J Immunol, 170:* 3621-3630, 2003.
22. Jnaoui, K., Lamarti, N., Paques, A. T., and Goubau, P. Prozone effect with the VIDAS HIV DUO Ultra assay. *J Clin Virol, 38:* 273-274, 2007.
23. Nnoruka, E. N. and Ezeoke, A. C. Evaluation of syphilis in patients with HIV infection in Nigeria. *Trop Med Int Health, 10:* 58-64, 2005.
24. Butch, A. W. Dilution protocols for detection of hook effects/prozone phenomenon. *Clinical Chemistry, 46:* 1719-1720, 2000.

CHAPTER 6

Matrix Stabilization of MRSw-based Assays

6.1 Summary

Superparamagnetic nanoparticle magnetic relaxation switches (MRSw) are being developed for aggregation-based diagnostic assays and *in vivo* detection of clinical conditions due to their simple mix-and-read methodology[1-4]. MRSw nanoparticles "switch" from dispersed to aggregated in the presence of an analyte, resulting in a change in the transverse relaxation time (T_2). Conditions that favor high sensitivity, however, cause uncontrolled formation of large aggregates, resulting in a limited dynamic range and spurious measurements. We present here a method for matrix stabilization of the MRSw that traps aggregates so that precipitation cannot

occur and produces stable MRSw measurements. This approach constitutes a significant step towards practical and reliable aggregation-based assays.

6.2 Introduction and Motivation

6.2.1 MRSw Instability

Biomedical applications rely on the colloidal stability of the nanoparticles at physiologic conditions, more specifically in an aqueous ionic solutions, neutral pH, and 37 °C[5]. Solution stability occurs when Brownian motion is sufficient to overcome gravitational forces. It depends on the particle size, charge, and surface chemistry. Recent work has identified some limitations of MRSw-based assays, which include a restricted dynamic range, uncontrolled aggregation, and erroneous T_2 measurements at high analyte concentrations[1, 6] (Section 5.4.9). All of these issues may be attributed to formation of aggregates that are unstable in solution and no longer produce a monotonically changing signal (Figure 6–1a-c). The instability appears to be the result of large aggregates no longer behaving as colloidal particles and beginning to settle under the influence of gravity. Aggregate size, for example, grows more rapidly with higher valency MRSw (Section 5.4.10). This is consistent with the formation of large networks as the underlying mechanism for the instability[6]. A recently reported multiparametric approach that successfully addresses drifting T_2 measurements requires reassaying the unstable sample with appropriate dilutions to be within the dynamic range of the assay[1]. This technique, however, is not always feasible for *in vitro* diagnostics and not possible for *in vivo* quantitation.

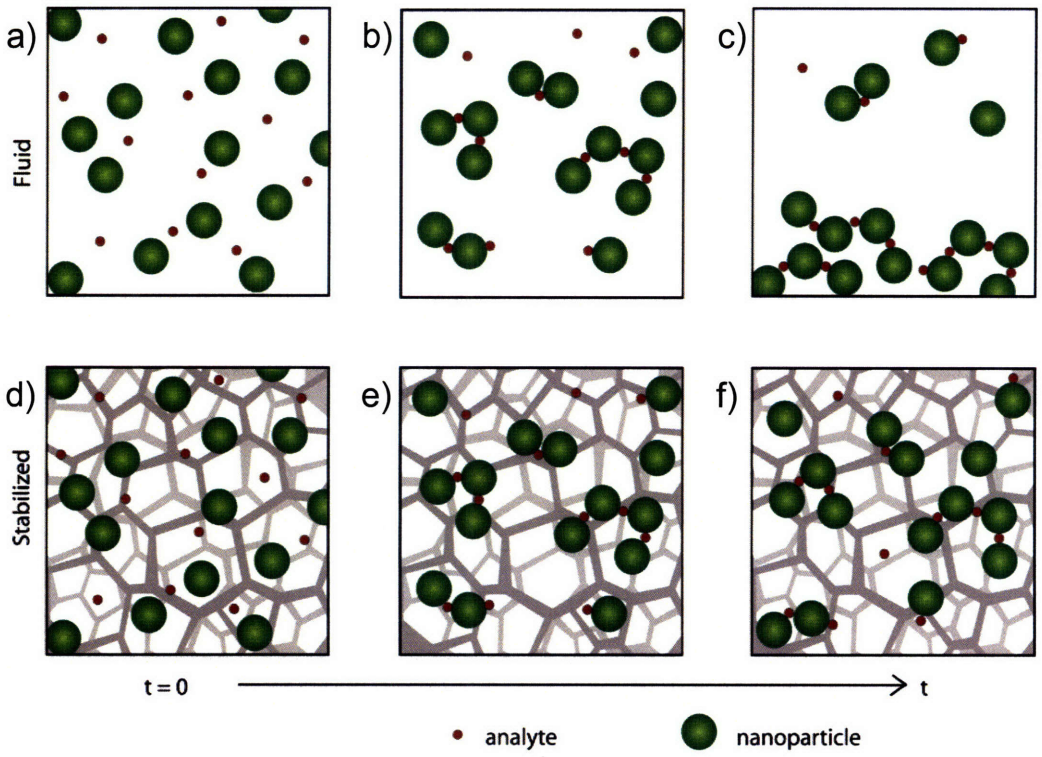

Figure 6–1. Schematic of aggregation-based assays. a) Aggregation-based assays involve mixing analytes with particles that have some specificity for the analyte through functional groups such as antibodies. b) Multivalency of the analyte or particle or both allows the particles to become crosslinked and aggregate. The degree of aggregation can be externally measured. MRSw show a change in T_2 which can be measured by MRI or magnetic relaxometer. c) Excess crosslinking can cause the particles to precipitate, preventing a stable measurement. d) A matrix can be used to stabilize the aggregates without significantly affecting the mobility of the unaggregated particle. e) The matrix controls the formation of particle aggregates and prevents precipitation. f) Stable measurements can be made.

6.2.2 Matrix Stabilization of Colloids

Control of aggregate formation is critical for further development of this technology. Matrix stabilization is an approach that is commonly used for colloids or particulates and involves modification of the matrix in which the particles reside.[7] The simplest case is to increase the viscosity of the matrix so that the time for aggregates to settle is long compared with the time of the measurements. A similar approach is to use a shear thinning matrix or a matrix with a yield stress. These methods mostly affect the behavior of the aggregates and minimize

impact on the motion of individual particles and analyte molecules. The stabilizing matrix allows unaggregated MRSw to diffuse but reduces the mobility of aggregates (Figure 6–1d). This matrix may also limit the aggregate size and hinder precipitation as clusters are trapped within the pores of the stabilizing matrix (Figure 6–1e). The net effect is to fix the particles in space and time, such that repeat measurements can be made (Figure 6–1f).

Matrix stabilization is preferred in this biological diagnostic application over approaches involving modification of surface chemistry or of the assay solution as the particle chemistry has already been optimized for magnetic properties, biocompatibility, and operation in physiologically compatible conditions. Hydrogels are just one material that can provide a matrix for the MRSw nanoparticles. The composition, pore size and density can be titrated to allow the appropriate level of mobility for the nanoparticles. Furthermore, hydrogels can be formed into a variety of shapes with either non-degradable or biodegradable chemistry depending on the application. Agarose is a common biocompatible hydrogel that is liquid-like at high temperature but physically crosslinked when cooled. A low gelling temperature agarose provides a longer working time over a wider temperature range. Other scaffold materials and structures may also be adapted for aggregate stabilization, such as an inverse opal morphology or micropatterned hydrogels[8-10]. Other additives and viscosity enhancers, such as alginate, PEG, and glass fibers, may also be beneficial. The matrix material should be compatible with a variety of physiologic buffers to extend the usage of aggregation-based assays for *in vitro* diagnostic testing and *in vivo* sensing.

Matrix stabilization is a technique that is used in the synthesis of iron oxide nanoparticles, but has not been extensively applied for assay applications. Particles are formed through a precipitation reaction within a cross-linked polymer network to prevent non-specific

aggregation and control particle size distribution [11]. Several applications do not require freely mobile single particles [12]. Nanoparticles for these applications are loaded within a larger polymeric particle to form composite materials for drug delivery or hyperthermia applications. Other notable applications of matrix stabilization involve immobilizing enzymes in a macroporous hydrogel. The enzymes were physical trapped within a PEG structure while still allowing access of the substrate through pores[8]. This technique resulted in higher rates of conversion than when the enzymes were not stabilized.

6.3 Materials and Methods

6.3.1 Aggregation Experiments

Aggregation experiments were performed by mixing equal volumes of C95-2/C97-2 CLIO reagent and analyte solutions in a microplate.[6] Analyte (hCG) were obtained from Sigma. CLIO reagent was prepared to have final concentrations of 8 μg/ml Fe C95-2 and 8 μg/ml Fe C97-2 after analyte addition. Agarose-stabilized CLIO (st-CLIO) reagent was prepared to have final concentrations of 8 μg/ml Fe C95-2, 8 μg/ml Fe C97-2, and 0.5% agarose (Low gelling temperature agarose, Sigma) after analyte addition. Analyte solutions were prepared in phosphate buffered saline pH 7.4 with 1% penicillin-streptomycin and 0.1% bovine serum albumin PBS, artificial urine solution (Surine®, Dynatek Industries, Lenexa, KS), DMEM cell culture media (Invitrogen), cell culture media + 10% fetal bovine serum (10% FBS, Invitrogen), and fetal bovine serum (100% FBS). Reported values are the final analyte concentrations obtained after mixing. Samples volumes of 100 to 300 μl were produced.

6.3.2 *^1H Transverse Relaxation Time Measurements*

Proton relaxation time measurements were performed on a single-sided MR (0.43 T and 25°C; Profile NMR MOUSE, ACT Center for Technology, Aachen, Germany). The single-sided MR sensor was retrofitted with a programmable motion stage and 96-well plate holder. Single-sided MR samples were directly pipetted and mixed in the wells of a 96-well plate and were read automatically in sequence. Transverse relaxation times for the single-sided MR ($T_{2,eff}$) were measured using a CPMG sequence with the following parameters: TE = 0.035 ms, 2143 echoes, 20 scans, and TR = 1.25 s. The echo peak intensities were fit to the equation $I = I_0 e^{-t/T_2}$ using a custom script running on MATLAB (The Mathworks, Natick, MA). $T_{2,eff}$ were plotted as measured or subtracted from the initial value and the difference reported as $\Delta T_{2,eff}$. All values are within 0.5 ms with 95% confidence. Initial measurements of non-stabilized aqueous samples were obtained within one minute after mixing for the first timepoint. Initial measurements of agarose-stabilized samples were obtained approximately 5 minutes after mixing to allow agarose to gel. Subsequent T_2 kinetic measurements were made after incubation times indicated.

6.3.3 *Diffusivity of CLIO Experiment*

The single-sided MR was fitted with an automated XYZ motion stage (Newport) with a repeatability of the positioning better than 1 μm. A sample was prepared by pipetting 150 μL of agarose into a well of a 96-well plate and allowing it to gel. The CLIO reagent was placed over the agarose gel in one well, and PBS over another. A 1-D $T_{2,eff}$ profile of each well was measured over a period of 40 hours. Each profile consisted of 5 slices approximately 250 μm apart

spanning a distance of 1 mm from the bottom of the well. The probe was tuned to measure a slice approximately 8 x 8 mm and 250 μm thick, located 2 mm above the probe center.

6.4 Results

MRSw-based assays require MRSw to be stable for the duration of the sample processing and batch measurement. Certain *in vivo* applications may require longer stability on the order of weeks to months. Agarose was chosen as a readily available stabilizing agent. It was evaluated for permitting CLIO mobility and allowing aggregation. The dynamic range and the length of stability were also investigated.

6.4.1 CLIO Diffusivity in Agarose Matrix

The diffusivity of the CLIO in agarose gel was measured to evaluate the potential of agarose as a stabilizing matrix for the aggregation based assay. The assay would not work if the nanoparticles were completely immobilized by the matrix. A CLIO solution was layered on top of agarose and the $T_{2,eff}$ of a thin section of agarose was measured over time (Figure 6–1). The single-sided MR probe's static field gradient allows for 1-D imaging of a section approximately 250 μm thick (16). The $T_{2,eff}$ of agarose covered in PBS was constant at around 70 ms, which is close to that of water. The $T_{2,eff}$ of agarose alone is much higher than most of the values reported here as it is does not contribute much to dephasing of protons. The $T_{2,eff}$ of the agarose covered in nanoparticle solution was found to decrease consistently over the monitored period as the CLIO diffused into the agarose (Fig 5b). There was an initial induction period because the agarose

could not be profiled at the liquid/agarose interface but 2 mm from the bottom of the well, or 1.5 mm from the interface. This limitation is due to physical reading region of the coil.

CLIO diffusivity in agarose, D, can be estimated using the following relation:

$$D \approx \frac{R^2}{\tau}$$

where R is a characteristic diffusion distance in a time τ. The nanoparticle concentration can be measured indirectly from the T_2 of the sample. Concentration profiles at two time points four hours apart were used to estimate the nanoparticle diffusivity in agarose. The CLIO concentration front diffused 0.8 mm in 4 hours, resulting in CLIO diffusivity in agarose on the order of 10^{-7} cm^2/s. This value is close to that expected of a nanoparticle in water as computed using Einstein's equation for a hard sphere of radius 50 nm diffusing in water at room temperature. The diffusion of non-aggregated CLIO, therefore, is not expected to be hinder by agarose at the concentration tested. The diffusion of analyte molecules that are smaller than the nanoparticles can also be assumed to be unaffected by the agarose matrix. Furthermore, the interaction of the analyte and nanoparticles is not expected to be impeded.

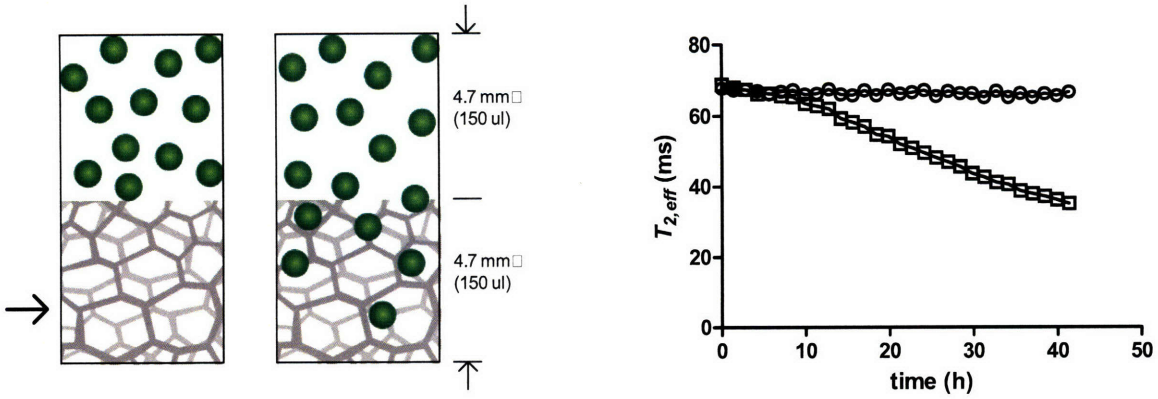

Figure 6–1. Diffusivity of CLIO in Agarose Matrix a) A solution containing CLIO nanoparticles was placed above the agarose and a 1-D transverse relaxation profile was made over a 1 mm span. b) The $T_{2,eff}$ decreased, indicating a mobile CLIO diffused into the agarose when the CLIO reagent was layered above the agarose (□). The $T_{2,eff}$ remained constant when PBS solution was layered above the agarose (○).

6.4.2 CLIO Aggregation in Agarose Matrix

The ability of the CLIO to aggregate in the matrix was examined. The experiment was conducted in parallel with the investigation of fluid CLIO reagent in various buffers (Section 5.4.9) Known hCG concentrations were prepared in the buffers as previously described and then mixed with the molten stabilized CLIO (st-CLIO) reagent, resulting in the same final hCG and CLIO concentrations as in the non-stabilized fluid experiment. The mixture was prepared directly in a 96-well plate and allowed to solidify for 5 minutes at room temperature before $T_{2,eff}$ measurements were taken. The addition of hCG in the stabilized samples resulted in $T_{2,eff}$ decreases compared with the controls. It should be noted that the agarose-stabilized samples have a slightly lower initial $T_{2,eff}$ (between 40-45 ms, Figure 6–1b) than the non-stabilized samples (47-48 ms, Figure 6–1a) due to the contribution of the agarose. The agarose did not hinder the ability of the CLIO to aggregate in response to hCG (Figure 6–1b). The profile is similar to the non-stabilized samples at the initial timepoint (Figure 6–1a). The $T_{2,eff}$ of stabilized samples were constant over 28 days (Figure 6–2, right) in distinct contrast to the fluid CLIO (Figure 6–2, left).

It is especially significant that the higher concentrations tested do not exhibit drift in $T_{2,eff}$, as they did in the non-stabilized samples. The final $T_{2,eff}$ value was reached during the 5 minutes allotted for solidification and did not significantly change thereafter. Agarose was successful in stabilizing T_2 measurements. Aggregation was not noticeably affected by the use of agarose matrix stabilization as evidenced by comparable $T_{2,eff}$ changes with and without matrix stabilization. The dynamic range also appears comparable.

A single concentration, 2.5 μg/ml, was investigated more closely (Figure 6–3). This is the concentration which was previously shown to be the most unstable with the fluid CLIO reagent (Section 5.4.9). Agarose-stabilization shows that the $T_{2,eff}$ drop is maintained throughout the period investigated. The percent change in T_2 was larger in magnitude with the st-CLIO than with fluid CLIO reagent. The reason for this is difficult to interpret as the agarose component of T_2 change is not easily subtracted out as it may have a non-linear behavior. It is also possible that the $T_{2,eff}$ of the fluid CLIO reagent exhibited a minimum value that was not captured by these timepoints.

The overall assay reaction time was lengthened by only 5 minutes when agarose matrix stabilization was used. Replicate experiments using a shorter solidification time (30 s) resulted in similar $T_{2,eff}$ measurements; however, larger variability was observed. This is perhaps due to measurements at various stages of solidification. Matrix stabilization with materials that do not require a solidification time may also be used. The viscosity and porosity of the stabilizing matrix in these applications must be modified to obtain measurements within acceptable time scales. Matrix stabilization would be most suitable in applications where simplicity and stability are needed rather than fast measurements.

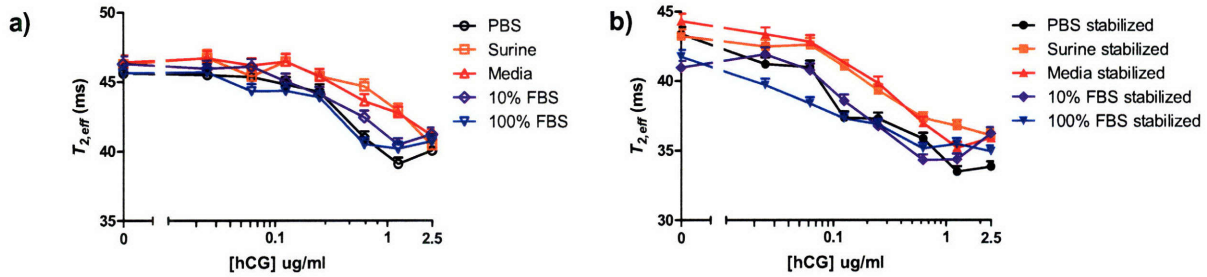

Figure 6–1. $T_{2,eff}$ of hCG in various buffers with a) fluid CLIO reagent (○ PBS, □ Surine, △ Media, ◇ 10% FBS, ▽100% FBS), and b) agarose-stabilized CLIO reagent (● PBS, ■ Surine, ▲ Media, ◆ 10% FBS, ▼ 100% FBS) immediately after mixing (0 hr).

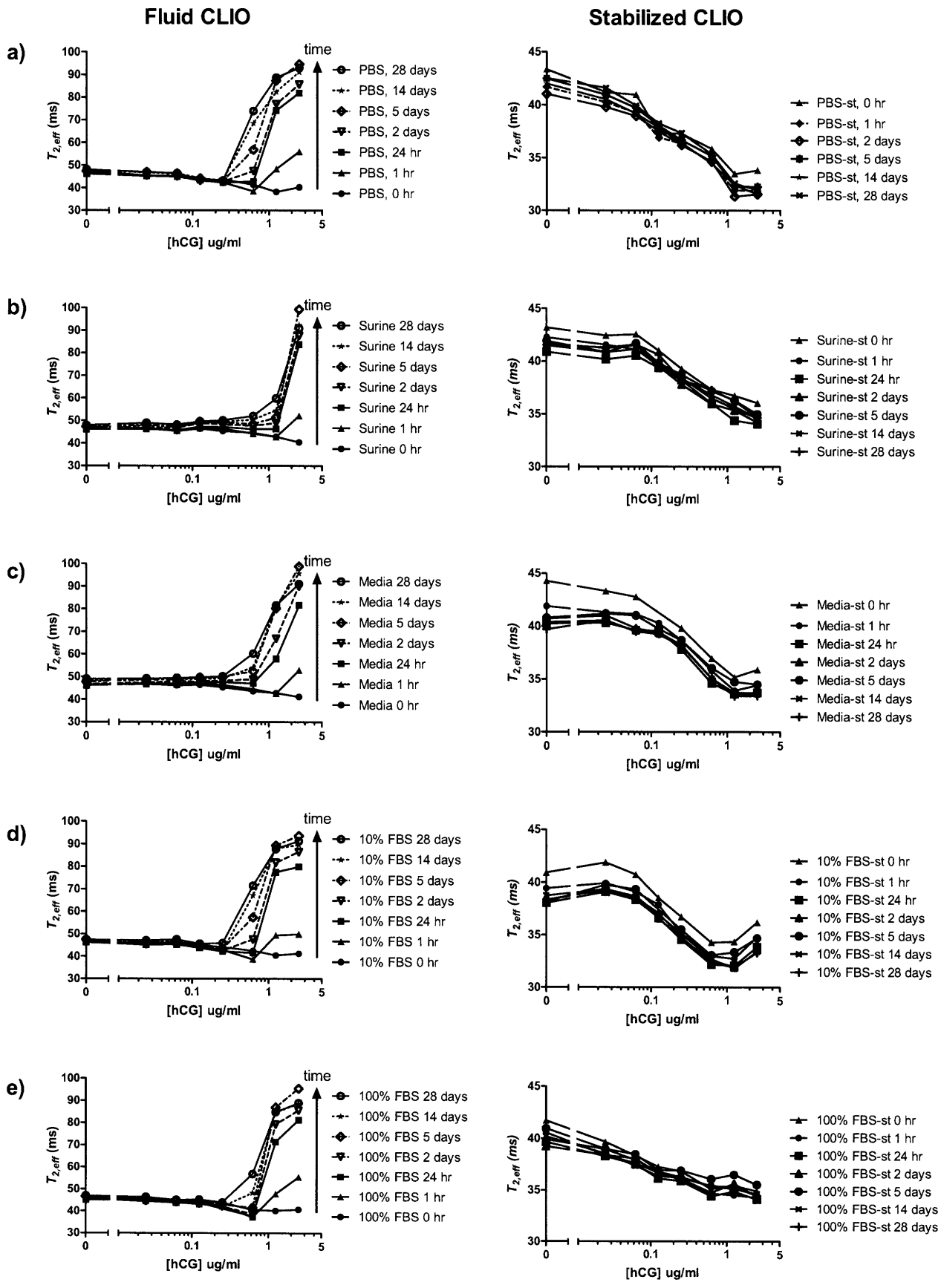
Fluid CLIO
Stabilized CLIO
a)
b)
c)
d)
e)
time
$T_{2,eff}$ (ms)
[hCG] ug/ml
PBS, 28 days
PBS, 14 days
PBS, 5 days
PBS, 2 days
PBS, 24 hr
PBS, 1 hr
PBS, 0 hr
PBS-st, 0 hr
PBS-st, 1 hr
PBS-st, 2 days
PBS-st, 5 days
PBS-st, 14 days
PBS-st, 28 days
Surine 28 days
Surine 14 days
Surine 5 days
Surine 2 days
Surine 24 hr
Surine 1 hr
Surine 0 hr
Surine-st 0 hr
Surine-st 1 hr
Surine-st 24 hr
Surine-st 2 days
Surine-st 5 days
Surine-st 14 days
Surine-st 28 days
Media 28 days
Media 14 days
Media 5 days
Media 2 days
Media 24 hr
Media 1 hr
Media 0 hr
Media-st 0 hr
Media-st 1 hr
Media-st 24 hr
Media-st 2 days
Media-st 5 days
Media-st 14 days
Media-st 28 days
10% FBS 28 days
10% FBS 14 days
10% FBS 5 days
10% FBS 2 days
10% FBS 24 hr
10% FBS 1 hr
10% FBS 0 hr
10% FBS-st 0 hr
10% FBS-st 1 hr
10% FBS-st 24 hr
10% FBS-st 2 days
10% FBS-st 5 days
10% FBS-st 14 days
10% FBS-st 28 days
100% FBS 28 days
100% FBS 14 days
100% FBS 5 days
100% FBS 2 days
100% FBS 24 hr
100% FBS 1 hr
100% FBS 0 hr
100% FBS-st 0 hr
100% FBS-st 1 hr
100% FBS-st 24 hr
100% FBS-st 2 days
100% FBS-st 5 days
100% FBS-st 14 days
100% FBS-st 28 days

Figure 6–2. Repeat measurements of hCG using fluid CLIO reagent (left) and stabilized CLIO reagent (right) in various buffers: a) PBS, b) Surine, c) Media, d) 10% FBS, e) 100% FBS. The fluid CLIO reagent at the indicated timepoints reveal rapidly fluctuating and unstable measurements, but with stabilized CLIO reagent show stable measurements up to 28 days later. Agarose does not interfere with the detection capability of the CLIO reagent.

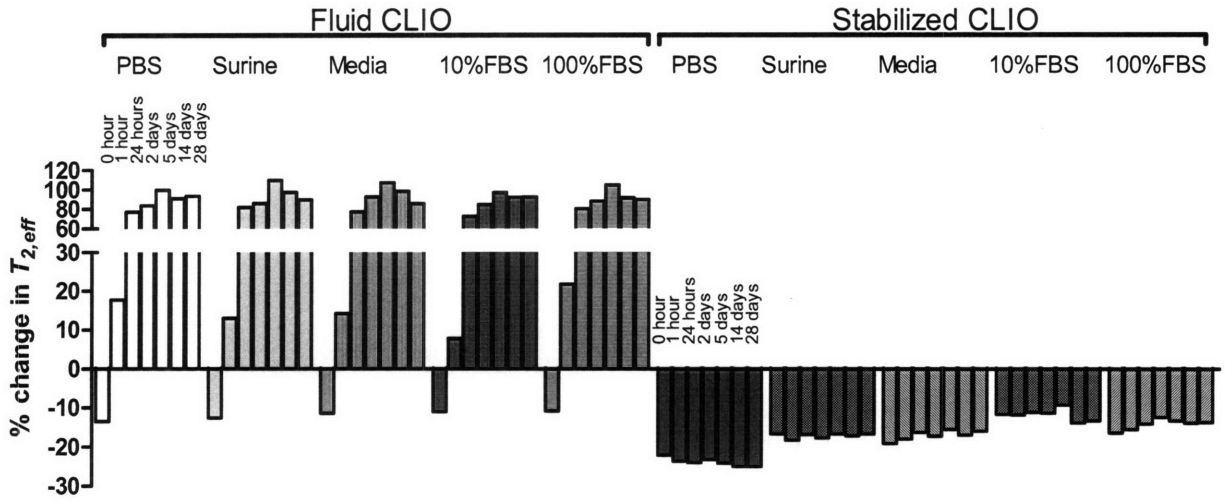

Figure 6–3. Stability of 2.5 µg/ml hCG in PBS analyte sample in various buffers. Comparison of fluid and agarose-stabilized CLIO reagent, represented as percent change in $T_{2,eff}$ from the 0 µg/ml hCG control in the respective buffer. Data were recorded at 0 h, 1 h, 24 h, 2 days, 5 days, 14 days, and 28 days. Note that $T_{2,eff}$ are initially low in fluid samples, indicating that hCG caused MRSw aggregation, but the values rise at 1 hr and continue to drift with time. Stabilized samples show no drift in $T_{2,eff}$ over 28 days.

6.5 Conclusion

MRSw-based assays require MRSw to be stable for the duration of the sample processing and batch measurement. Certain *in vivo* applications may require longer stability on the order of weeks to months. Agarose was chosen as a readily available stabilizing agent. It was evaluated for permitting CLIO mobility and allowing aggregation. The dynamic range and the length of stability were also investigated. Matrix stabilization allows stable sensing of analytes in aggregation-based chemical assays. Stable T_2 measurements were demonstrated for 28 days by mixing analyte solution and CLIO reagent containing agarose.

It is hypothesized that matrix stabilization slows aggregate formation and limits final aggregate size by trapping clusters within the pores so that precipitation cannot occur (Figure 6–1). Matrix stabilization controls T_2 by decreasing the mobility of the aggregates in solution whereas previously aggregate growth was primarily limited only by the availability of reactants. Dynamic light scattering cannot be conducted on the slightly opaque agarose samples, but future work may employ other techniques to investigate the particle size distribution in the stabilizing matrix. Transmission electron microscopy may be useful for testing this hypothesis.

We have also demonstrated the assay in a high-throughput mode in a standard 96-well plate format with the single-sided MR, which is essential for screening and development of magnetic nanoparticle assays. The combination of these two aspects, an industry standard sample format and matrix stabilization, provides high-throughput simplified sample handling essential for a mix-and-read plate assay. Agarose was used for its gelling ability and stabilizing property to demonstrate the use of matrix stabilization; however, other materials should be investigated as a matrix stabilization agent depending on required viscosity and porosity. Materials that do not require a solidification time may be of particular interest. This study constitutes a significant step towards practical and reliable aggregation-based assays for *in vitro* diagnostics. Long-term *in vivo* applications, in particular, may benefit from matrix stabilization of MRSw by allowing longitudinal tracking of local biomarker or drug concentrations during treatment.

6.6 References

1. Taktak, S., Sosnovik, D., Cima, M. J., Weissleder, R., and Josephson, L. Multiparameter magnetic relaxation switch assays. *Anal Chem, 79:* 8863-8869, 2007.
2. Sun, E. Y., Weissleder, R., and Josephson, L. Continuous analyte sensing with magnetic nanoswitches. *Small, 2:* 1144-1147, 2006.
3. Yigit, M. V., Mazumdar, D., Kim, H. K., Lee, J. H., Dintsov, B., and Lu, Y. Smart "Turn-on" magnetic resonance contrast agents based on aptamer-functionalized superparamagnetic iron oxide nanoparticles. *ChemBioChem, 8:* 1675-1678, 2007.
4. Lowery, T. J., Palazzolo, R., Wong, S. M., Prado, P. J., and Taktak, S. Single-coil, multisample, proton relaxation method for magnetic relaxation switch assays. *Anal Chem, 80:* 1118-1123, 2008.
5. Tartaj, P., Morales, M. D., Veintemillas-Verdaguer, S., Gonzalez-Carreno, T., and Serna, C. J. The preparation of magnetic nanoparticles for applications in biomedicine. *Journal of Physics D-Applied Physics, 36:* R182-R197, 2003.
6. Kim, G. Y., Josephson, L., Langer, R., and Cima, M. J. Magnetic relaxation switch detection of human chorionic gonadotrophin. *Bioconjug Chem, 18:* 2024-2028, 2007.
7. Ortega-Vinuesa, J. L. and Bastos-Gonzalez, D. A review of factors affecting the performances of latex agglutination tests. *Journal of Biomaterials Science-Polymer Edition, 12:* 379-408, 2001.
8. Choi, D., Lee, W., Lee, Y., Kim, D. N., Park, J., and Koh, W. G. Fabrication of macroporous hydrogel membranes using photolithography for enzyme immobilization. *Journal of Chemical Technology and Biotechnology, 83:* 252-259, 2008.
9. Stachowiak, A. N. and Irvine, D. J. Inverse opal hydrogel-collagen composite scaffolds as a supportive microenvironment for immune cell migration. *J Biomed Mater Res A,* 2007.
10. Barnes, C. P., Sell, S. A., Boland, E. D., Simpson, D. G., and Bowlin, G. L. Nanofiber technology: designing the next generation of tissue engineering scaffolds. *Adv Drug Deliv Rev, 59:* 1413-1433, 2007.
11. Gupta, A. K. and Gupta, M. Synthesis and surface engineering of iron oxide nanoparticles for biomedical applications. *Biomaterials, 26:* 3995-4021, 2005.
12. Rebolledo, A. F., Fuertes, A. B., Gonzalez-Carreno, T., Sevilla, M., Valdes-Solis, T., and Tartaj, P. Signatures of clustering in superparamagnetic colloidal nanocomposites of an inorganic and hybrid nature. *Small, 4:* 254-261, 2008.

CHAPTER 7

Interleukin-2 MRSw-based Assay

7.1 Summary

Magnetic relaxation switches (MRSw) were prepared to detect interleukin-2 (IL-2). IL-2 is a cytokine that activates anti-cancer immune activity and is used for cancer therapy. Polyclonal antibodies against IL-2 were conjugated to crosslinked iron oxide (CLIO) nanoparticles using standard peptide chemistry. The polyclonal antibody CLIO conjugate should also create aggregates as the multiple clones may recognize different epitopes on IL-2. This approach was attempted as polyclonal antibodies more readily available than matched pairs of antibodies. The addition of IL-2 to CLIO-anti-IL-2 resulted in transverse relaxation time ($T_{2,eff}$)

increases compared to a blank control as seen by single-sided MR, in contrast with the T_2 decreases reported in Chapter 5 and 6. Kinetic experiments show that $T_{2,eff}$ increases over 2 days in a concentration dependent manner from 0.01 to 5 μg/mL.

7.2 Introduction & Motivation

IL-2 is large protein (15 kDa) cytokine with a variety of immune responses. Stimulated CD4+ T-cells, B-cells, lymphokine activated killer cells and natural killer cells produce IL-2, which in turn induces T-cell proliferation and a natural killer response. It can be exogenously delivered as an immunotherapeutic in cancer treatment. Paracrine delivery of exogenous IL-2 alone been show to be effective against tumors in animal experiments [1, 2] Paracrine or local delivery of IL-2 may be more efficacious than systemic administration it mimics the natural biological action by establishing an IL-2 gradient and facilitating cytotaxis.

Combinations of IL-2 and chemotherapeutic drugs may have a synergistic anti-tumor effect due to complementary mechanisms of action. Carmustine or 1,3-Bis(2-chloroethyl)-1-nitrosourea (BCNU) is a 214.1 MW nitrosourea that acts directly on DNA and is the most commonly used chemotherapeutic agent for the treatment of brain cancer (Chapter 8). Animal work has shown that combinations of IL-2 and BCNU have a synergistic effect for brain cancer therapy[3-6]. Combination local therapy is particularly promising as it seems to stimulate tumor-specific immunity to a subsequent second tumor challenge. Sampath et al.[6] found that survival was prolonged to 70 days after tumor implantation in 7 of 10 animals compared to 10% survival with IL-2 alone or no survival with BCNU alone (Figure 7–1). The method of delivery was via the implantation of a replication-incompetent genetically modified tumor cell line transfected to

produce 80 ng of IL-2 per 10^6 cells per day. The limitations of this approach include all of the risks associated with cellular transplantation and gene therapy: transplantation rejection of allografts or difficulties in isolating tissue for autografts, potentially oncogenic genomic integration of inserted genes, and variation in transfection stability and gene expression efficiency. Efforts to avoid these dangers involve targeted approaches, including direct injection, targeted particulate formulation, or microchip platform delivery of the recombinant protein (Chapter 8)[5, 7, 8].

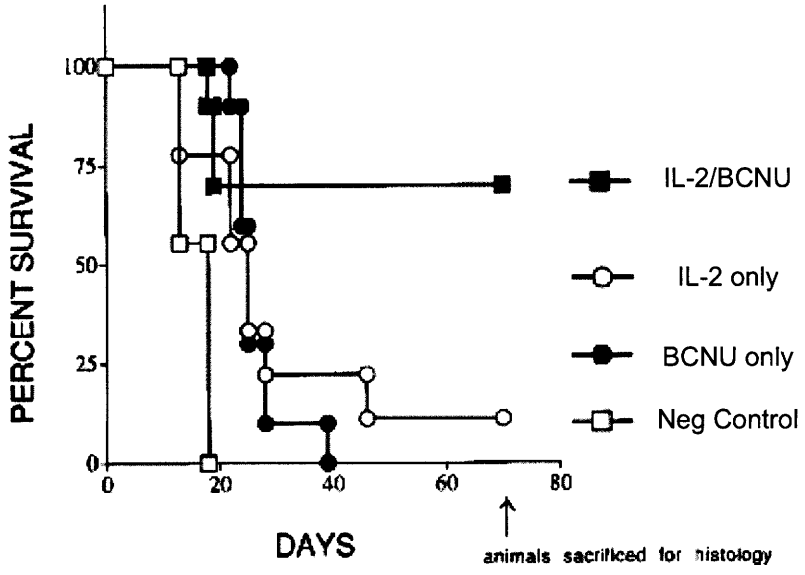

Figure 7–1: Kaplan-Meier survival curve showing survival for animals after IC B16/F10 melanoma challenge treated with empty polymer (□), IL-2-transduced cells alone (○), 10% BCNU polymer alone (•), or combination of 10% BCNU polymer and IL-2-transduced cells (■). Reproduced with permission from [6]. Copyright 1999 American Association for Cancer Research.

The multiple dosing regimens used clinically suggest that the most effective release profiles have yet to be determined. Intravenous IL-2 administration limits the achievable release profiles for these combination therapies as serum half-life is on the order of minutes after systemic injection[9]. Development of local or targeted delivery methods would benefit from biodistribution measurements to test the extent of local delivery.

Polyclonal antibodies against IL-2 were conjugated to CLIO. Previously, a matched pair of *monoclonal* antibodies was conjugated to CLIO for detection of hCG. Polyclonal antibodies should also create aggregates as the multiple clones may recognize different epitopes on IL-2. It should be noted that polyclonal antibodies are an ill-characterized mixture of antibodies and thus cannot be associated with a single K_d. This approach was attempted as polyclonal antibodies more readily available than matched pairs of antibodies and thus would demonstrate a wider and more cost-effective use for MRSw assays.

7.3 Materials and Methods

7.3.1 Aggregation Experiments

Aggregation experiments were performed by mixing equal volumes of CLIO-anti-IL-2 reagent and analyte solutions in the wells of a 96-well microplate. CLIO-anti-IL-2 nanoparticles were prepared in PBS to have final concentrations of 10 μg/ml Fe and were mixed with various IL-2 concentrations. IL-2 (Tecin^{TM}, Teceleukin, recombinant human IL-2) was generously provided by the Biological Research Branch (BRB, National Cancer Institute). Analyte dilutions of IL-2 were prepared in phosphate buffered saline pH 7.4 with 1% penicillin-streptomycin and 0.1% bovine serum albumin (PBS) to reduce nonspecific adsorptive loss of analyte. Reported concentrations are the final analyte concentrations obtained after mixing. The limit of detection (LOD) is defined as the concentration where the standard deviation does not overlap with the standard deviation of the PBS control.

7.3.2 Device Fabrication

Cylinders of HDPE were cut from a 3 mm thick sheet to make the device substrate with a 5 mm inner diameter and 10 mm outer diameter. Double-sided pressure sensitive adhesive was used to attach the polycarbonate membrane (10 nm pores, $6x10^8$ pores/cm^2, SPI Supplies) to the top of the device. The reservoir was filled with 80 μL of fluid CLIO-anti-IL-2 reagent or agarose stabilized CLIO-anti-IL-2 reagent. The final CLIO concentration in the devices in both cases was 10 μg/ml Fe. The reservoir was then sealed with single-sided pressure sensitive adhesive. The devices were immediately placed in 1 ml of PBS containing various IL-2 concentrations and kept at 37°C. Devices were removed periodically and carefully blotted dry before being measured on the single-sided MR.

7.3.3 ^1H Relaxation Time Measurements

Proton relaxation time measurements were performed on a single-sided MR (0.43 T and 25°C; Profile NMR MOUSE, ACT Center for Technology, Aachen, Germany). The single-sided MR sensor was retrofitted with a programmable motion stage and 96-well plate holder. Samples were directly pipetted and mixed in the wells of a 96-well plate at room temperature and were read automatically in sequence. Measurements were obtained within one minute after mixing or at the specified times for T_2 kinetic experiments. Washers were measured without the programmable motion stage and placed by hand over the reading region of the single-sided MR. Transverse relaxation times for the single-sided MR ($T_{2,eff}$) were measured using a CPMG sequence with the following parameters: TE = 0.035 ms, 2143 echoes, 20 scans, and TR = 1.25 s. The echo peak intensities were fit to the equation $I = I_0 e^{-t/T_2}$ using a custom script running on

MATLAB (The Mathworks, Natick, MA). $T_{2,eff}$ were plotted as measured or subtracted from the initial value and the difference reported as $\Delta T_{2,eff}$. All values are within 0.5 ms with 95% confidence.

7.4 Results

7.4.1 CLIO-anti-IL-2 + Interleukin-2 Aggregation

MRSw for IL-2 was tested by mixing CLIO-anti-IL-2 with increasing concentrations of IL-2 from 0.01 to 5 μg/mL in a microplate. $T_{2,eff}$ were subtracted from the initial value immediately after mixing and the difference was plotted as $\Delta T_{2,eff}$ (Figure 7–1d). The $T_{2,eff}$ relaxation time of all solutions was initially the same. The start value for the 8 samples was 42.3 +/- 0.4 ms (average +/- standard deviation). The $\Delta T_{2,eff}$ of devices placed in IL-2 increased over time. The degree of increase varied with concentration such that the solutions with the highest IL-2 concentration showed the largest $\Delta T_{2,eff}$. The device placed in 5 μg/ml IL-2, for example, showed 9 ms increase in 12 hours. The trend appears to continue up to 48 hours (Figure 7–1b) although, unfortunately, more regular timepoints were not taken to determine if the response slows down. The data were also plotted to show the concentration response (Figure 7–1c). The samples did not exhibit a concentration dependent response with immediate measurement, but repeat measurements of CLIO-anti-IL-2 reagent revealed the $\Delta T_{2,eff}$ rises in a concentration dependent manner. Decreases in $T_{2,eff}$ were not observed at all for the CLIO-anti-IL-2 reagent.

This behavior is in contrast with that observed for other CLIO reagents. C95-2/C97-2 , for example, showed concentration dependent $T_{2,eff}$ measurements only at the initial timepoint. $T_{2,eff}$ that either decreased and remained stable at a lower value or eventually increased to a very

high value (80-100 ms) such that there was no differentiation of the various concentrations from one another. The $T_{2,eff}$ of the CLIO-anti-IL-2 reagent rises slowly and maintains resolution of the different concentrations even at 48 hours. The relationship becomes steeper with time and may lead to higher sensitivity at the lower concentrations. It is possible that longer monitoring would reveal that the $T_{2,eff}$ would eventually also reach a very high value and lose the concentration dependent relationship. The CLIO-anti-IL-2 reagent aggregates may also be precipitating but at a slower rate that for the C95-2/C97-2 reagent (Section 5.4.9). The LOD is 0.01 μg/mL IL-2 at the iron concentration tested. A lower Fe concentration may yield an even lower LOD as fewer IL-2:CLIO binding events would be necessary to see a relative change in the solution (Section 5.4.8). This reaction is not an endpoint read, however, and the hours of incubation required for the development of the $\Delta T_{2,eff}$ makes this reagent impractical for applications where fast measurements are required. The slower response here may be related to the effective K_d of the ensemble of polyclonal antibodies. The CLIO-anti-IL-2 reagent produced here may be useful in an application where a slower response to environmental conditions is acceptable.

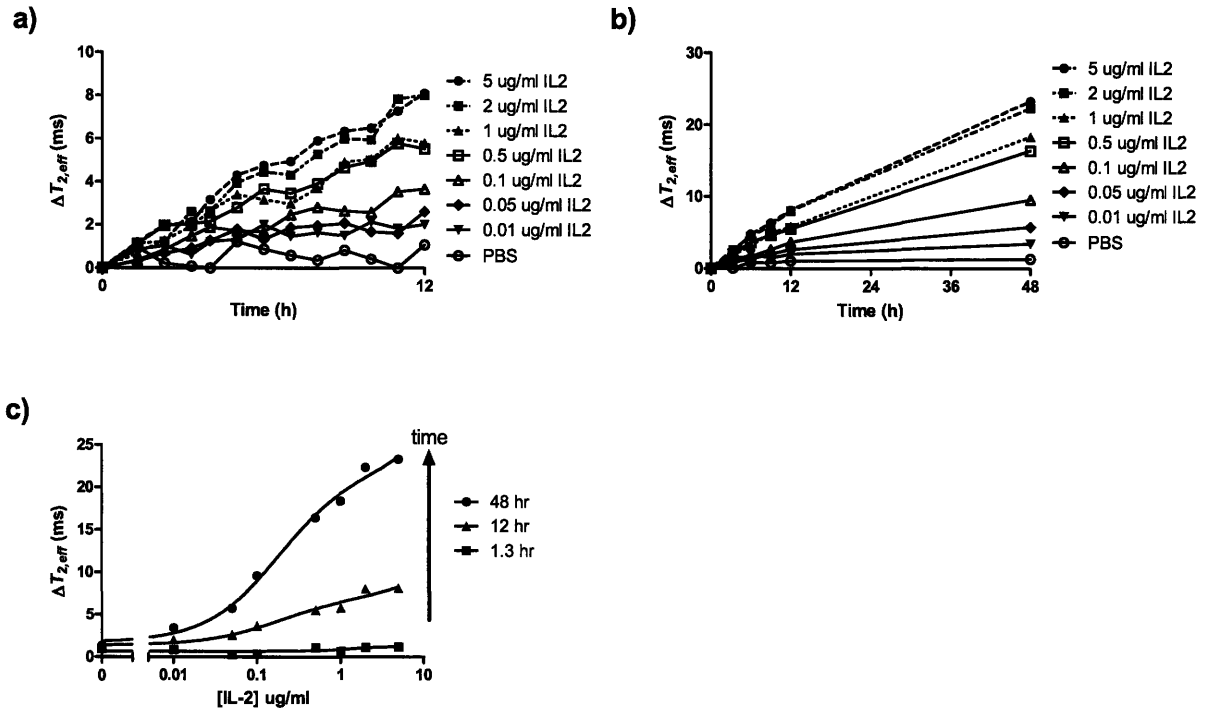

Figure 7–1. $\Delta T_{2,eff}$ of fluid IL-2 CLIO-anti-IL-2 reagent mixed with IL-2 using in plate format. Several IL-2 concentrations were measured on the single-sided MR. a) The control sample shows relatively little change. $\Delta T_{2,eff}$ of all samples containing IL-2 increased over 12 hours. The magnitude of the increase varied with IL-2 concentration. b) $\Delta T_{2,eff}$ of fluid IL-2 CLIO-anti-IL-2 over 48 hours shows that the values continue to change in a concentration dependent manner. c) The data are replotted showing the $\Delta T_{2,eff}$ versus concentration at three timepoints (1.3 hr, 12 hr, and 48 hr).

7.4.2 Fluid CLIO-anti-IL-2 Reagent in Device Format

Fluid CLIO-anti-IL-2 reagent was placed into a washer-like device format. These washers have a semipermeable membrane on one side that allows analytes to enter the device and interact with the MRSw. They are similar in concept to that reported earlier in by our group[10], but are made in a disc shape of a harder material. These devices were incubated in various concentrations of IL-2, removed periodically, and measured on the single-sided MR (Figure 7–1a). Trends were similar to that observed with CLIO-anti-IL-2 reagent in a microplate (Section). The start value of all devices was the same, 42.2 +/- 0.5 ms (average +/- standard deviation). The $\Delta T_{2,eff}$ of devices placed in IL-2 increased over time, varying with concentration

such that the solutions with the highest IL-2 concentration showed the largest $\Delta T_{2,eff}$. This response was observed as early as 4 hours and continued for more than 2 days. It is of note that the time scale of $\Delta T_{2,eff}$ changes was similar in the microplate well and in the washers (Figure 7–1b). It was expected that the response in the washers would be slower because IL-2 would need to diffuse into device. There may be a slight induction time with the washer, and further studies should be conducted to explore this.

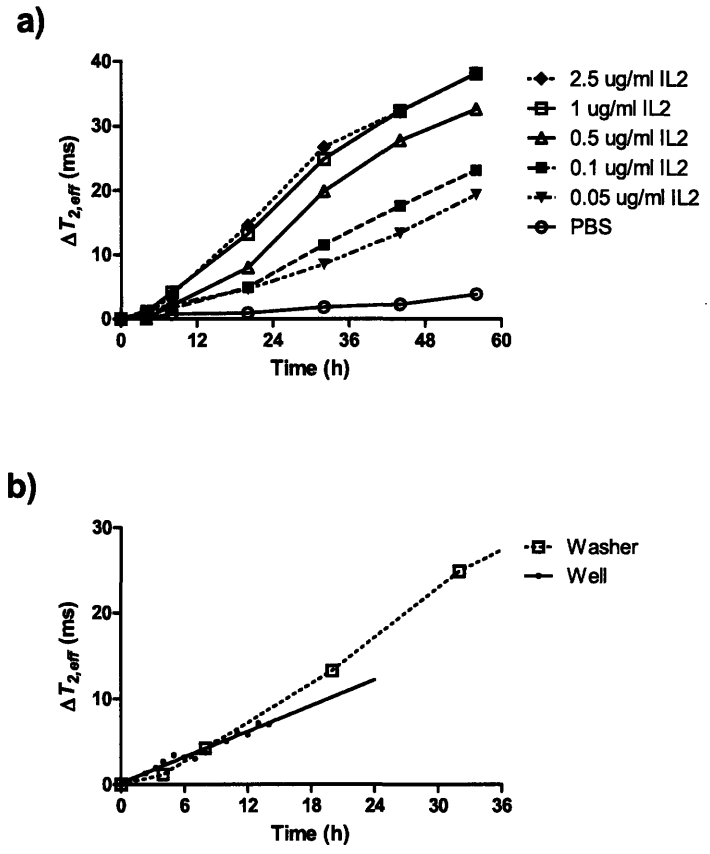

Figure 7–1. $\Delta T_{2,eff}$ of fluid IL-2 CLIO-anti-IL-2 washers incubated in various IL-2 concentrations. a) $\Delta T_{2,eff}$ of all devices incubated in IL-2 increased. b) The $\Delta T_{2,eff}$ response of fluid IL-2 CLIO-anti-IL-2 to IL-2 in wells was compared to washers.

7.4.3 Agarose Stabilized CLIO-anti-IL-2 Reagent in Device Format

The different behavior of the CLIO-anti-IL-2 reagent from the CLIO-95-X/CLIO-97-X reagent motivated investigation of the effect of matrix stabilization on CLIO-anti-IL-2 reagent. Agarose stabilization may reveal the mechanism of T_2 change and facilitate comparison with results from CLIO-95-X/CLIO-97-X. It was expected from our previous results that the $T_{2,eff}$ would decrease when stabilized and remain constant after aggregation has occurred. However, no $T_{2,eff}$ decreases were ever recorded using the fluid CLIO-anti-IL-2 reagent even at the first timepoint.

Washers containing stabilized CLIO-anti-IL-2 reagent were incubated in 1 ug/ml IL-2 (Figure 7–1a). $\Delta T_{2,eff}$ increased with fluid CLIO-anti-IL-2 reagent as demonstrated previously; however, $\Delta T_{2,eff}$ decreased with stabilized CLIO-anti-IL-2 reagent. Additional agarose concentrations were also tested (Figure 7–1a). Larger $\Delta T_{2,eff}$ decreases were observed with lower agarose concentrations. This result suggests that stabilization of aggregation is occurring, and the lower $\Delta T_{2,eff}$ with the softer gels suggests that perhaps the CLIO-anti-IL-2 reagent in those gels may be able aggregating more extensively or in a manner that more efficiently dephases the protons. It may also be that it is more difficult for the analyte to diffuse through the washers containing higher agarose percentage. The mobility calculation was previously conducted with 0.5% agarose (Section 6.4.1), and it is possible that 2% agarose is sufficient to hinder CLIO mobility. Another possibility is that the assumption that the analyte does not interact with the agarose matrix may be incorrect, and additional forces due to charge or steric effects may be affecting the analyte mobility.

The stabilized CLIO-anti-IL-2 washers were also incubated in increasing concentrations of IL-2 (Figure 7–1b). This experiment was performed with stabilization by a single agarose

concentration (1%). An approximate concentration dependence is observed though at longer times, and the $\Delta T_{2,eff}$ converge such that it is difficult to discriminate between the samples. A majority of the $T_{2,eff}$ drop occurs within one day. IL-2 is diffusing through the membrane into device and aggregating CLIO in the washer in this period of time. The reaction time does not appear to be significantly longer different in the agarose washers from the fluid washers. Previous work has suggested that the rate limiting step is the movement of analyte across the semi-permeable membrane[10]. A faster response may be obtained by using devices with a higher permeability membrane. Device-based sensing of IL-2 is feasible. The saturation of the T_2 response at long times may be addressed by titrating the particle concentration for the desired dynamic range. The PBS sample slightly increased in $T_{2,eff}$ over first two days. This may be due to leakage of CLIO from the device from membrane defects, leakage of CLIO from the membrane-substrate interface, or swelling of the agarose gel. All of these would effectively lower the CLIO concentration in the device and cause an increased in $T_{2,eff}$. This effect may be masked in the devices incubated in IL-2 as the decrease in $T_{2,eff}$ may be large enough to offset any effect that increases the $T_{2,eff}$ and aggregates are less likely to leak from the device than single particles.

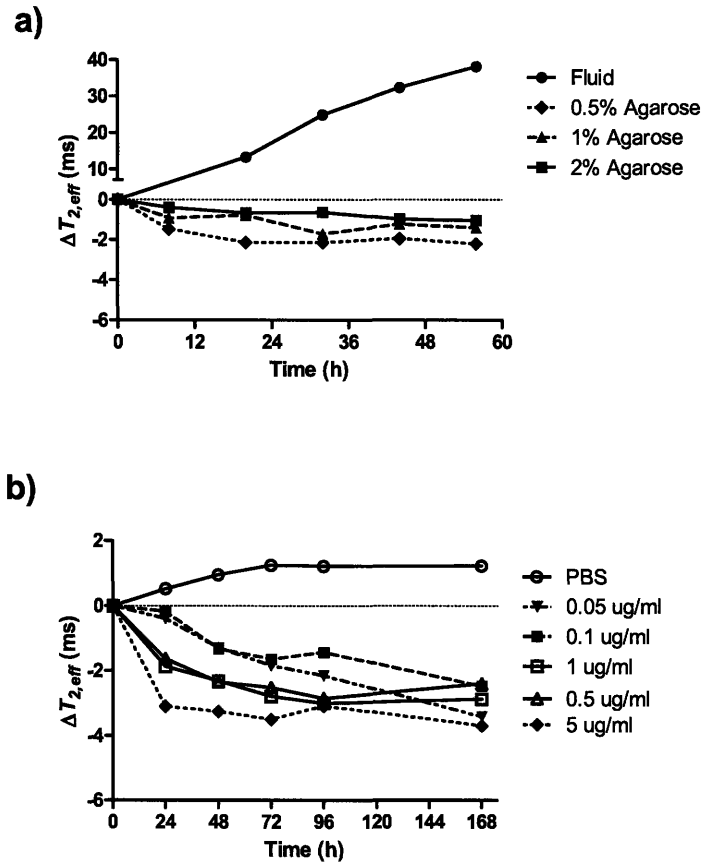

Figure 7–1. $\Delta T_{2,eff}$ of IL-2 CLIO-anti-IL-2 washers incubated with a single IL-2 concentration (1 ug/ml). IL-2 CLIO-anti-IL-2 devices were either fluid, stabilized with 0.5% agarose, stabilized with 1% agarose, or stabilized with 2% agarose. $\Delta T_{2,eff}$ increases for fluid devices but decreases for stabilized devices. b) Concentration response of IL-2 CLIO-anti-IL-2 washers stabilized with 1% agarose. $\Delta T_{2,eff}$ increases slightly for control device, and all devices incubated in IL-2 decreases. Magnitude of T_2 change roughly corresponds with IL-2 concentration, but correlation in stabilized devices not as strong as in fluid devices.

7.5 Conclusion

MRSw for IL-2 was tested. IL-2 is a cytokine that activates anti-cancer immune activity and is used for cancer therapy. Polyclonal antibodies to IL-2 were conjugated to CLIO using standard peptide chemistry. The polyclonal CLIO-anti-IL-2 conjugate should also create aggregates as the multiple clones may recognize different epitopes on IL-2. This approach was attempted as polyclonal antibodies more readily available than matched pairs of antibodies. The

resulting CLIO-anti-IL-2 reagent was then assessed as an MRSw agent by mixing with IL-2 solutions and measuring $T_{2,eff}$. The solutions did not initially show a change in $T_{2,eff}$, but a concentration dependent response developed after incubation and was maintained up to 2 days later. This result showed that conjugation of a polyclonal antibody can successfully generate an MRSw reagent.

This reagent behaves differently from the two previously described analytes assayed by MRSw. The $T_{2,eff}$ *increased* with IL-2 concentration. CLIO-anti-IL-2 reagent was also encapsulated into washer devices and covered with a semi-permeable polycarbonate membrane. The devices were then placed in IL-2 solutions and the IL-2 was allowed to diffuse into the devices. Devices containing fluid CLIO-anti-IL-2 reagent also showed a concentration dependent increase in $T_{2,eff}$, but devices containing agarose stabilized CLIO-anti-IL-2 reagent showed a decrease in $T_{2,eff}$. CLIO-anti-IL-2 reagent appears to aggregate and precipitate at a slower rate than the CLIO-95-X/CLIO-97-X blend. Longer monitoring would reveal whether the concentration dependent response will persist. It is not clear if the difference in $T_{2,eff}$ behavior is due to the polyclonal nature of the conjugate, its affinity (indeterminable, but most likely lower than monoclonal antibodies), the analyte properties, or a combination of these factors.

7.6 References

1. Thompson, R. C., Pardoll, D. M., Jaffee, E. M., Ewend, M. G., Thomas, M. C., Tyler, B. M., and Brem, H. (1996) Systemic and local paracrine cytokine therapies using transduced tumor cells are synergistic in treating intracranial tumors. *J Immunother Emphasis Tumor Immunol 19*, 405-13.
2. Hanes, J., Sills, A., Zhao, Z., Suh, K. W., Tyler, B., DiMeco, F., Brat, D. J., Choti, M. A., Leong, K. W., Pardoll, D. M., and Brem, H. (2001) Controlled Local Delivery of Interleukin-2 by Biodegradable Polymers Protects Animals from Experimental Brain Tumors and Liver Tumors. *Pharmaceutical Research 18*, 899 - 906.
3. Farone, A. L., and Cox, D. C. (1992) 1,3-Bis(2-chloroethyl)-1-nitrosourea (BCNU)/interleukin-2 chemoimmunotherapy of murine L1210 leukemia. *Cancer Immunol Immunother 34*, 279-81.
4. Lesniak, M. S., Sampath, P., DiMeco, F., Viglione, M. P., Tyler, B. M., Pardoll, D. M., and Brem, H. (2000) Comparative Analysis of paracrine immunotherapy in experimental brain tumors. *Neurosurg Focus 9*.
5. Rhines, L. D., Sampath, P., DiMeco, F., Lawson, H. C., Tyler, B. M., Hanes, J., Olivi, A., and Brem, H. (2003) Local Immunotherapy with Interleukin-2 Delivered from Biodegradable Polymer Microspheres Combined with Interstitial Chemotherapy: A Novel Treatment for Experimental Malignant Glioma. *Neurosurgery 52*, 872 - 879.
6. Sampath, P., Hanes, J., DiMeco, F., Tyler, B. M., Brat, D., Pardoll, D. M., and Brem, H. (1999) Paracrine Immunotherapy with Interleukin-2 and Local Chemotherapy is Synergistic in the Treatment of Experimental Brain Tumors. *Cancer Research 59*, 2107-2114.
7. Thomas, T. T., Kohane, D. S., Wang, A., and Langer, R. (2004) Mircoparticulate formulations for the controlled release of interleukin-2. *Journal of Pharmaceutical Sciences 93*, 1100-1109.
8. Grayson, A. C. R., Choi, I. S., Tyler, B. M., Wang, P. P., Brem, H., Cima, M. J., and Langer, R. (2003) Multi-pulse Drug Delivery from a Resorbable Polymeric Microchip Device. *Nature Materials 2*, 767-772.
9. Donohue, J. H., and Rosenberg, S. A. (1983) The fate of interleukin-2 after in vivo administration. *J Immunol 130*, 2203-8.
10. Daniel, K. D., Kim, G. Y., Vassiliou, C. C., Jalali-Yazdi, F., Langer, R., and Cima, M. J. (2007) Multi-reservoir device for detecting a soluble cancer biomarker. *Lab Chip 7*, 1288-93.

CHAPTER 8

Microchip Delivery of Brain Chemotherapy Drug

8.1 Summary

Sustained local delivery of single agents and controlled delivery of multiple chemotherapeutic agents are sought for the treatment of brain cancer. A resorbable, multi-reservoir polymer microchip drug delivery system has been against a tumor model. The microchip reservoirs were loaded with 1,3-bis(2-chloroethyl)-1-nitrosourea (BCNU). BCNU was more stabile at 37°C within the microchip compared to a uniformly impregnated polymeric wafer (70% intact drug vs. 38%, at 48 hours). The half-life of the intact free drug in the microchip was 11 days, which is a marked enhancement compared to its half-life in normal saline and 10%

ethanol (7 and 10 minutes, respectively) [1, 2]. A syngeneic Fischer 344 9L gliosarcoma rat model was used to study the tumoricidal efficacy of BCNU delivery from the microchip or homogeneous polymer wafer. A dose-dependent decrease in tumor size was found for 0.17, 0.67, and 1.24 mg of BCNU-microchips. Tumors treated with 1.24 mg BCNU-microchips showed significant tumor reduction ($p=0.001$) compared to empty control microchips at two weeks. The treatment showed similar efficacy to a polymer wafer with the same dosage. The microchip array of reservoirs allows for delivery of multiple drugs with independent release kinetics and formulations.

8.2 Introduction and Motivation

Brain cancer is still associated with poor prognosis with survival being less than one year when surgical resection is combined with radiation and chemotherapy[3-6]. Although brain cancers account for only 2 percent of all cancers, brain cancers are often associated with the poorest prognosis[3]. Patients with untreated brain metastases survive an average of four months and only increases from 12 to 15 months after some combination of surgery, radiation therapy, and local drug therapy (Gliadel™)[7-10]. Research is ongoing for sustained intracranial delivery of single agents as well as controlled delivery of combination chemotherapeutics via systemic injection, polymers, pumps, and convection enhanced delivery[11-19]. In particular, local controlled treatment of brain tumors with a homogeneous biodegradable polymer, Gliadel® wafer, has been particularly successful in improving survival[10, 20-22]. However, only the non-degradable and degradable microchip platform is able to deliver multiple agents in distinct rounds from a single device[23, 24].

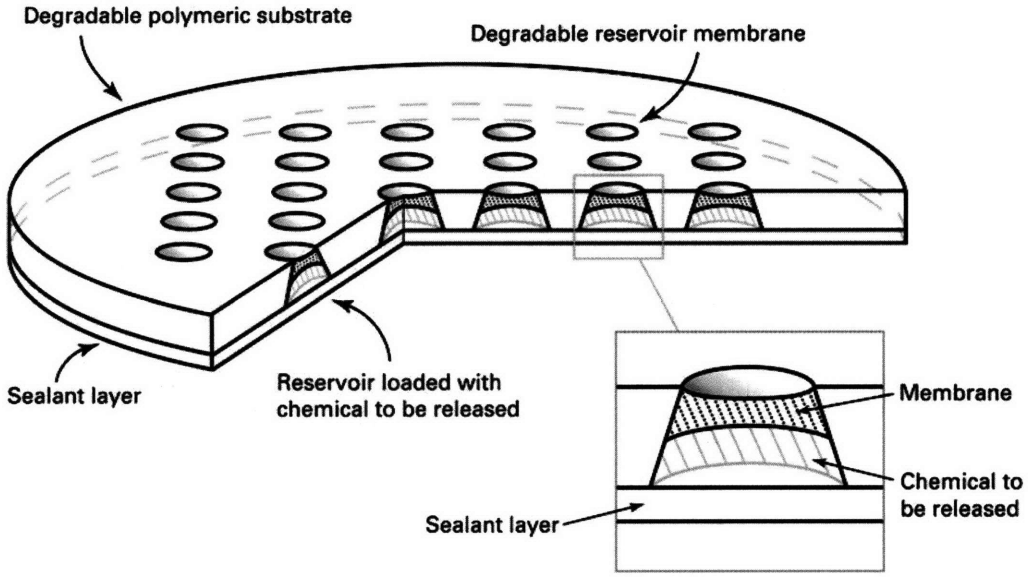

Figure 8–1: Schematic showing the polymer microchip. Reprinted with permission from Macmillan Publishers Ltd: Nature Materials[26]. Copyright 2003.

The microchip system has a unique array of reservoirs, which enables 1) delivery of multiple drugs, 2) independent modulation of drug release profiles, and 3) several drug formulations in a single implantation procedure, which is not possible with other drug delivery technologies. The microchip has the potential to deliver subsequent doses of therapeutic agents at a later time to prevent or to treat recurrence of neoplasm. Local delivery by microchips can increase the concentration of chemotherapeutic agent at the tumor site while reducing systemic toxicity. This spatial control is particularly beneficial for brain tumors because they rarely spread outside the brain [25].

Delivery of 1,3-bis(2-chloroethyl)-1-nitrosourea (BCNU), a commonly used brain cancer chemotherapeutic agent, from a non-degradable microchip was shown to have a dose-dependent inhibiting effect on tumor growth with an efficacy comparable to a subcutaneous injection of an

equal dose of the drug[27]. This technology was validated in a similar device for long-term repeat dosing by the triggered release of leuprolide (MW 1,205) for up to six months in beagle dogs[28]. These devices are not self-contained, however, and require a transcutaneous or wireless interface. A passively actuated, biodegradable controlled release system can avoid the complications of these components in select applications. Our group has previously reported on the behavior of biodegradable microchips that contain an array of drug reservoirs, each sealed by a thin membrane that degrades according to a predetermined schedule to release drug[23]. The substrate hydrolyzes after all the doses have been released. Herein, we compare the efficacy of this new device to an existing clinical therapy.

Our studies show that the use of a biodegradable polymer-based microchip containing BCNU can significantly limit tumor growth of 9L gliosarcoma challenge in a rat model. The performance of this new drug delivery device is comparable to a polymer wafer uniformly impregnated with BCNU, similar to the FDA-approved Gliadel® therapy. This study provides the foundation for potentially significant improvements in cancer therapies by means of precise local administration of single or multiple drugs in a predetermined manner from a self-contained degradable microchip.

8.3 Materials and Methods

8.3.1 Microchip Fabrication and Packaging

The polymer microchips (Figure 8–1) were fabricated as previously reported[23]. Briefly, purified poly(L-lactic acid) (PLA, MW 194,000; Medisorb 100L; Alkermes, Cambridge, MA) tablets were compression-molded against a patterned aluminum die and followed by polishing to

form the reservoirs. A 12% v/v solution of poly(lactic-co-glycolic) acid (PLGA, MW 11,000; Medisorb 50:50 DL 2A; Alkermes) in 1,1,3,3,- hexafluoro-2-propanol was injected to form a membrane inside each reservoir. The microchip was then dried in a vacuum oven for 2 days at 80 °C. A mixture of BCNU (Bristol-Myers Squibb Co., Evansville, IN) and $_{14}$C-BCNU (Moravek Biochemicals, Brea, CA) was injected into the microchips using a microinjector (UltraMicroPump II; World Precision Instruments, Sarasota, FL). Each microchip was loaded with a final mass of 0.17, 0.67, or 1.24 mg of BCNU. The final microchip dimensions are approximately 10 mm in diameter and 1 mm in thickness.

Control devices of polymer wafers fabricated from polycarboxyphenoxypropane:sebacic acid (pCPP:SA) were incorporated with 1.24 mg BCNU. Briefly, pCPP:SA in a 20:80 formulation (Guilford Pharmaceuticals, Inc., Baltimore, MD) and BCNU were dissolved together in dichloromethane followed by vacuum desiccation. Polymer disks were then formed by compression molding. Polymers were stored at −80 °C prior to implantation. A detailed protocol is described elsewhere[29].

8.3.2 BCNU Stability and In Vitro Release

The stability of BCNU within the multi-reservoir microchips and the uniformly impregnated wafers was studied. BCNU was microinjected into the polymer microchip and then sealed on both sides with pressure sensitive adhesive. Similarly, BCNU was incorporated into the wafers as described above. The devices were incubated at 37 °C in a capped glass vial for various times. BCNU was extracted from the microchip for 3 min in 3 ml 20:80 ethanol:water. BCNU was extracted from wafers by dissolving with 99.7:0.3 dichloromethane:acetonitrile. The extracted solutions were immediately assayed using the Bratton–Marshall assay.

Intact BCNU was quantified via a colorimetric assay using the Bratton–Marshall method[30]. The assay is sensitive to only the whole BCNU molecule. One part of sulfanilamide solution (5 mg/ml in 2 M HCl) was added to two parts of each BCNU solution to be tested, sealed, and heated in a water bath at 50 °C for 45 min. The samples were chilled on ice to room temperature, and 200 μl of the resulting solution and 10 μl of the Bratton–Marshall reagent (3 mg/ml of N-(1-naphthyl)ethylenediamine in deionized water) were transferred to a 96 well plate and the absorbance was read 5 min later at λ=540 nm. The absorbance followed a linear relationship with BCNU concentration from 0 to 50 μg/ml. Samples were diluted in appropriate solvent before performing the assay to be within the linear range as necessary. The percent of intact BCNU was calculated by dividing the amount of intact BCNU as determined from the Bratton–Marshall assay by the initial amount of BCNU as estimated by radioactive-labeling or mass. All stability measurements were performed in triplicate, and the average value was reported.

Microchips were filled with BCNU, sealed and placed into 3 ml PBS at 37 °C to determine in vitro release kinetics. Periodically, the PBS was removed and replaced with fresh PBS. The radioactivity of the release medium was measured using a liquid scintillation counter (Packard TriCarb 2200CA; Perkin Elmer Life Sciences, Wellesley, MA) using ScintiSafe Plus 50% scintillation fluid (Fischer Chemicals, Fairlawn, NJ). The radioactivity per timepoint was divided by the total radioactivity loaded and integrated over time to describe the cumulative release profile. The results are reported as the median with error bars representing the 25th and 75th percentiles.

8.3.3 Ectopic Tumor Model

Two separate experiments were performed to evaluate the efficacy of BCNU when delivered via the biodegradable microchip. An initial efficacy study examined two dosages of BCNU (0.16 and 0.67 mg) released from the microchip, and a second experiment included a higher dosage of BCNU (1.24 mg).

Forty-one F344 Fischer rats underwent implantation of 9L gliosarcoma in the left flank in the first study. The ratswere divided into six groups and received one of the following treatments directly beneath the tumor at ten days: 1) a PLGA microchip containing 0.16 mg BCNU (n=8); 2) a PLGA microchip containing 0.67 mg BCNU (n=8); 3) an injection of 0.16 mg BCNU (n=4); 4) an injection of 0.67 mg BCNU (n=4); 5) an empty microchip (n=8); and 6) no treatment (n=9).

Forty F344 rats underwent 9L gliosarcoma flank implantation in the second study. The rats were randomly divided into five groups and received one of the following treatments: 1) a PLGA microchip containing 1.24 mg BCNU (n=8); 2) a pCPP:SA wafer containing 1.24 mg BCNU (n=8); 3) an empty PLGA microchip (n=8); and 4) empty pCPP:SA wafer (n=8); and 5) no treatment (n=8).

The microchips and wafers were sterilized by a gamma radiation dose of 480 Gy from a Cesium-137 source (Mark1-68 irradiator; JLS Shepherd, Glendale, CA) prior to implantation. A 2 mm_3 piece of solid 9L glioma, an experimental gliosarcoma syngeneic to the Fischer 344 rat (Brain Tumor Research Center; University of California, San Francisco), was implanted into the left flank of experimental animals as described previously[29]. Initial tumor sizes were measured at ten days after tumor implantation, and animals were randomized to experimental groups. The treatment was then placed between the flank muscle and the tumor under aseptic conditions.

Microchips were placed with the drug-eluting side facing the tumor. The incision was then closed with sterile autoclips. Tumors were measured three times a week with calipers, and the tumor volume was approximated as an ellipsoid (Eq. 1). Median tumor volumes vs. time were plotted and the delay of tumor growth vs. untreated controls was used as the measure of efficacy. The asymmetric, two-tailed Mann-Whitney U test was used to compare tumor sizes at various timepoints. p-values > 0.05 were considered significant.

$$V_{tumor} = Length \times Width \times Height \times \frac{\pi}{6} \qquad \text{Eq. 1}$$

8.3.4 Kinetics of BCNU Release In Vivo

Some animals were individually housed in metabolic cages (Nalgene model #650-0100, Braintree Scientific Inc., Braintree, MA) to assess drug release by radioactive excretion. Radioactivity measurements were conducted on urine after determining that no radioactivity was detected in the fecal samples. One ml urine samples were taken twice daily and mixed with 5 ml scintillation gel (Ready Gel, Beckman Coulter Inc., Fullerton, CA) in a 7 ml scintillation vial. The radioactivity was measured using a liquid scintillation counter (Beckman Coulter Inc., Fullerton, CA). The amount of radioactivity (nCi) was multiplied by the total volume of urine collected at that timepoint, and integrated over time to produce the drug recovery curves. Selected explanted microchips were sonicated in methanol and then allowed to soak for 1.5 h to extract the remaining radioactive BCNU. The radioactivity was quantified as above.

8.3.5 Rodent Model

Fischer 344 rats (female, 150–200 g) were obtained from Charles River Laboratories (Wilmington, MA). All animals implanted with radioactive BCNU and two animals from the other groups (serving as controls) were individually housed in metabolic cages, which separate feces and urine into tubes outside the cage. All other animals were housed in standard cages. All animals were given standard rat chow and water *ad libitum*. Animals housed in metabolic cages were given sugar water (4 tsp/500 ml), which encouraged the animals to drink more and allowed more frequent collection of urine samples. Animals were checked daily for physical or behavioral evidence of toxicity, such as decreased alertness, impaired grooming, or gait disturbances. Animals were housed and treated in accordance with the policies and principles of laboratory care of the Johns Hopkins University School of Medicine Animal Care and Use Committee and the MIT Committee on Animal Care. All in vivo experiments were carried out at the Johns Hopkins Animal Care Facility.

8.4 Results

8.4.1 Stability of BCNU and In Vitro Release

The half-life of BCNU within the microchip measured by the Bratton–Marshall assay at 37 °C was 11 days (Figure 8–2). The stability of BCNU in the microchip and wafer was directly compared in a separate experiment. The microchips contained 74% intact BCNU in the microchip and 62% intact BCNU in the wafer after incubation at 37 °C for 24 h when compared to the initial BCNU content. These values drop to 70% and 38% respectively at 48 h.

BCNU was released from the microchips in two distinct phases (Figure 8–3). Approximately 50% of the BCNU from microchips containing 1.24 mg of BCNU was released during the initial 12 h. This initial burst was followed by a much slower release of the majority of the remaining contents during the next 5 days.

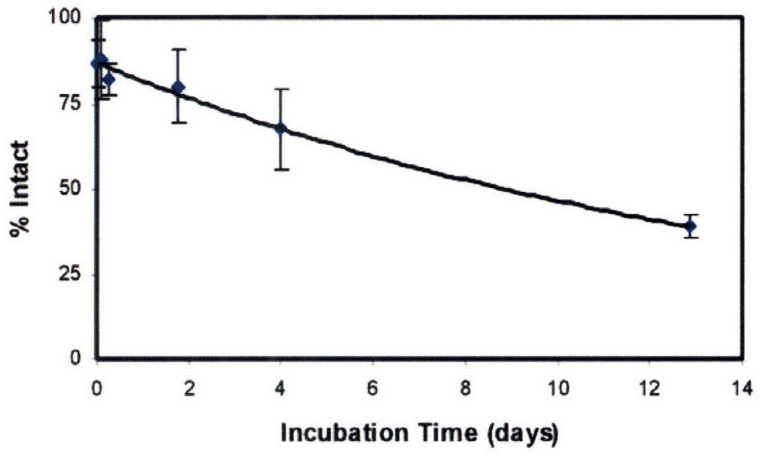

Figure 8–2. Intact BCNU in the sealed microchip. The mean±SD is plotted (n=3). BCNU in the polymer microchip has a half-life at 37 °C of 11 days.

8.4.2 Stability of BCNU and In Vitro Release

Microchips containing 0.17, 0.67 and 1.24 mg were implanted into the flank of 9L tumor-bearing rats. Animals receiving either no treatment or empty microchips were used as negative controls. The latter group was included to account for possible effects due to the polymer platform itself. The urine from all animals in treatment groups (n=8 or 9) and selected animals in negative control groups (both n=2) was collected and the BCNU recovered in the urine was

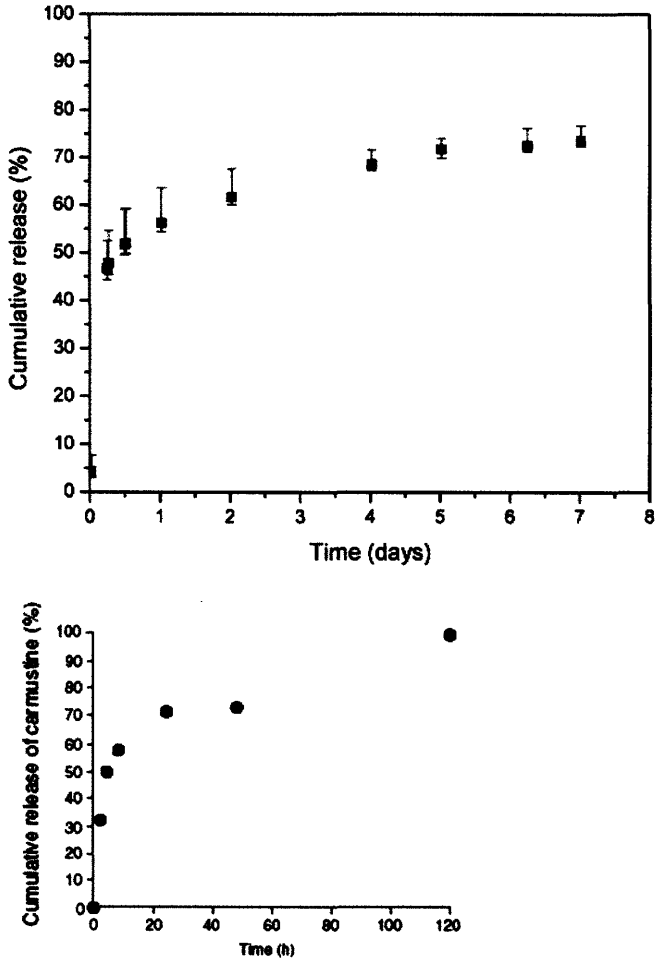

Figure 8–3. A) Cumulative release of BCNU from microchip into PBS at 37 °C (n=6). The median value is reported with the error bars representing the 25th and 75th percentiles. B) Release of BCNU from pCPP:SA wafers implanted into rat brains. (Reprinted by permission from Elsevier: J Control Release, 42:83–92, 1996).

integrated over time (Figure 8–4 and Table 8–1). The two control groups showed no radioactivity as expected. The release kinetics from the three BCNU-microchip groups were similar, reaching a plateau around day 6. An average of 37, 39, and 33% of the loaded radioactivity was recovered in the urine at 12 days after microchip implantation from the 0.17, 0.67, and 1.24 mg dose microchips, respectively. The urinary recovery shows that BCNU was released immediately upon implantation as was expected from the in vitro data.

The amount of radioactivity recovered from the microchips after sacrifice was approximately 5% of the initial loading for the 0.17 mg dose microchips, and 10% for the 0.67 mg dose microchips. Data for the residual radioactivity in the 1.24 mg microchips were not available, but is presumed to be of the same order. The unaccounted radioactivity may be distributed in various tissues, feces, or expired as CO21.

Table 8–1

Table 1
Urinary recovery of ^{14}C from rats with polymer microchips by day 12 (n=8 for each group)

BCNU dosage (mg)	Urinary recovery of ^{14}C (% of initial loading)
0.16[a]	37+10
0.67[a]	39+13
1.24[a]	33+8
1.24[b]	44+4

[a] Data from dose escalation study.
[b] Data from comparison of microchip *vs.* wafer delivery.

8.4.3 Microchip Delivery Inhibits 9L Glioma Tumor Growth

A study was performed to examine if the BCNU delivered from the passive microchip retained its tumoricidal activity and to observe the effect of this delivery vehicle on tumor

growth. The efficacy of three different doses of BCNU from the microchip was tested against the 9L gliosarcoma. Then, a side-by-side comparison of one dose in the microchip was tested against the wafer formulation with the same amount of BCNU.

The resulting tumor growth data are shown in Figure 8–5 for the different treatment groups. No treatment, empty microchips, and empty wafers were used as negative controls to account for possible effects on the tumor growth or growth measurement due to the polymer delivery platform. Overall, the BCNU treatment groups showed a smaller median tumor size than the control groups that received either empty microchips or no treatment. The lowest doses (0.16 mg) showed no significant difference in tumor size from the empty control microchips (p=0.074). The difference was significant, however, for the 0.67 mg dose (p=0.016), and for the 1.24 mg dose (p=0.001), which showed markedly reduced tumor size. Median tumor sizes in treatment groups were compared to empty microchip control at 12 days. Tumors in the low and middle dose groups were 43% and 65% smaller. The tumors receiving high dose microchips were 87% smaller than untreated tumors. The 1.24 mg dose was considered the minimum effective dose and selected for the subsequent study.

The efficacy of BCNU from the microchip was directly compared to that from a uniformly impregnated wafer (Figure 8–6). The minimum effective dose of 1.24 mg was microinjected into the polymer microchip or uniformly impregnated throughout the polymer wafers. Negative control groups included blank microchips and blank wafers. The negative control groups showed that the tumor grew by day 14 after microchip implantation to a median of 15.0 and 20.9 cm3 for the blank microchip and the blank wafer, respectively. In contrast, the tumors in the microchip treatment group grew only to a median of 1.5 cm3 and the wafer treatment group to 1.2 cm3. The microchip and the wafer produced significant tumor reduction

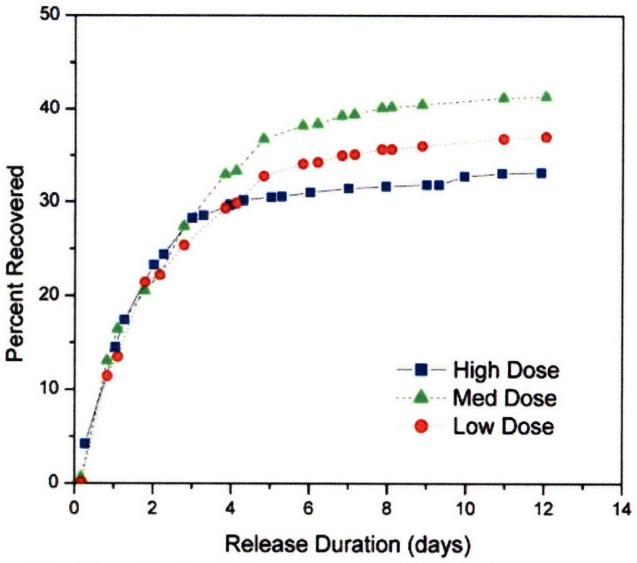

Figure 8–1. BCNU release kinetics obtained from quantification of 14C-BCNU excreted in urine after device implantation, normalized by loading amount. There is no statistical difference among three different doses administered (0.17, 0.67, and 1.24 mg). No radioactivity is excreted from the negative controls (not shown).

compared to their respective empty controls (p=0.032 and p=0.001 respectively). There was no significance in the difference in tumor sizes between the two treatment groups (p=0.156). These results show that the release of BCNU from the microchip is as effective as the release from the wafer.

8.5 Discussion

This study demonstrates the *in vivo* efficacy for cancer treatment of a self-contained degradable microchip that provides precise spatial administration of chemotherapeutics. Specifically, the microchip was used to deliver BCNU against a tumor model and showed significant reduction in tumor growth (Figure 8–5). Tumors treated with the highest loaded microchip showed marked diminished growth compared to empty control microchips (p=0.001).

The microchip was found comparable to that of the pCPP:SA wafer in release profile (Figure 8–3b) and efficacy in reducing tumor size. This demonstrates the first validation of proper microchip operation and efficacy in an *in vivo* model. Previously, only the *in vitro* activity of heparin released from the polymer microchip had been quantified[23], but no *in vivo* results had been demonstrated. A dose-dependent behavior was observed, with the highest dosage of BCNU delivering the strongest inhibiting effect on the tumor growth.

The release of the chemotherapeutic agent, BCNU, from the microchip starts on day 1 and continues for nearly 2 weeks (Figure 8–3). BCNU is released quickly from the polymer devices after implantation. This is necessary considering the hydrolytic instability of BCNU. The

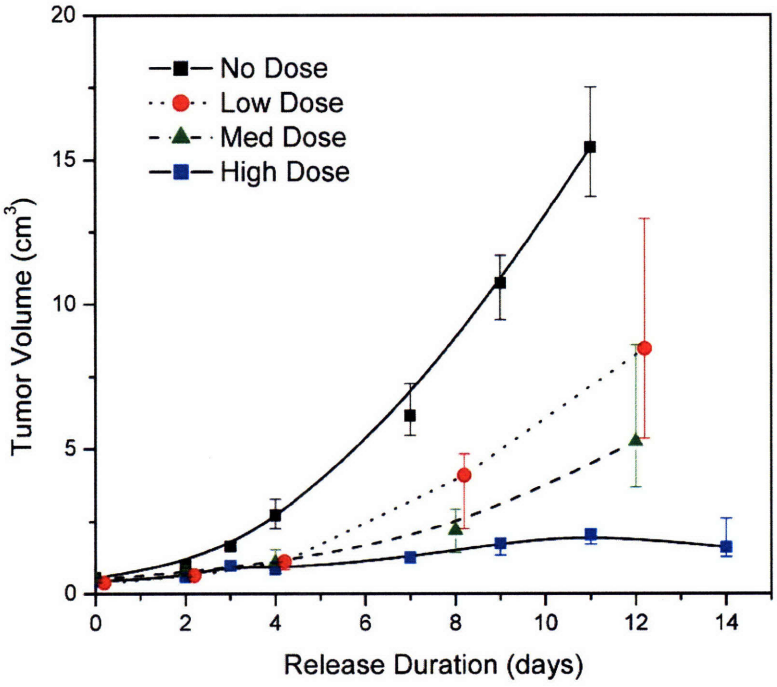

Figure 8–1. Dose response to BCNU from the polymer microchip. The high and medium doses showed statistical significance from the negative controls (p=0.001 and 0.016 respectively). The tumor reduction from the low dose was not statistically significant (p=0.074). The median values are plotted with error bars representing the 25th and 75th percentiles. Values for the medium dose were offset for clarity

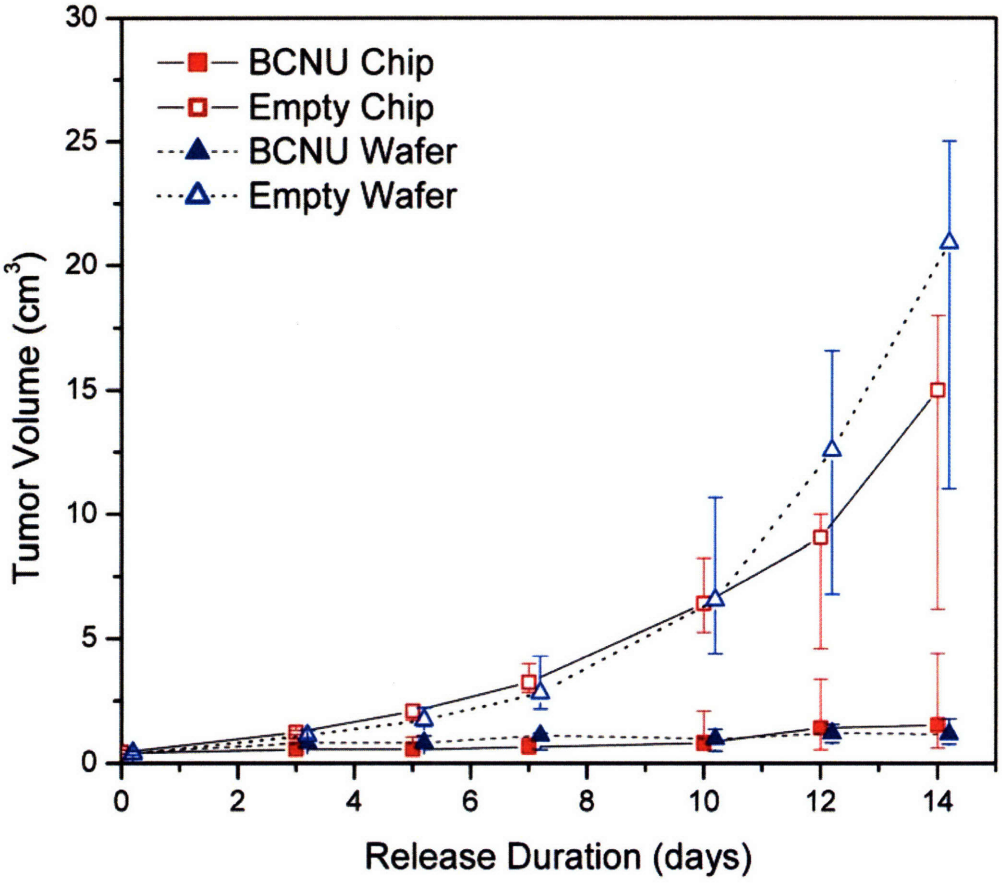

Figure 8–2: Tumor response to the same loaded dose of BCNU from the polymer microchip and the polyanhydride wafer. Both microchip and wafer showed tumor reduction compared to their empty control (p=0.032 and p=0.001 respectively) and were not statistically different from each other (p=0.156). The median values are plotted with error bars representing the 25th and 75th percentiles. Values were offset for clarity.

release profile of BCNU from the microchip is comparable to release from a uniformly impregnated pCPP:SA wafer (Figure 8–3b), which when released in rat brains at 37°C occurred over a period of approximately 5 days[31]. Dang, et al, measured the amount of BCNU recovered from pCPP:SA wafer explants and subtracted that amount from the initial loading to calculate the amount released.

High-pressure liquid chromatography (HPLC) and a colorimetric assay using the Bratton-Marshall reagent can both be used to quantify BCNU[2, 30-32]. The Bratton-Marshall method was

preferred for this study to quantify the *intact* BCNU molecule due to ability to process larger numbers of samples in parallel. Serial measurement of sample as in HPLC was considered undesirable BCNU has a short half-life in aqueous solution. BCNU was shown to have a half-life of 11 days when contained within the microchip at 37°C (Figure 8–2). This represents a substantial extension of the half-life compared to the free drug molecule in normal saline and 10% ethanol ($t_{1/2}$= 7 and 10 minutes, respectively)[1, 2]. BCNU is also more stable within the microchip compared to the wafer. At 48 hours, the microchip contains nearly twice as much intact BCNU as the wafer (70% and 38% respectively). BCNU acts by alkylating DNA, and it is known that its metabolites also have tumoricidal activity. Free BCNU powder dissolved in cell culture medium has been shown to be cytotoxic to XF498 cells after incubation for up to 12 hours, at which time the intact BCNU molecule is unmeasurable[32]. The microchip can release BCNU or its metabolically active degradation products, but for long term, or repeat release, the ability of the microchip to enhance stability of BCNU may also translate to increased effectiveness of other unstable molecules, especially with the use of excipients or stabilizers.

BCNU is reported here to begin release from the 11 kDa PLGA membrane within minutes of incubation in PBS. Previous work from our group has reported release of dextran (MW 70000), human growth hormone (MW 21500), or heparin (MW 6000-20000) from the microchip with the same 11 kDa membrane from between 6 and 17 days in PBS at temperatures from 28-33°C[23]. We believe this earlier release may have occurred for several reasons. All release profiles reported here were performed in a controlled 37°C incubator. BCNU is small (MW 214.1) and lipophilic compared to the model compounds used previously. It diffuses through the PLGA membrane and may facilitate swelling and opening of the membrane. This is supported by the observation that the membranes showed a visible swelling as early as a few

hours after the BCNU-loaded microchips were submersed in PBS at 37°C, whereas swelling of the membranes in PBS at 28-33°C was observed later to coincide with the released of dextran[33].

The urinary recovery shows BCNU was released on day 1 of implantation (Figure 8–4) as was expected from the *in vitro* data. Approximately one third of the initial loading was recovered by day 12 with a majority being released by day 5 (Table 1). The rate of recovery, however, is slower than the rate of release *in vitro*, attributed to the pharmacokinetics of rodent renal clearance. The total urinary recovery is lower than values reported by other groups (78%, 55%)[34, 35], which used different style metabolic cages, animal models, and administration locations. The recovery reported here is consistent with data from our previous injected control groups and release kinetics measurements[24].

The results from this study show that release of BCNU from the microchip is as effective as release from a clinically approved homogenous polymer matrix. The pCCP:SA wafer with BCNU is widely used to treat brain tumor patients and is commercially available as the Gliadel® Wafer [10, 20]. Gliadel® is FDA approved for the treatment of recurrent glioblastoma multiforme and newly diagnosed, high grade malignant gliomas. Six to eight wafers are placed in the cavity that remains after tumor resection, and the BCNU is released as the copolymer degrades. Gliadel® is now used routinely to improve survival in patients with malignant gliomas, but it is capable of delivering only one compound [10, 21, 22].

It is expected that delivery of a combination of synergistically acting chemotherapeutic agents can reduce tumor size with fewer side effects beyond that achieved by a monotherapy. Drug resistance and genetic profiling information[36] can be combined with the microchip to customize treatment of tumors. Future studies should exploit combination therapies and the synergistic action of potent combinations using additional anti-cancer drugs, such as

temozolomide[37-39] to achieve greater cytotoxicity with lower drug amounts. The use of solid dosage forms allows the microchip to potentially achieve smaller device dimensions and higher drug:polymer ratios than polymer matrix formulations. An optimized reservoir shape and configuration can deliver the same amount of drug with one tenth less polymer. This represents a solid foundation for improvement in treatments of diseases that can benefit from precise administration of multiple drug cocktails from a self-contained degradable microchip.

8.6 Conclusion

BCNU delivered from the polymer microchip inhibited the tumor growth of the 9L glioma in rats. The inhibiting effect on tumor growth was dose-dependent. These results are the first demonstration of in vivo efficacy of a polymer microchip brain cancer therapy. The efficacy validation of this platform as well as important dose response information indicates further evaluation of combination chemotherapy using a polymer platform with multiple reservoirs.

8.7 References

1. Tepe, P., Hassenbusch, S. J., Benoit, R., and Anderson, J. H. (1991) BCNU stability as a function of ethanol concentration and temperature. *J Neurooncol 10*, 121-7.
2. Kari, P., McConnell, W. R., Finkel, J. M., and Hill, D. L. (1980) Distribution of Bratton-Marshall-positive material in mice following intravenous injections of nitrosoureas. *Cancer Chemother Pharmacol 4*, 243-8.
3. Legler, J. M., Ries, L. A., Smith, M. A., Warren, J. L., Heineman, E. F., Kaplan, R. S., and Linet, M. S. (1999) Cancer surveillance series [corrected]: brain and other central nervous system cancers: recent trends in incidence and mortality. *J Natl Cancer Inst 91*, 1382-90.
4. Gloeckler Ries, L. A., Reichman, M. E., Lewis, D. R., Hankey, B. F., and Edwards, B. K. (2003) Cancer survival and incidence from the Surveillance, Epidemiology, and End Results (SEER) program. *Oncologist 8*, 541-52.
5. Lagerwaard, F. J., and Levendag, P. C. (2001) in *Forum (Genova)* pp 27-46.
6. Surawicz, T. S., Davis, F., Freels, S., Laws, E. R., Jr., and Menck, H. R. (1998) Brain tumor survival: results from the National Cancer Data Base. *J Neurooncol 40*, 151-60.
7. Zimm, S., Wampler, G. L., Stablein, D., Hazra, T., and Young, H. F. (1981) Intracerebral metastases in solid-tumor patients: natural history and results of treatment. *Cancer 48*, 384-94.
8. Lagerwaard, F. J., Levendag, P. C., Nowak, P. J., Eijkenboom, W. M., Hanssens, P. E., and Schmitz, P. I. (1999) Identification of prognostic factors in patients with brain metastases: a review of 1292 patients. *Int J Radiat Oncol Biol Phys 43*, 795-803.
9. Vecht, C. J., Haaxma-Reiche, H., Noordijk, E. M., Padberg, G. W., Voormolen, J. H., Hoekstra, F. H., Tans, J. T., Lambooij, N., Metsaars, J. A., Wattendorff, A. R., and et al. (1993) Treatment of single brain metastasis: radiotherapy alone or combined with neurosurgery? *Ann Neurol 33*, 583-90.
10. Brem, H., Piantadosi, S., Burger, P. C., Walker, M., Selker, R., Vick, N. A., Black, K., Sisti, M., Brem, S., Mohr, G., Muller, P., Morawetz, R., and Schold, S. C. (1995) Placebo-controlled Trial of Safety and Efficacy of Intraoperative Controlled Delivery by Biodegradable Polymers of Chemotherapy for Recurrent Gliomas. *Lancet 345*, 1008-1012.
11. (2001) Randomized trial of procarbazine, lomustine, and vincristine in the adjuvant treatment of high-grade astrocytoma: a Medical Research Council trial. *J Clin Oncol 19*, 509-18.
12. Chae, G. S., Lee, J. S., Kim, S. H., Seo, K. S., Kim, M. S., Lee, H. B., and Khang, G. (2005) Enhancement of the stability of BCNU using self-emulsifying drug delivery systems (SEDDS) and in vitro antitumor activity of self-emulsified BCNU-loaded PLGA wafer. *Int J Pharm 301*, 6-14.
13. Gallia, G. L., Brem, S., and Brem, H. (2005) Local treatment of malignant brain tumors using implantable chemotherapeutic polymers. *J Natl Compr Canc Netw 3*, 721-8.
14. Giussani, C., Carrabba, G., Pluderi, M., Lucini, V., Pannacci, M., Caronzolo, D., Costa, F., Minotti, M., Tomei, G., Villani, R., Carroll, R. S., Bikfalvi, A., and Bello, L. (2003) Local intracerebral delivery of endogenous inhibitors by osmotic minipumps effectively suppresses glioma growth in vivo. *Cancer Res 63*, 2499-505.

15. Hamstra, D. A., Moffat, B. A., Hall, D. E., Young, J. M., Desmond, T. J., Carter, J., Pietronigro, D., Frey, K. A., Rehemtulla, A., and Ross, B. D. (2005) Intratumoral injection of BCNU in ethanol (DTI-015) results in enhanced delivery to tumor--a pharmacokinetic study. *J Neurooncol 73*, 225-38.
16. Lesniak, M. S., and Brem, H. (2004) Targeted therapy for brain tumours. *Nat Rev Drug Discov 3*, 499-508.
17. Mardor, Y., Rahav, O., Zauberman, Y., Lidar, Z., Ocherashvilli, A., Daniels, D., Roth, Y., Maier, S. E., Orenstein, A., and Ram, Z. (2005) Convection-enhanced drug delivery: increased efficacy and magnetic resonance image monitoring. *Cancer Res 65*, 6858-63.
18. Quinn, J. A., Desjardins, A., Weingart, J., Brem, H., Dolan, M. E., Delaney, S. M., Vredenburgh, J., Rich, J., Friedman, A. H., Reardon, D. A., Sampson, J. H., Pegg, A. E., Moschel, R. C., Birch, R., McLendon, R. E., Provenzale, J. M., Gururangan, S., Dancey, J. E., Maxwell, J., Tourt-Uhlig, S., Herndon, J. E., 2nd, Bigner, D. D., and Friedman, H. S. (2005) Phase I trial of temozolomide plus O6-benzylguanine for patients with recurrent or progressive malignant glioma. *J Clin Oncol 23*, 7178-87.
19. Rhines, L. D., Sampath, P., DiMeco, F., Lawson, H. C., Tyler, B. M., Hanes, J., Olivi, A., and Brem, H. (2003) Local Immunotherapy with Interleukin-2 Delivered from Biodegradable Polymer Microspheres Combined with Interstitial Chemotherapy: A Novel Treatment for Experimental Malignant Glioma. *Neurosurgery 52*, 872 - 879.
20. Gliadel (R) Wafer (polifeprosan 20 with Carmustine implant), P. I., Baltimore, MD: Guilford Pharmaceuticals, 2003.
21. Westphal, M., Hilt, D. C., Bortey, E., Delavault, P., Olivares, R., Warnke, P. C., Whittle, I. R., Jaaskelainen, J., and Ram, Z. (2003) A Phase 3 Trial of Local Chemotherapy with Biodegradable Carmustine (BCNU) Wafers (Gliadel Wafers) in Patients with Primary Malignant Glioma. *Neuro-Oncology 5*, 79-88.
22. Valtonen, S., Timonen, U., Toivanen, P., Kalimo, H., Kivipelto, L., Heiskanen, O., Unsgaard, G., and Kuurne, T. (1997) Interstitial Chemotherapy with Carmustine-loaded Polymers for High-grade Gliomas: A Randomized Double-blind Study. *Neurosurgery 41*, 44-48.
23. Grayson, A. C. R., Choi, I. S., Tyler, B. M., Wang, P. P., Brem, H., Cima, M. J., and Langer, R. (2003) Multi-pulse Drug Delivery from a Resorbable Polymeric Microchip Device. *Nature Materials 2*, 767-772.
24. Li, Y., Shawgo, R. S., Tyler, B., Henderson, P. T., Vogel, J. S., Rosenberg, A., Storm, P. B., Langer, R., Brem, H., and Cima, M. J. (2004) In vivo release from a drug delivery MEMS device. *J Control Release 100*, 211-9.
25. Giese, A., Kucinski, T., Knopp, U., Goldbrunner, R., Hamel, W., Mehdorn, H. M., Tonn, J. C., Hilt, D., and Westphal, M. (2004) Pattern of recurrence following local chemotherapy with biodegradable carmustine (BCNU) implants in patients with glioblastoma. *J Neurooncol 66*, 351-60.
26. Grayson, A. C. R. (2003) in *Massachusetts Institute of Technology, Doctoral Thesis* pp 293, Massachusetts Institute of Technology, Cambridge, MA.
27. Li, Y., Ho Duc, H. L., Tyler, B., Williams, T., Tupper, M., Langer, R., Brem, H., and Cima, M. J. (2005) In vivo delivery of BCNU from a MEMS device to a tumor model. *J Control Release 106*, 138-45.
28. Prescott, J. H., Lipka, S., Baldwin, S., Sheppard, N. F., Jr., Maloney, J. M., Coppeta, J., Yomtov, B., Staples, M. A., and Santini, J. T., Jr. (2006) Chronic, programmed

polypeptide delivery from an implanted, multireservoir microchip device. *Nat Biotechnol 24*, 437-8.

29. Tamargo, R. J., Myseros, J. S., Epstein, J. I., Yang, M. B., Chasin, M., and Brem, H. (1993) Interstitial Chemotherapy of the 9L Gliosarcoma: Controlled Release Polymers for Drug Delivery in the Brain. *Cancer Research 53*, 329-333.
30. Loo, T. L., and Dion, R. L. (1965) Colorimetric Method for the Determination of 1,3-Bis(2-chloroethyl)-1-nitrosourea. *Journal of Pharmaceutical Science 54*, 809 - 810.
31. Dang, W., Daviau, T., Ying, P., Zhao, Y., Nowotnik, D., Clow, C. S., Tyler, B., and Brem, H. (1996) Effects of GLIADEL® wafer initial molecular weight on the erosion of wafer and release of BCNU. *Journal of Controlled Release 42*, 83-92.
32. Seong, H., An, T. K., Khang, G., Choi, S. U., Lee, C. O., and Lee, H. B. (2003) BCNU-loaded Poly(D,L-lactide-co-glycolide) Wafer and Antitumor Activity Against XF-498 Human CNS Tumor Cells InVitro. *International Journal of Pharmaceutics 251*, 1-12.
33. Grayson, A. C. R., Cima, M. J., and Langer, R. (2004) Molecular release from a polymeric microreservoir device: Influence of chemistry, polymer swelling, and loading on device performance. *Journal of Biomedical Materials Research Part A 69A*, 502-512.
34. DeVita, V. T., Denham, C., Davidson, J. D., and Oliverio, V. T. (1967) The physiological disposition of the carcinostatic 1,3-bis(2-chloroethyl)-1-nitrosourea (BCNU) in man and animals. *Clinical pharmacology and therapeutics 8*, 566-77.
35. Domb, A., Rock, M., Schwartz, J., Perkin, C., Yipchuck, G., Broxup, B., and Villemure, J. G. (1994) Metabolic disposition and elimination studies of a radiolabelled biodegradable polymeric implant in the rat brain. *Biomaterials 15*, 681-688.
36. Leuraud, P., Taillandier, L., Medioni, J., Aguirre-Cruz, L., Criniáere, E., Marie, Y., Kujas, M., Golmard, J. L., Duprez, A., Delattre, J. Y., Sanson, M., and Poupon, M. F. (2004) Distinct responses of xenografted gliomas to different alkylating agents are related to histology and genetic alterations. *Cancer research. 64*, 4648-53.
37. Stupp, R., Mason, W. P., van den Bent, M. J., Weller, M., Fisher, B., Taphoorn, M. J., Belanger, K., Brandes, A. A., Marosi, C., Bogdahn, U., Curschmann, J., Janzer, R. C., Ludwin, S. K., Gorlia, T., Allgeier, A., Lacombe, D., Cairncross, J. G., Eisenhauer, E., and Mirimanoff, R. O. (2005) Radiotherapy plus concomitant and adjuvant temozolomide for glioblastoma. *N Engl J Med 352*, 987-96.
38. Gururangan, S., Cokgor, L., Rich, J. N., Edwards, S., Affronti, M. L., Quinn, J. A., Herndon, J. E., 2nd, Provenzale, J. M., McLendon, R. E., Tourt-Uhlig, S., Sampson, J. H., Stafford-Fox, V., Zaknoen, S., Early, M., Friedman, A. H., and Friedman, H. S. (2001) Phase I study of Gliadel wafers plus temozolomide in adults with recurrent supratentorial high-grade gliomas. *Neuro-oncol 3*, 246-50.
39. Brem, S., Tyler, B., Li, K., Pradilla, G., Legnani, F., Caplan, J., and Brem, H. (2007) Local Delivery of Temozolomide by biodegradable polymers is superior to oral administration in a rodent glioma model. *Cancer Chemother Pharmacol.*

CHAPTER 9

Summary of Results

& Suggestions for Future Work

9.1 Summary of Results

The results presented in this thesis clearly demonstrated the ability of a polymeric reservoir-based device to achieve sensing and drug delivery. We present here two tools/two applications to help in the war on cancer. MRI contrast agents have been used to obtain qualitative information in vivo, but the use of a semi-permeable device with a constrained volume allows quantitative determination. For the drug delivery project, this is the first time in vivo efficacy has been shown from a multi-reservoir controlled-release platform.

9.1.1 Reservoir-based Sensing Device

The operation of molecular relaxation switches (MRSw) was successfully demonstrated. Several CLIO were conjugated to antibodies to produce MRSw that detect several classes of analytes, protein A (PA), human chorionic gonadotrophin (hCG), and interleukin-2 (IL-2) (Chapter 4). Protein A served as a simple multivalent protein analyte; HCG was used as an example of a tumor-secreted cancer biomarker; and IL-2 was chosen as an example of a cancer therapeutic.

The diagnostic application of MRSw was described in detail with specific attention to the analyte concentration response, T_2 kinetic profile, and particle size kinetic profile (Chapter 5, 6, and 7). MRSw experiments with PA showed expected decreases in T_2 and concomitant increases in particle size. The favorable results with PA led us to commence more extensive investigations with hCG. The hCG concentration response was found generally to decrease T_2 from 0.01 to 1 μg/ml for CLIO concentrations of 8 μg/ml. The concentration profile was maintained in a variety of biological buffers and selective in the presence of other proteins, which is particularly important to establish for extending the diagnostic applications of MRSw (Chapter 5). MRSw, for example, can be used directly with unprocessed cell culture media, serum or urine samples. A low valency and high valency MRSw for hCG were specifically compared. The valency refers to the degree of antibody functionalization per CLIO. The concentration response was found to be steeper, viz. more sensitive with higher valency MRSw. T_2 and particle size kinetic profiles were also conducted for determining the ideal incubation time and the window for T_2 measurements. The MRSw reaction was found to be fast. Changes in T_2 and particle size were observed within 30 seconds of mixing analyte solutions and CLIO reagents.

Stability of the MRSw assay was investigated and found to favor lower analyte concentrations and lower valency CLIO. The advantage of the higher sensitivity, higher valency CLIO was difficult to exploit and was mitigated as it was more susceptible to precipitation and unstable T_2 measurements. A method to improve the stability of CLIO aggregates was introduced (Chapter 6). MRSw were embedded in agarose and exposed to analyte (either by directly mixing in with the agarose (Section 6.4.2). This matrix stabilization approach was shown to produce stabilized T_2 measurements for 28 days *in vitro* after which the experiment was terminated. There are no indications that the stability would not continue for longer if the experiment had been continued. This matrix stabilization approach constitutes a significant step towards practical and reliable aggregation-based assays.

The stoichiometric nature of MRSw was also investigated in Chapter 5. Specifically, the ratio of C95 to C97 and the effect changing the total CLIO concentrations was studied. Nontrivial gains can be made the LOD by adjusting the CLIO concentration. Magnetic relaxometer parameters may be adjusted accordingly to accurately measure high T_2 within acceptable acquisition times.

We have also demonstrated the MRSw assay in a high-throughput mode in a standard 96-well plate format with the single-sided MR, which is essential for screening and development of magnetic nanoparticle assays. The combination of these two aspects, an industry standard sample format and matrix stabilization, provides high-throughput simplified sample handling essential for a mix-and-read plate assay.

Chapter 7 focused on MRSw for IL-2. IL-2 was found, in contrast, to *increase* the T_2 of the CLIO-anti-IL-2 reagent solution in a concentration-dependent manner. The solutions did not initially show a change in $T_{2,eff}$, but a concentration dependent response developed after

incubation and was maintained up to 2 days later. A polyclonal antibody was used for the detection of IL-2; however, it is not clear if this different result was due generally to the use of a polyclonal antibody, due to the effective K_d of the ensemble of polyclonal antibodies, specifically to this conjugate, or the properties of IL-2. The desired dynamic range may be achieved by adjusting the initial CLIO concentration appropriately.

CLIO-anti-IL-2 reagent was also encapsulated into washer devices with a semi-permeable polycarbonate membrane. The devices were then placed in IL-2 solutions and the IL-2 was allowed to diffuse into the devices. Devices containing fluid CLIO-anti-IL-2 reagent also showed a concentration dependent increase in $T_{2,eff}$, but devices containing agarose stabilized CLIO-anti-IL-2 reagent showed a decrease in $T_{2,eff}$. The CLIO-anti-IL-2 reagent produced here may be useful in an application where a slower response to environmental conditions is acceptable.

9.1.2 Reservoir-based Drug Delivery Device

The chemotherapeutic drug 1,3-bis(2-chloroethyl)-1-nitrosourea (BCNU) was delivered from the polymer microchip and inhibited the tumor growth of the 9L glioma in rats. The tumor growth was inhibited in a dose-dependent manner from 0.16, 0.67, and 1.24 mg of BCNU. These results are the first demonstration of *in vivo* efficacy of a polymer microchip delivered therapeutic. The effect of the same dose of BCNU delivered from the microchip and a polycarboxyphenoxypropane:sebacic acid (pCPP:SA) polymer wafer were compared. The microchip and the wafer produced significant tumor reduction compared to their respective empty controls ($p=0.032$ and $p=0.001$ respectively). There was no significance in the difference

in tumor sizes between the two treatment groups (p=0.156). These results show that the release of BCNU from the microchip is as effective as the release from the wafer.

9.2 Suggestions for Future Work

9.2.1 Reservoir-based Sensing Device

The primary aim of this thesis was to develop MRSw sensors for quantitative measurement of soluble signals. A great deal of characterization has been done, but the next steps would involve translating this body of knowledge for *in vivo* use. The main steps would include the following:

1) to employ high sensitivity MRSw with a stabilizing matrix

2) to miniaturize the device, ultimately for delivery through a biopsy needle

3) to demonstrate multi-reservoir sensing

4) to achieve faster device operation, namely with a high permeability membrane

5) to correlate the MRSw device measurements with local analyte concentration

6) to identify additional analytes of interest

7) to test the hypothesis that the local biomarker concentration may lead to earlier diagnosis and detection of metastasis

We are already making progress on the use of MRSw for *in vivo* applications. T_2 behavior of devices containing CLIO were investigated using MRI (Figure 9–1)[1]. The MRSw were enclosed inside PDMS substrates and a polycarbonate membrane containing 10 nm pores. The devices were then immersed in baths containing various concentrations of hCG-β. T_2 was found

to decrease at one day in response to the analyte concentration (Figure 9–2). This successful demonstration of *in vitro* MRSw device performance led us investigate *in vivo* performance in a proof-of-principle study. A human cell line producing hCG was used to produce ectopic tumors in the flanks of nude mice. A washer type device (Chapter 7) containing CLIO reagent was subcutaneously implanted near the tumor. Preliminary data show that the devices do respond to the hCG produced by the tumors. Correlation with serum concentrations is not strong, as expected, and methods to determine local hCG concentrations are being pursued.

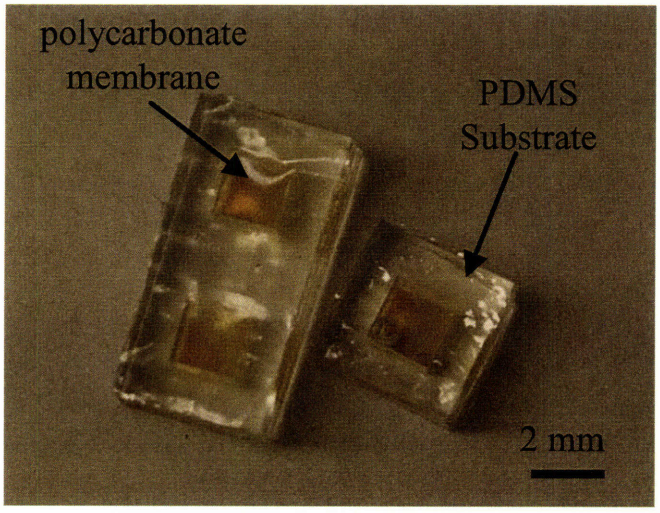

Figure 9–1. Photograph of sensing devices filled with a concentrated MRS solution. The polydimethylsiloxane (PDMS) substrate contains reservoirs which are covered by a semi-permeable polycarbonate (10 nm pore) membrane. The membrane will allow analyte to diffuse into the reservoir and induce MRS aggregation, which is measured by MRI. Reproduced from [1].

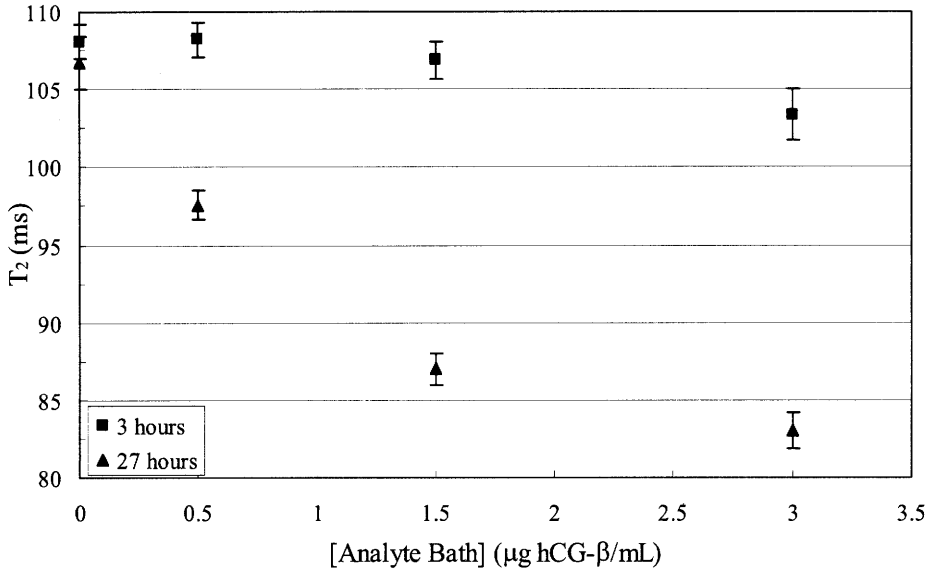

Figure 9–2. Sensing of hCG-β using a PDMS device and MR imaging. CLIO solutions (6 μ g Fe/mL) were contained in the reservoirs with polycarbonate membranes. Sample devices were placed in baths of known hCG-β concentrations. T_2 shortening of the sample devices are reported as a percent change in T_2 compared to control devices (same CLIO concentration, but the device was placed in a bath of PBS only). Reproduced from [1].

It is hypothesized that local biomarker concentration may provide a more accurate method of categorizing patients for staging and treatment. Early categorization into low and high risk status may allow the appropriate treatment to be given sooner rather than waiting for failure with the single agent and then giving the more hazardous multi-drug treatment later. Ultimately, we hope this approach will allow earlier detection of cancer as well as monitoring of treatment efficacy. Further extensions of this work may allow measurement of local drug concentration in conjunction with a targeted or local drug delivery method. This device-based approach may have impact on the development of targeted drug delivery and personalized cancer treatment. Individualized treatment may be especially important in cancer because each cancer is unique, with respect to genesis, location, burden, and spread, resulting in a highly variable response to

therapy. We hope that this work contributes to the development of multiplexed sensors for clinical oncology applications.

9.2.2 Reservoir-based Drug Delivery Device

The microchip array of reservoirs allows for delivery of multiple drugs with independent release kinetics and formulations. The efficacy validation of this platform as well as important dose response information indicates further evaluation of combination chemotherapy using a polymer platform with multiple reservoirs. Compounds which have shown synergistic anti-tumor effect are the first that should be tested with microchip delivery. BCNU and IL-2 have been extensively studied against glioma. Temozolimide is second-generation alkylating agent that has achieved clinical success. Microchip delivery of combinations of temozolimide and other agents should also be explored.

9.3 References

1. Daniel, K. D., Kim, G. Y., Vassiliou, C. C., Jalali-Yazdi, F., Langer, R., and Cima, M. J. (2007) Multi-reservoir device for detecting a soluble cancer biomarker. *Lab Chip 7*, 1288-93.

CHAPTER 10

Acknowledgements

First, I want to thank God for his infinite mercy, wisdom, persistence, and patience. He has led me all the way through this journey. Surprisingly, the most important things I learned during my Ph.D. were not technical but were about myself and His perfect nature.

The work described in this thesis was the result of much professional collaboration and would not have been possible without much personal support.

My mother, my father, my sister Shirley, and her husband Andrew, who have been constant supporters.

My thesis committee members:

Professor Darrell Irvine, who helped me through all the major Ph.D. milestones and all the different turns of this thesis. His career and research have been a model for me.

Professor Robert Langer, who encourages creativity, vision, and hard work as a paragon example. His generosity and guidance were instrumental to this research and will continue to direct me.

Professor Michael Cima, who instilled in me his love of gizmos and science, and challenged me to work on the most difficult problems. His incredible teaching and mentorship were critical to my growth and confidence as a scientist.

Collaborators and consultants on the Sensor project:

Ralph Weissleder, Lee Josephson, Isaac Koh, Suelin Chen, and the other dedicated researchers at the Center for Molecular Imaging Research-MGH

Tyler Jacks, Philip Sharp, Alain Charest and the entire CCCE team

Tom Lowery at T_2 Biosystems

Collaborators and consultants on the drug delivery project:

Amy Richards Grayson, who developed the polymeric multi-reservoir microchip, taught me about drug delivery, and was invaluable in getting me started in the lab.

Henry Brem and Betty Tyler at Johns Hopkins University, who provided the expertise regarding brain cancer and performed the drug delivery animal experiments.

Lenny, Barb, Connie, Ilda, Nancy, Tiffany, for making things run smoothly in and out of the lab.

The actual writing process would not have gone as well without Susan at the Writing center and my thesis cheer group (Lisa, Sylaja, and Sasha). Thanks!!!

I am grateful for the funding that has made this research possible, the NIH Bioengineering Research Partnership grant and NCI Center for Cancer Nanotechnology Excellence grant; as well as personal support through the NSF Graduate Research Fellowship and HST Fellowship, especially the Martinos Scholarship.

The camaraderie and commiseration of my fellow graduate students, especially all those who completed their thesis this past year, kept me going through all the tough spots. We made it!!!

I want to especially thank David Nguyen, my DMSE-HST-Langer Lab twin, one of my closest friends and supporters, who has been a cherished companion through classes, research, numerous practice talks, and life itself.

Everyone in the Langer and Cima labs has been wonderful.

Classmates, colleagues and officemates in particular who've had an impact on me and the direction of this thesis:

Jenny Mu, Ying Chau, Tommy Thomas, Amy Richards Grayson

Jessica Liao, Benjamin Larman

Heejin Lee, Honglinh Ho Duc, Dan Wesolowski, Christophoros Vassiliou, Noel Elman

Karen Daniel, Seth Townsend, Christopher Bettinger, Divya Bolar, and Mikhail Shapiro

Best wishes to those continuing the sensing and drug delivery projects!!! Alex, Byron, Yibo, and Yoda

UROPS Robert Batten, Helen Tsai, Christine Lee, Ryan Huang, Sina Omran, Marilyn Galindo, Melinda Valdez, and Farzad Jalali-Yadzi. I hope they learned as much from me as I learned from them.

The DMSE community, especially Angelita Mireles and Kathleen Farrell for recruiting, and welcoming me to my new home at MIT, and being my foster mothers

The HST community, for their passion to integrate science, engineering, and medicine to solve problems in human health, especially:

Biju Parakaddan, Kyle Smith, and my JT Lisa "LT" Treat, with whom I lived for two months and shared profound experiences on the HST-India program

Drs. Shiladitya Sengupta, Neerja Bhatla, and MP Sharma, the HST-India coordinators

Cathy Modica, Valerie Pronio-Stelluto, and Jeannie Bruno, who believed in me always

and Peter Mack, my ICM partner for reminding me to keep a positive mental attitude.

Thanks to my girlfriends: Blanca, Lara, and my dearest Bonnie, for flying in from California to hold my hand through the thesis defense presentation

The Edgerton Bible Study Group: Jeff Blackburne, Steven Lulich, Jialu Yeh, Taemie Kim, Kenneth Arnold, Peter James "and John"

My Ashdown House community: Eveline, Rachelle, Aditi, Stacy, Marisa, Himani, Anton, Brad, Yoshi, Brian Chan, Albert Chow, Bhuwan, Barun, Marcus, Vivek, Tor, Matt Guyton, Ann & Terry Orlando, Denise Lanfranchi, John, Mike, Lenny, and Maria, for making our 200 year old house a wonderful place to live. I will treasure my years there.

MIT Sport Taekwondo, always training for first place. Go Tech!

MIT Salsa Club, Chris, Meagan, Steve, for sharing their love of salsa

and the dinner-dance-poi crew, Ashley Evans, Ravi Purushotma, Divya Bolar, Mara MacDonald, and Rahmat Cholas. Words can't adequately describe how awesome it was to tear up the floor (literally) with you guys, but "Afghani Pumpkin" comes close.

Thanks also to the following for helping, relaxing, sustaining and chillaxing me through the years: LSC, free food, grad women group, DMSE grad lounge, Quake, Starcraft, HST grad lounge, Ashdown House & AHEC, GSC, MIT Sport TKD, GoCrossCampus, MIT Salsa Club, Charles River and the esplanade, MIT Sailing Pavilion, Pistol, Park Street Church, and Ph.D. Comics

It was a privilege to work on cancer therapy and diagnosis. I admit that during the daily grind, I easily forgot that my work has the real potential to help people in the near future. Fortunately, my HST ICM hospital rotations introduced me to the patients that may benefit one day from translational research such as mine and put a face to the disease. One of the most striking memories I will hold onto was when I met a young girl through the Make-A-Wish Foundation, which grants wishes to terminal cancer patients. Her wish was to visit MIT and the world-class research laboratories here. Although she was too weak to pick up the Langer autographed textbook that we presented her with, her excitement and hope for the future glowed strong.

May we all have true hope.